University of Louisville

ThinkIR: The University of Louisville's Institutional Repository

5-2012

# Exciton generation and dissociation mechanisms in organic bulk heterojunction solar cell materials.

Hemant M. Shah 1981-
*University of Louisville*

EXCITON GENERATION AND DISSOCIATION MECHANISMS IN ORGANIC
BULK HETEROJUNCTION SOLAR CELL MATERIALS


By

Hemant M. Shah

M.S. University of Louisville, 2008

EXCITON GENERATION AND DISSOCIATION MECHANISMS IN ORGANIC
BULK HETEROJUNCTION SOLAR CELL MATERIALS


By
Hemant M. Shah
Master of Science, University of Louisville, 2008



A Thesis approved on
December 14, 2011



By the following Thesis Committee:


_____

Dr. Bruce W. Alphenaar (Thesis Director)


_____

Dr. Robert W. Cohn


_____

Dr. Mahendra K. Sunkara


_____

Dr. Gamini Sumanasekara


_____

Dr. Shamus McNamara

## DEDICATION

This dissertation is dedicated to my parents

Mr. Mahesh K. Shah

and

Mrs. Gopi M. Shah

I thank my parents for the confidence and support they have shown for me throughout my life.

I would also like to dedicate this dissertation to my elder sister

Mrs. Neeta C. Mehta

Neeta has been a great inspiration for me my entire life

## ACKNOWLEDGMENTS

This thesis was developed over a period of four years. First and foremost I would like to thank my advisor Dr. Bruce W. Alphenaar for giving me this wonderful opportunity to work in his lab for this prolonged period of time. His unique ideas have helped design and develop some of the most amazing experiments I ever got a chance to work on. Over the years I have tried to develop his way of thinking and I believe this has made me a better researcher. Second I would like to thank Dr. Mahendra K. Sunkara for the unprecedented access to his lab in Chemical Engineering. It was an amazing experience to work on collaborative projects with his group. I had never imagined I would be able to gain such different perspectives from a different branch of engineering.

I would like to thank Dr. Robert W. Cohn for the useful discussions I have had the opportunity to have with him over the years. His class on Nanotechnology proved to be vitally important for my research. I also thank him for sharing his lab with our group. His lab proved to be very lucky for me as majority of the research work in this thesis was performed in his lab. I thank Dr. Gamini Sumanasekara for his useful insights on my research. His ideas have helped make this work better. Over the years I have asked him tons of questions about my work and have always learned something new about it.

I thank Dr. Shamus McNamara for his useful evaluation of my thesis and being a part of my committee. The new courses he introduced in the ECE department at University of Louisville have helped me a lot of graduate students to a great extent.

I would like to thank all the current and former post docs and research engineers with whom I had the pleasure to work closely. Dr. Aditya D. Mohite, Dr. Adam Willitsford and Dr. Tanesh Bansal helped me a lot with the laser training and related issues. I thank Dr. George Lin who was always very instrumental in challenging me with all my ideas which always helped me refine my work. I thank Dr. Suresh Gubbala, Dr. Praveen Meduri and Dr. Chandrashekar Penyala from Chemical Engineering for training and helping me with several equipments.

Over the course of my stay at the University of Louisville I have worked with almost every staff member in Schumaker Research Building and I thank all of them for their help. All the Graduate students I had the opportunity to work with has been a pleasure.

# ABSTRACT

## EXCITON GENERATION AND DISSOCIATION MECHANISMS IN ORGANIC BULK HETEROJUNCTION SOLAR CELLS MATERIALS

Hemant M. Shah

December 14th, 2011

Characterization of the optical and electrical properties of organic solar cell materials is of prime importance to organic solar cell design. This thesis describes the use of capacitive photocurrent measurements to study the exciton generation and dissociation mechanisms of organic solar cell materials. The emphasis is on the study of the methanofullerene derivatives (e.g., PCBM) which act as the electron acceptor material. This is because much work has already been done studying electron donating polymers used in organic solar cells (in an effort to enhance their absorbance coefficient), but less information is available on the acceptor material.

In the blend films of MDMO-PPV: PCBM, the charge generation rate in PCBM was discovered to be much higher than would be expected from the absorbance cross-section. This observation led to design of a photovoltage bleaching experiment to examine the charge generation mechanism.

Here the effect of illumination by a tunable light source on the open circuit photovoltage of a MDMO-PPV: PCBM bulk heterojunction solar cell was measured.

Illumination of light at the PCBM ground state singlet exciton causes a sharp decrease in the photovoltage, while illumination at the ground state MDMO-PPV exciton shows no change. A direct pathway of recombination of above gap generated charge carriers was identified. Photovoltage bleaching results suggests that excitation at the PCBM ground singlet state exciton increases the recombination rate of higher energy excitations, either by acting as a recombination center or by forcing higher energy carriers into short lived states that recombine before reaching the contacts. The fact that the photovoltage bleaching correlates with the ground state PCBM singlet exciton suggests that charge dissociation from PCBM preferentially generates long-lived localized states.

Capacitive photocurrent measurements were then performed on isolated methanofullerene derivatives, with the polymer donor material absent. Several low energy transitions were resolved in the optical spectroscopy of methanofullerene derivatives. These low energy states lay below the optical energy band-gap of these materials, so that their presence was unexpected. It was determined that the low energy states overlapped with the plasmon state of the highly conducting substrates (Indium Tin Oxide) which were in close proximity with the PCBM. Plasmon states in ITO have been observed previously, but the results presented in this thesis are unique in that this is the first evidence

of charge transfer from the plasmon state of ITO to a high electron affinity fullerene derivative.

The results show the evidence of charge transfer from PCBM to ITO over a broad wavelength range of 400 – 2400 nm (3 eV – 0.5 eV). Few materials have been observed to have absorbance and charge transfer over such a large range of energies in the infra-red regime. These results open a new direction for development of organic solar cell design with higher power conversion efficiencies.

# TABLE OF CONTENTS

**PAGE**

**CHAPTERS**                                                                                         **PAGE**

## 1. INTRODUCTION

## Chapter 2: Background

# LIST OF TABLES

# LIST OF FIGURES

# CHAPTER I: INTRODUCTION

## 1.1 Energy Issues



Figure 1.1: Estimated U.S. Energy usage graph from Lawrence Livermore National Laboratory

On April 24th, 2004 American Scientist and Chemistry Nobel prize winner, Dr. Richard E. Smalley was invited to the US Oversight hearing on sustainable, low emission and electricity generation. When asked what his opinion was as to the main challenge facing humanity, he said, "Energy is the single most important

problem facing humanity today – not just the U.S., but also worldwide. The magnitude of this problem is incredible. Energy is the largest enterprise on Earth– by a large margin... While conservation efforts will help the worldwide energy situation, the problem by mid-century will be inadequate supply".[1] This strongly worded opinion projects the urgent need for innovative ways to find alternative sources of energy and reduce the dependence on oil. Figure 1 shows an energy usage graph for the United States in 2009, developed by Lawrence Berkeley National Laboratory and Department of Energy. [2] As seen, of the total energy consumed in 2009, about 80% came from some form of fossil fuels leading to greenhouse gas emissions. The addition of $CO_2$ to the atmosphere through fossil fuel use is a major threat to the global environment. However, little will has been shown by government agencies (especially from the world's most polluting countries) to deal with this significant problem. [3]



Figure 1.2: The volatility in the price of Crude oil over a period of 72 months. [4]

The price of oil and atmospheric pollution caused by its consumption has generated a renewed urgency to the search for alternative sources of energy. [5]

One of the most promising forms of renewable energy is solar energy. [6] Large scale, economical and high efficiency solar cells have the potential to satisfy a large portion of the energy demand across the globe. Solar cells made of single crystal silicon, gallium arsenide and other III-IV compounds have high power conversion efficiency. The main drawback of these cells is the price of manufacturing single crystal structures, especially on a large scale. [7]

## 1.2 Photovoltaic principles
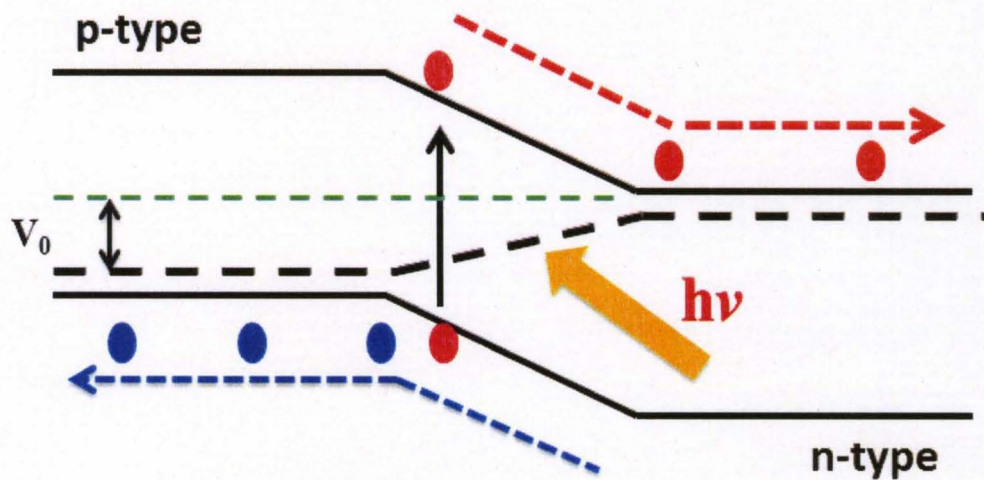


Figure 1.3: Working principle of a p-n junction photovoltaic cell

In single crystal inorganic solar cells, above gap light is absorbed by the photo-sensitive material to create electron-hole pairs (ehps). These charges are then separated from each other by an internal electric field, or built-in potential barrier. Once the charges are isolated from each other, they can move freely into

the circuit generating electric current to power a load. Figure 1.3 shows a schematic of how electrons and holes are created by light absorbance and then separate across the built-in potential formed by a p-n junction. Silicon solar cells with p-n junction charge separation schemes routinely achieve efficiencies of 21% or more. [8]

## 1.3 Inorganic vs. Organic (Excitonic) Solar cells

Organic solar cells behave very differently from their inorganic counterparts. Organic semiconducting materials do not show extensive regular 3-D lattices, and instead are made up of collections of single molecules or polymer chains. As such, charge transport in these materials occurs much more slowly than in inorganics, and is characterized by 'hopping' from molecule to molecule rather than by free-carrier like conduction. Furthermore, the absorption of light in organic materials forms stable excited state (excitons) that do not readily dissociate into free electrical charges at room temperature. (For this reason, organic solar cells are often referred to as "excitonic" solar cells.) [9] In organic materials, the formation of freely propagating charge states following photon absorption is rare, and occurs only when the exciton is quenched by an impurity or by a metal contact. [9] Single layer organic solar cells therefore tend to show low power conversion efficiencies (PCE <<1%) due to poor current generation. [10] A breakthrough came in 1986, when Tang et al created the first donor-acceptor junction (D-A junction) at the interface between two organic materials of different electronegativity. [11] The difference in electron affinity creates a driving force for electron transfer in the excited state, splitting the excitons formed during

4

light absorption into separate electrical charges. In the Tang solar cell, the donor-acceptor junction was formed between the electron donor CuPC, and a perylene derivative acting as an electron acceptor. The working principle of a D-A junction is shown in figure 4. [12]
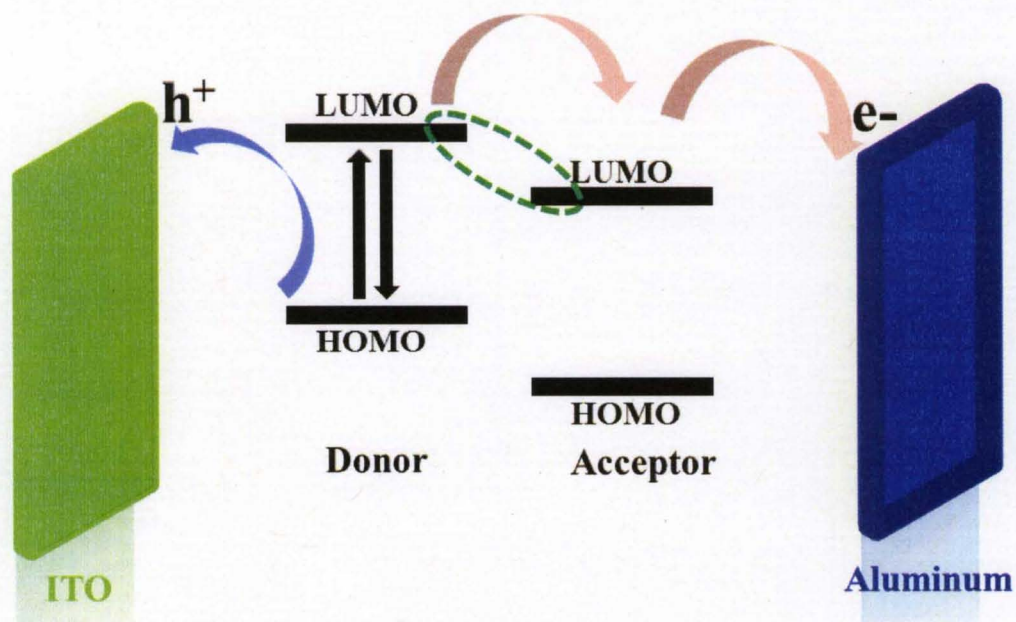


Figure 1.4: Schematic of charge separation in a D-A junction

The offset in the lowest unoccupied molecular orbital (LUMO) level positions of the donor and acceptor materials facilitates the charge separation between the two materials. The charge then percolates through the materials and is collected by the electrodes.

## 1.4 Overview of current excitonic solar cells

A short description of existing excitonic solar cells is now provided, together with their most recently reported efficiencies. Table 1 summarizes the properties for the different types of excitonic solar cells.

| Classification | Efficiency (%) | $V_{oc}$ (V) | $J_{sc}$ (mA/cm$^2$) | FF (%) | Test Center | Reference |
|---|---|---|---|---|---|---|
| Dye-Sensitized solar cells | 10.9 ± 0.3 | 0.736 | 21.7 | 68.0 | AIST (1/11) | Sharp (13) |
| Dye-Sensitized (sub-module) | 9.9 ± 0.4 | 0.719 | 19.4 | 71.4 | AIST (8/10) | Sony, eight parallel cells (14) |
| Organic polymer | 8.3 ± 0.3 | 0.816 | 14.46 | 70.2 | NREL (11/10) | Konarka (15) |
| Organic (sub-module) | 3.5 ± 0.3 | 8.620 | 0.847 | 48.3 | NREL (11/89) | Solarmer (16) |
| Quantum-Dot Polymer | 1.3 | 0.47 | 4.2 | 62 | MIT | Bulovic (17) |
| Inorganic-Organic | 4.1 | 1.1 | 10.9 | 0.35 | MIT | Bulovic (18) |
| Inorganic Nano-dot | 6 | 0.48 | 20.2 | 62 | University of Toronto | Sargent (19) |
| Polymer-Polymer | 2 | 1.19 | 4 | 0.42 | Kyoto University | Ito (20) |

Table 1: Cell and sub-module efficiencies measured under the global AM1.5 spectrum (1000W/m$^2$) at258$^0$C (IEC 60904-3: 2008, ASTM G-173-03 global).

$V_{oc}$: Open circuit voltage
$J_{sc}$: Short circuit current
FF:Fill factor
AIST: Japanese National Institute of Advanced Industrial Science and Technology.
NREL: National renewable energy laboratory
AM 1.5: Atmosphere air mass conditions

## 1.4.1 Dye sensitized solar cells

Dye sensitized solar cells (DSSC) were invented more than ten years ago by Michael Gratzel and co-workers, Since this time, they have achieved calibrated efficiencies of approximately 11%. [21] In DSSCs, an inorganic nanoporous membrane (usually $TiO_2$) is coated with a light absorbing dye. Upon illumination, an electron is injected from the dye into the inorganic membrane, and then collected by a conducting electrode acting as the cathode. The hole charge is carried to the anode by an electrolyte, usually based on a $I_2/I_3$ redox couple. Recent developments have tried to avoid the use of a liquid electrolyte by using a solid state hole transporter. Unfortunately cells using these new hole transporters have reduced efficiencies (only 4%). [22-23]

## 1.4.2 Inorganic-Organic hybrid solar cells

Inorganic-organic hybrid solar cells combine the good electron transport properties of inorganic materials, with the light absorbance and hole transport of organic semiconducting polymers. Typical examples are ZnO or $TiO_2$ particles combined with polyphenyl vinylenes (PPV) or polythiophene (PHT) polymers. [24-26]Ultimately, the use of a carefully nano-structured inorganic semiconductor

7

may allow control over the desired film morphology, however to date the highest efficiencies have been reached with random blending of the conjugated polymer and inorganic nanoparticles (1.5% efficiency). If finer mixing of the inorganic and organic components in film or solution can be achieved, then improvements in efficiency are expected.

### 1.4.3 Nanocrystal (Quantum Dot) –Polymer solar cells

Nanocrystal-Polymer solar cells are a variation on the inorganic-organic solar cell in which nanometer size quantum dots act as the electron transporter (usually CdSe or CdTe). Nanorods (rather than nanocrystals) have also been explored due to their improved charge transport properties [27]. The best efficiencies achieved to date are using tetrapod nanocrystals. The main problem for nanocrystal-polymer solar cells is the aggregation and separation of the nanocrystal and polymer in solution and in the film, which requires surfactants to help bring the two components together. It is thought that the presence of these surfactants is detrimental to the device, and efficiencies can be improved with thermally removable surfactants. Efficiencies of up to 1.3% have been reported. [17]

### 1.4.4 All inorganic nano-dot solar cells

All inorganic nano-dot solar cells are a blend mixture of two inorganic nanocrystal types (e.g., CdS and CdTe). Using an all inorganic phase potentially creates higher charge transport properties. Also, because there are no organic

materials present, there is less degradation and a greater working lifetime. Although these types of solar cells have only recently emerged, they already show efficiencies of 2.9%. [28] This is the only known type of solar cell which can in principle break the Shockley-Queisser efficiency limit for photovoltaics, a limit imposed because the energy of a photon greater than the band gap is lost as heat. [29] Due to carrier multiplication (a reverse Auger recombination effect) absorbed light of more than two times the band gap energy can be used to create two excitons instead of one. While carrier multiplication has not yet been seen in a working photovoltaic device, in principle, the effect raises the maximum theoretical device efficiency to 70%.

### 1.4.5 Polymer-Polymer solar cells

Polymer-Polymer solar cells are made from a mixture of two conjugated polymer materials, one more electronegative than the other, with complementary absorption spectra so both components can harvest light throughout the solar spectrum. Advantages favoring their commercialization include efficient light harvesting, ease of customizability and solution processability of polymers. However, to date polymer-polymer solar cells have shown disappointing efficiencies. Despite showing the highest open circuit voltages of all solar cells (>1V), low fill factors caused by poor current collection badly limit polymer-polymer solar cell efficiencies. [30] The highest reported polymer-polymer device efficiency to date is 1.9% (using POPT and MEH-CN-PPV) [31]. Blend films of two polymer materials, F8BT and PFB, show much promise as polymer: polymer

devices, however photoluminescence quenching of the donor PFB, often used as a measure of charge formation, is only 70% in a 1:1 PFB:F8BT film. This represents up to a 30% loss in device efficiency from the initial charge generation step alone, even before any recombination losses. The mechanism leading to and the efficiency of charge generation therefore are crucial parameters to device efficiency and need to be studied carefully.

### 1.4.6 Polymer-Fullerene solar cells
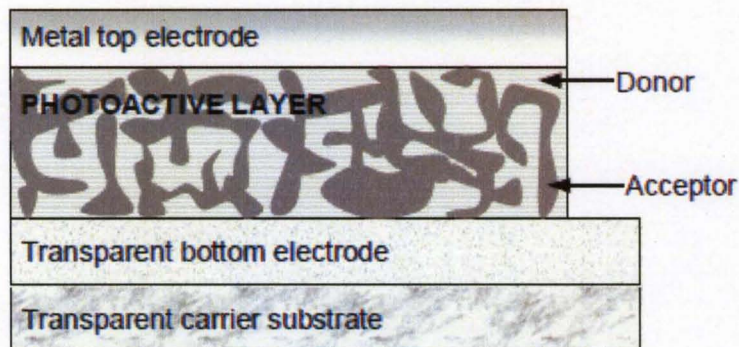


1.5 Device schematic of polymer-fullerene solar cell

Polymer-fullerene solar cells belong to the class of excitonic solar cells in which an electron donating polymer is mixed with an electron acceptor. [32] The concept of light induced electron transfer from a polymer to an acceptor at ultrafast scales has increased the attention given to polymer-fullerene solar cells to a large scale. Two commonly used techniques for forming polymer-fullerene based solar cells are (a) bi-layer and (b) bulk heterojunction architectures which are commonly known as BHJs. A bi-layer device configuration consists of a thin

10

film of polymer on which a thin film of fullerene is deposited either by spin coating or evaporation. Although bi-layer device configuration have shown promising results, by far the highest power conversion efficiencies have been observed for polymer-fullerene based bulk heterojunction device architectures. As seen in figure 1.5 bulk heterojunction devices is similar to a bi-layer but it exhibits a larger interfacial area which facilitates the charge separation easier than in other configurations. Bulk heterojunction devices can be formed by co-deposition of donor and acceptor pigments or spin coated from solutions polymers/fullerenes. These device configurations will be discussed in more detail in chapter 2.

This thesis will primarily focus on fabrication and characterization of various bulk heterojunction device configurations blends based on polymers, methanofullerene derivatives and conducting metal oxide nanoparticles.

## 1.5 Open Questions Facing Polymer-Fullerene Solar cells

Despite the relatively high efficiencies of polymer-fullerene solar cells, there is only limited information about how these devices work and what parameters limit their performance. It has been reported that for a thin MDMOPPV:PCBM film, 90% of the absorbed photons are collected as electrons, suggesting that both charge formation and charge recombination processes are near their optimal levels. Such high internal efficiencies are only possible however if the photoactive blend layer is thin enough that more than 40% of the incident light is lost through transmission through the sample. Thicker blend films absorb more of the incident light, but tend to show much lower efficiencies due to recombination losses in the low mobility materials. Studies of charge

recombination loss mechanisms are therefore necessary if greater efficiencies are to be achieved in thicker blend layers. Recent optical studies on MDMOPPV: PCBM films have detected the presence of charge trap sites in the photoactive blend. These sites prolong the lifetime of the hole charges in the device by preventing their recombination. The prolonged lifetime of charges in trap sites offers one potential avenue for decreasing recombination losses in polymer-fullerene devices; however the origin and nature of the trap states are not yet understood.

There is considerable debate over the exact process for the exciton dissociation in the polymer-fullerene solar cells, and work still remains to understand the charge separation mechanism in these materials. Charge recombination is one factor that competes with charge generation and charge separation. Recently, however, the charge recombination rate has been shown to be relatively low, therefore it must not be the only factor limiting the power conversion efficiency. The photo-generated charge decay dynamics are also very complicated in polymer-fullerene solar cells. The decay process has different characteristics for the excitons generated in the polymers, in the electron acceptors and at the donor-acceptor interfaces. It is important to understand the decay dynamics and to identity processes which impede the charge dissociation process and enhance or favor the charge recombination process.

## 1.6. Outline of the thesis

This thesis describes an experimental study focused on two main areas: the charge generation and dissociation mechanism in polymer-fullerene solar

cells and the optical characterization of methanofullerene derivatives to understand the charge generation mechanisms in the electron acceptors. Various techniques were used to study photo-generated charge mechanism in these materials including: UV-Vis-IR absorbance, open circuit photo-voltage measurement, capacitive photocurrent spectroscopy (CPS), and incident photon to current conversion (IPCE).

Chapter 1 gives an introduction on the energy issues around the globe, principles of photovoltaics and a comparison between inorganic and organic solar cells. Some of the currently reported high efficiency organic solar cells will be discussed next.

Organic solar cells that showed promising results were either on a bi-layer or bulk heterojunction device configuration. Chapter 2 discusses the background these two device configurations. New results of high power conversion efficiency have also raised new questions about the precise process of charge generation, separation and free carrier transport in bi-layer and BHJs devices. The proposed charge separation and transport mechanism and previously unseen results that have raised a debate over the exact process will also be discussed.

A major study was undertaken to understand and operate the femtosecond pulsed laser source which was one of the main excitation sources used for experimental study in this thesis. Theoretical notes explaining the lasing mechanism, the complexity in its cavity and operating procedure of the Optical

parametric amplifier (which acts as a wavelength tunable source) will be discussed in chapter 3.

Initial experiments were performed to compare the obtained results with the data published in the literature to ensure the quality of the fabricated devices. Chapter 4 will present results of absorbance and open circuit photovoltage of polymers, methanofullerene derivatives and organic solar cells based on bulk heterojunction device configurations.

A unique technique similar to surface photovoltage measurement (developed in our lab) was used to characterize the bulk heterojunction solar cell materials due to its sensitivity to photo-excited charge. Capacitive photocurrent spectroscopy (CPS) technique; the experimental setup and operational principle will be discussed in Chapter 5. Preliminary results of CPS of bulk heterojunction devices showed interesting results of certain materials having a high dissociation rate at low absorbance cross-section which will be discussed later. Finally results from CPS led to design of a new experiment; photovoltage bleaching experiment. Results of photovoltage bleaching experiments identified a direct path of recombination process in bulk heterojunction devices; results of photovoltage bleaching experiment and the discussion on the reason for enhancement in the recombination process will be presented in the conclusion of Chapter 5.

Some of the highest power conversion efficiencies in organic bulk heterojunction solar cells have been shown for devices consisting of methanofullerene derivatives as the primary constituent, however little work has

been done to understand the charge generation and dissociation process in these derivatives. Published results also raise questions about the ambiguity of the data. A thorough experimental study was undertaken to understand the charge separation mechanism in these materials. Experimental results and their theoretical assignments of methanofullerene derivatives will be discussed in chapter 6.

Chapter 7 provides general conclusions of the optical study of bulk heterojunction solar cells including capacitive photocurrent measurement, photovoltage bleaching results and methanofullerene derivatives optical spectroscopy. Chapter 8 sheds light at some of the future work that could be undertaken to advance these results in a new direction.

## CHAPTER II - BACKGROUND

In organic polymers, photo-excitation results in the formation of coupled electron-hole pairs (referred to as excitons) which are bound together by the Coulomb force of attraction. [19] In order for the photo-excited charge to be available for conduction, the exciton needs to be broken apart (or dissociated). This means that energy in excess of the Coulomb potential needs to be provided to generate a photo-current. The energy needed to break apart the electron-hole pair can be generated by the relaxation of high energy charge carriers, but in most cases this energy is lost in the form of heat. Combining the polymer with an acceptor material like PCBM, dramatically improves the exciton dissociation efficiency. The reason for this improvement is that the high energy photo-generated charge no longer simply relaxes to the ground state. It can also be donated to a neighboring electron acceptor which, due to the built-in band off-set, provides enough energy to physically break apart the bound electron-hole pair and make the photo-generated carriers available for conduction. [33-34]

### 2.1 Bi-layer and Bulk heterojunction device configurations

Various donor / acceptor configurations have been tried to enhance the power conversion efficiencies of organic solar cells. Two that have showed promise are donor-acceptor bi layer structures and bulk heterojunction (BHJ) devices (see Fig. 2.1 and Fig 2.2). [35-37]In both the bi-layer configuration and

bulk heterojunction device architecture, the dissociation of excitons and generation of charge carriers occurs primarily at the donor / acceptor interface. Thus, the formation of an optimal interfacial layer between the electron donors and acceptors becomes extremely crucial in these systems.
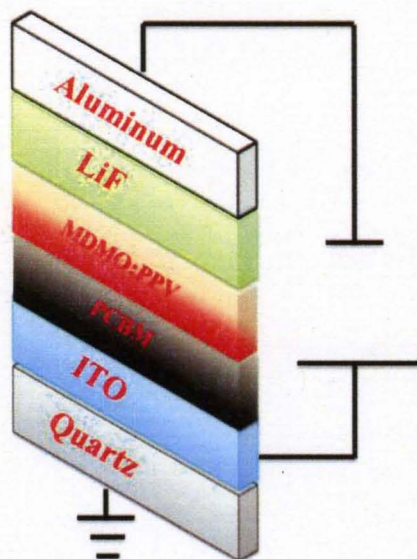


Figure 2.1: Device schematic for a bi-layer heterojunction device

The exciton diffusion length, or the distance that photo-generated excitons travel before recombining, is an important factor in organic solar cell design. If the photo-generated exciton has to travel a distance larger than the exciton diffusion length to reach a dissociation site, it will recombine before dissociation occurs, and the generation of free electrons and holes will not occur. The bi-layer device configuration contains only a single donor-acceptor interface so that all the photo-generated excitons have to travel to this single interface for efficient charge generation. For maximum power conversion in a bi-layer device

configuration the thickness of the donor and acceptor layers must therefore be below the exciton diffusion lengths. For polymers, this is between 5-14 nm. [38] Being limited to such a thin active region greatly reduces the amount of light that can be absorbed by the solar cell.
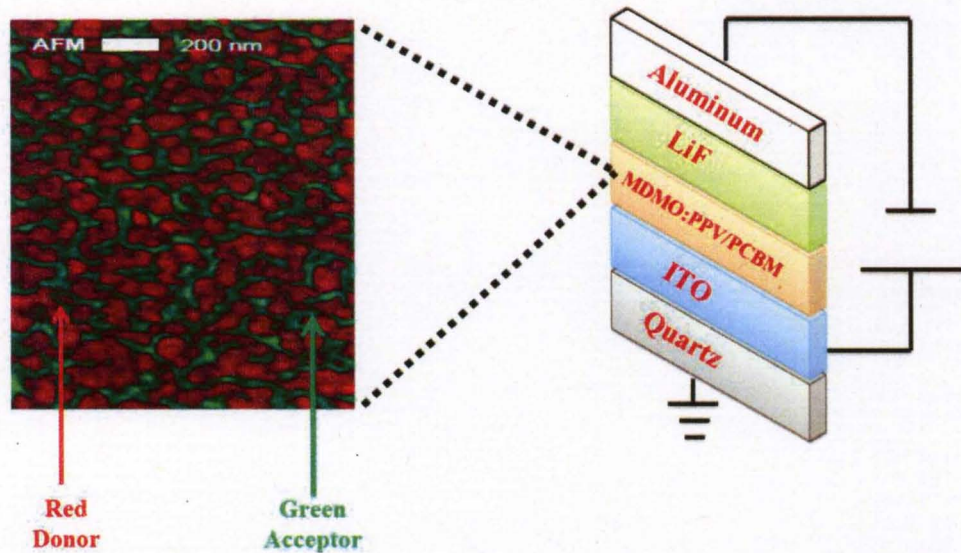


Figure 2.2: Device schematic for a bulk heterojunction device

This exciton diffusion length limitation is overcome by using the bulk heterojunction device architecture. The bulk heterojunction architecture contains many interfaces between electron donor and acceptor materials. The electron donating polymer is combined with an electron acceptor material dispersed in an organic solvent. Mixing the two materials together creates multiple donor / acceptor interfaces. The mixture of the electron donor and acceptor is prepared to maximize the amount of electron accepting material that adheres to the electron donating polymers chains, each of which creates an interfacial layer between them.

In comparison to a bi-layer structure, the excitons in a BHJ do not have to travel large distances to reach the electron donor-acceptor interfaces. Photo-generation due to dissociation of the electron-hole exciton happens throughout the bulk rather than just at one interface. This leads to improved power conversion efficiencies. The BHJ mixture must have good morphology, in that phase separated regions should exist between the donor and the polymer. Lack of good morphology in the mixture produces an uneven active layer film. This impedes the charge generation process by blocking the excitons from traveling to the donor-acceptor interface. A second consideration in BHJs is that the charge transport takes place through a mixture of both donor and acceptor materials. This complicates the charge separation and collection process.

## 2.2 Charge separation mechanisms in bulk-heterojunction solar cells

In bulk heterojunction solar cells, the electron donating polymer absorbs the majority of the light. Organic semiconducting polymers are known for their relative high absorption coefficients which can be as high as $10^7 m^{-1}$.[38] Because of this, only a few hundred nanometer thick acceptor-donor films can provide satisfactory absorbance characteristics. This means that the excitons do not have to diffuse as long of distance as would be necessary if the absorption was comparable to an inorganic material, like Silicon or Gallium Arsenide. (In inorganic solar cells, layer thicknesses of many microns are typically used.)

Excitons in organic semiconductors are referred to as Frenkel excitons,[38] indicating that they have relatively high binding energy compared to

the thermal energy at 300K. (Low binding energy excitons are referred to as Wannier-Mott excitons.) Another important distinction is between singlet and triplet excitons. A singlet exciton is a combination of electron and hole that has a total spin of zero (The name "singlet" refers to the fact that there is only a single electron-hole combination that results in zero spin).[38] The triplet exciton is a combination of electron and hole that has a total spin one. (As the name implies, there are three possible combinations that lead to triplet excitons.) The difference in spin means that there is a fundamental difference in the generation and recombination of singlet and triplet excitons.[38]

Because photons have zero spin, the optical generation of singlet excitons can proceed without requiring additional spin, while the optical generation of triplet excitons requires additional spin coupling. Because of this, only singlet excitons can be generated due to absorbance of light (as determined by certain optical selection rules), but both triplet and singlet excitons can be generated due to interaction following charge transfer. This is also why the primary photo-generated excitons in organic semiconductors are the singlet, rather than the triplet excitons. Most organic semiconductors are also known to exhibit photoluminescence. Because of the possibility for radiative recombination the excitons have a relatively short life span following photo-excitation. The singlet exciton lifetime is approximately 1ns—if they are not dissociated in this time, they recombine to emit a photon. Because the triplet exciton cannot recombine by emitting a photon, triplet exciton lifetimes are much longer, up to hundreds of microseconds.

## 2.2.1 General model of charge separation in BHJs

Figure 2.3 outlines the basic steps necessary for photocurrent generation in a bulk heterojunction solar cell. [39] These are:

**1.** Light absorption and exciton generation

**2.** Diffusion of excitons

**3.** Dissociation of excitons at the donor / acceptor interface resulting in charge generation

**4.** Charge transport and collection
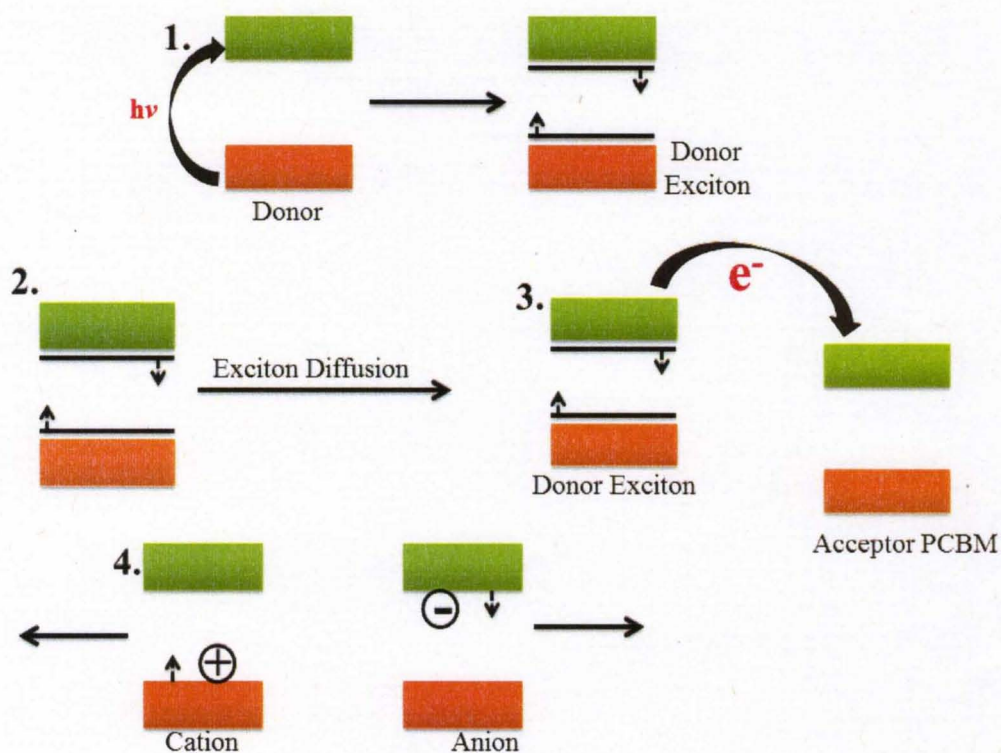


Figure 2.3 Photocurrent generation steps in an organic solar cell.

Figure 2.4 lists the steps involved in the charge separation process in more detail, using chemical reaction notation. [40-41] Here, D refers to the donor material and A refers to the acceptor material. In Step 1, light absorption occurs, generating an exciton in the donor, and raising the donor molecule to an excited state (D → D*). In Step 2, the donor diffuses to the donor / acceptor interface, and encounters and acceptor molecule, forming an "encounter pair" [D*, A]. Encounter pair refers to the fact that the exciton must "encounter" the acceptor molecule for any subsequent reaction to occur. In Step 3, the single exciton is broken apart so that the electron now resides on the acceptor material and the hole resides in the donor material (indicated as $[D^{+0}, A^{-0}]$). The charges are not

Step 1    $D + A \longrightarrow D^* + A$

Step 2    $D^* + A \longrightarrow [D^*, A]$

Step 3    $[D^*, A] \longrightarrow [D^{+0}, A^{-0}]$

Step 4    $[D^{+0}, A^{-0}] \longrightarrow D^{+0} + A^{-0}$
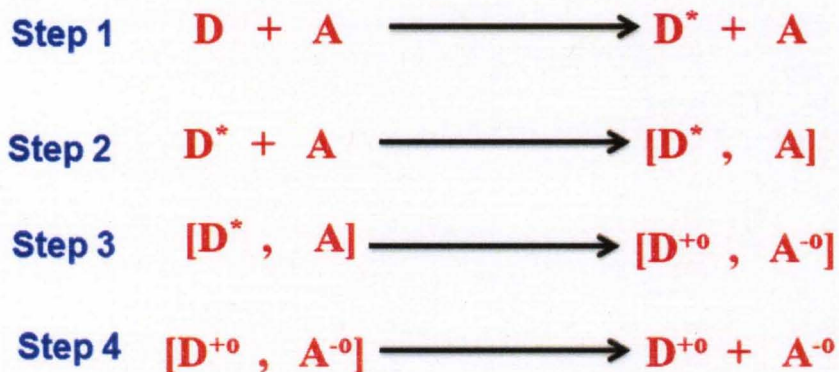
Figure 2.4 Model 2 from light absorption to free charge carrier generation

free, however, but are still bound together by the Coulomb force. This bound pair of electron and hole resting on either side of the donor acceptor interface is referred to as a polaron pair. The term polaron in general refers to an electron or a hole (i.e. charge) along with the distortion of the electron or hole's surrounding environment. [42 ]Polarons are particularly important in organic materials. In an

inorganic material, forces binding the crystal lattice are very strong so that an extra electron or hole at a site does not change its crystal surroundings. Organic semiconductors do not have strongly bound crystal lattice structures, so that when a charge is placed on a molecular site it can deform the entire lattice structure surrounding the molecular site. [38]

The final step (Step 4) is the dissociation of the polaron pair into the free hole and electron states ($D^{+0}$ and $A^{-0}$) which travel in the donor and acceptor materials respectively. The total energy required for the formation of the polaron pair and dissociation into free electrons and holes is less than that required for the direct dissociation of the exciton. Despite this, the mechanism whereby the energy necessary for dissociation is provided to the system is still unclear.

### 2.2.2 Forster resonance energy transfer in BHJs

A somewhat different charge dissociation mechanism that has been proposed involves Forster resonance energy transfer, or FRET. In FRET, an excited state can be directly transferred between two materials in close proximity with each other, provided that the energy of the excited state is similar in the two materials. The FRET based charge dissociation process is outlined in Fig. 2.5. Following photoexcitation (Step 1) the exciton state is directly transferred from the donor to the acceptor material (Step 2). Once in the acceptor material, exciton dissociation proceeds by the transfer of a free electron from the donor to

the acceptor, which generates the energy needed for exciton dissociation.
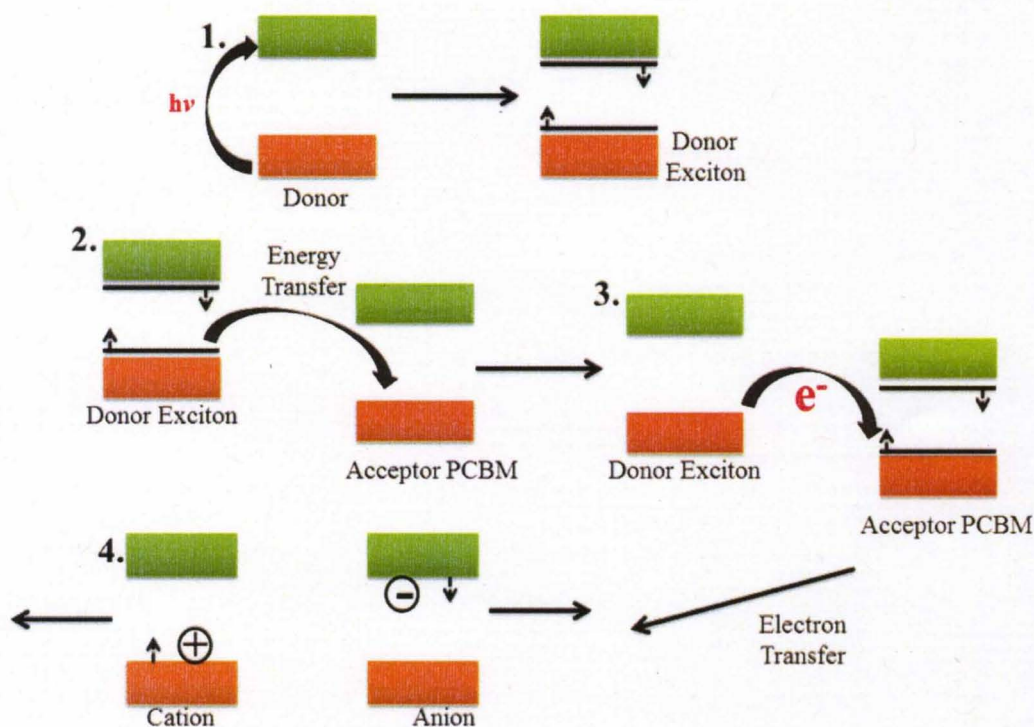


Figure 2.5 FRET mechanisms in charge separation

The FRET energy transfer process is thought to dominate in situations where the emission spectra of the polymer overlaps with the weak absorption of PCBM molecules. Evidence for FRET has been observed in Nile Red dye (500-700 nm emission) combined with PCBM [43-44]. The experiments measured the fluorescence quenching of the Nile red dye when PCBM molecules were added. The study concluded that resonance energy transfer between polymer and fullerenes can increase the diffusion length of the exciton beyond their ideal limit of 5-10 nm.

## 2.2.3 Existence of Charge transfer complex (CTC) in BHJs

One possible path by which the polaron pair can dissociate is through an additional interfacial state (as shown in Fig. 2.6) known as the charge transfer complex (or CTC). [45] The CTC is formed by the interaction of the donor and the acceptor. Its energy with respect to the ground state of free electron hole pairs is equal to the energy difference between the highest unoccupied molecular orbital of the donor and the lowest unoccupied orbital of the acceptor. The CTC provides an intermediate state between the polaron pair and the dissociated free carriers. Electron hole pairs occupying the CTC can directly relax into free carrier states without any additional energy. Evidence for the existence of the CTC in polymer-fullerene molecules has been provided by photo-thermal deflection spectroscopy (to measure absorbance) and photoluminescence measurements [46].
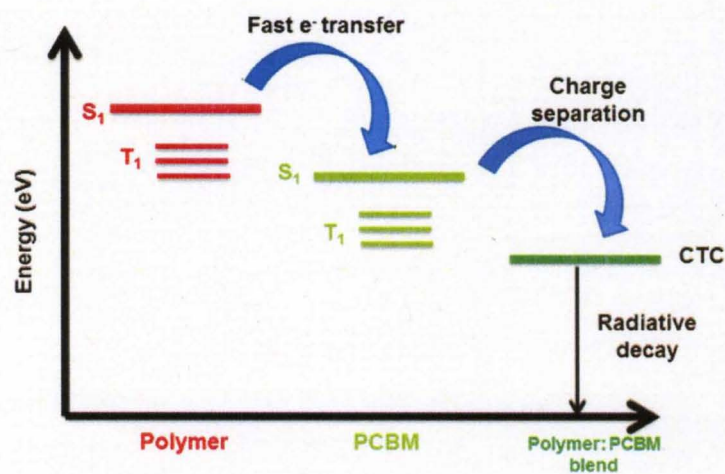


Figure 2.6: Polymer-fullerene blends with CTC below S1 state of PCBM

The energy of the CTC varies depending on the polymer chosen for the BHJ cell. It has been shown that the relative photogeneration efficiency of a particular polymer / PCBM mixture is determined by this CTC energy. As seen in figure 2.6, if the energy of the CTC falls below the singlet S1 and triplet T1 exciton levels in the PCBM, the CTC can relax directly into the free carrier states, and photocurrent generation will be high. If, however, as seen in figure 2.7, the energy of the CTC is above other available excited states, the CTC will relax through the long lived triplet excitons, resulting in minimal photo current activity.
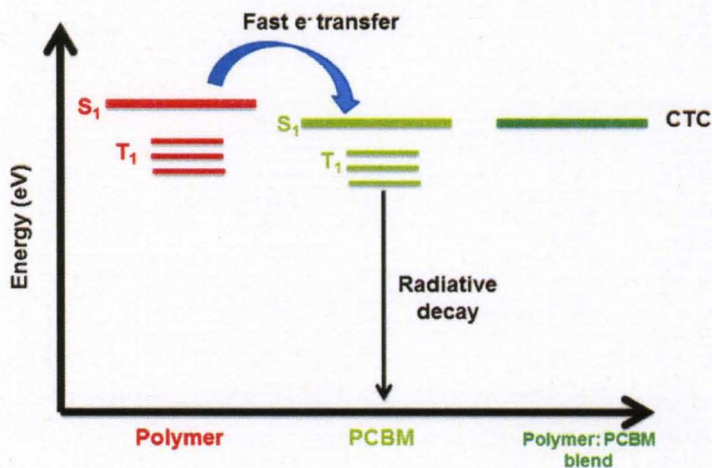


Figure2.7: Polymer-fullerene blends with CTC above S1 state of PCBM

## 2.3 Recombination processes

Recombination is a major obstacle for increased efficiencies of bulk heterojunction solar cells . Recombination processes are broadly characterized in two categories. The charge can either combine geminately or non-geminately. Geminate recombination is when the charge recombines between a single photo-generated charge pair. The charge from the same molecules could recombine

(termed monomolecular decay), thus the recombination rate is independent of excitation density. In a non-geminate charge recombination process the charge from different photogenerated charge pairs recombines. Individual charges from several charge pairs could recombine with charges of opposite signs of other charge pairs, which makes this recombination process dependent on excitation density. It has been noted that non-geminate charge recombination processes usually occur at high excitation densities. Non-geminate recombination process shows different behavior in presence and absence of trap states in the active film. When trap states are absent in the active film, the non-geminate recombination process shows a bimolecular reaction and occurs at a single reaction site. When high densities of trap states are present the non-geminate recombination process shows dispersive recombination kinetics. [47] If recombination process is dependent on and limited by de-trapping rate of charge carriers, it shows a decay rate which is independent of light intensity which makes is hard to distinguish between non-geminate recombination processes and geminate recombination process. [48-50]

## 2.4. Optical properties of methanofullerene derivatives

Since the first demonstration of photo induced electron transfer from an electron donating polymer to an electron acceptor, methanofullerenes have been the almost unanimous choice for the active electron acceptor material due to their high electron affinity. Only recently have there been efforts to use alternative acceptor materials, such as single and multi-walled carbon nanotubes, and none has demonstrated superior properties. One of the most common electron

27

acceptors from the methanofullerene family is 1-[3-(Methoxycarbonyl) propyl]-1-phenyl-[6.6] C61a functionalized derivative of C60. C60 has very low solubility in organic solvents such as toluene, dichlorobenzene and ortho-dichlorobenzene. [51-52] When functionalized with a methyl ester butyric side chain,the solubility is enhanced by an order of magnitude or more. Functionalized C60; PC60BM has its highest solubility in ortho-dichlorobenzene (as compared to toluene or dichlorobenzene).  Ortho-dichlorobenzene is also the most common organic solvent for polymer semiconductors used in the fabrication of bulk heterojunction solar cells.
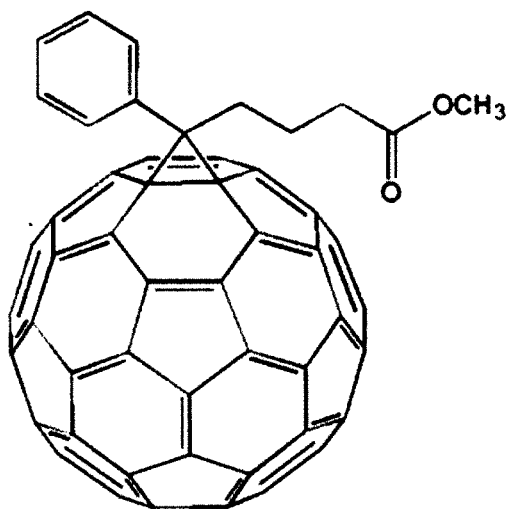
Figure 2.8: Chemical structure of PCBM

Over the past three decades, work to improve the efficiencies of organic solar cells has primarily focused on the electron donating polymers. For example, efforts have been made to tailor the polymer band-gap to extend their light absorbing range into the infra-red regime.  Attempts have been made to dope

polymers with heavy metal particles to enhance spin orbit coupling, and make the triplet state accessible. Much less work has focused on the electron acceptor PCBM. There have been recent reports suggesting that the hole transfer process form the methanofullerene electron acceptor back to the electron donor occurs at the rate of femtosecond timescales. [53] More studies are required to understand the process in its entirety to enhance the efficiency of organic solar cells.

It has been widely reported that the first allowed transition below the band gap in C60 occurs at 1.7 eV (~ 720 nm), which is attributed to the ground state singlet exciton transition (S1). [54] Theoretical calculations of the density of states reported by several groups suggest that there are no allowed optical transitions below this energy, Recently, several groups working on the interaction effects of nano structures with different substrates have demonstrated theoretical calculations suggesting that the density of states for methanofullerene can be perturbed when placed in close proximity of highly conducting substrates [55]. Although, the work was focused on fundamental understanding of methanofullerene, it opens a new area which needs to be explored to find avenues which could be correlated with organic solar cells as methanofullerene constitute a major part of the organic bulk heterojunction solar cells.

# CHAPTER III – OPTICAL EXCITATION SOURCES

A big part of this thesis was dedicated in understanding the operation and maintenance of a femtosecond pulsed laser system. Following section will discuss "Hurricane" laser; introduction, operation and OPA (Optical parametric amplifier). [56]

## 3.1 Introduction

The femtosecond pulse train consists of oscillator, stretcher, an amplifier and a compressor combined as a system package called "Hurricane" as shown in Figure 3.1, while the OPA (Optical parametric amplifier) feeds on the output of the Hurricane to provide the wavelength tuning capabilities. "Hurricane" is a solid-state femtosecond pulsed laser with a constant output wavelength of 800nm. Hurricane laser output is used to excite OPA consisting of a Beta Barium Borate (BBO) crystal which tunes the wavelength over broad range (300 - 2400 nm).

Generation of a typical high power femtosecond chain includes an oscillator that produces 100fs pulses at a repetition rate of typically 100 MHz. After passing through the stretcher the pulse duration increases up to 400ps and can be amplified. The gain medium is a Ti: sapphire (titanium-doped sapphire) crystal pumped by the second harmonic of a Q-switched Nd:YAG running at 1KHz. Once trapped in the cavity the pulse is amplified at each pass in the crystal with a typical gain per pass of two. After 15-20 round trips the pulse

saturates the gain and reaches its maximum energy. It is extracted from the amplifier and sent into multi pass power amplifier and finally into the Compressor. There it recovers its initial duration and pulses as short as 30fs with energies in the joule range can be obtained.
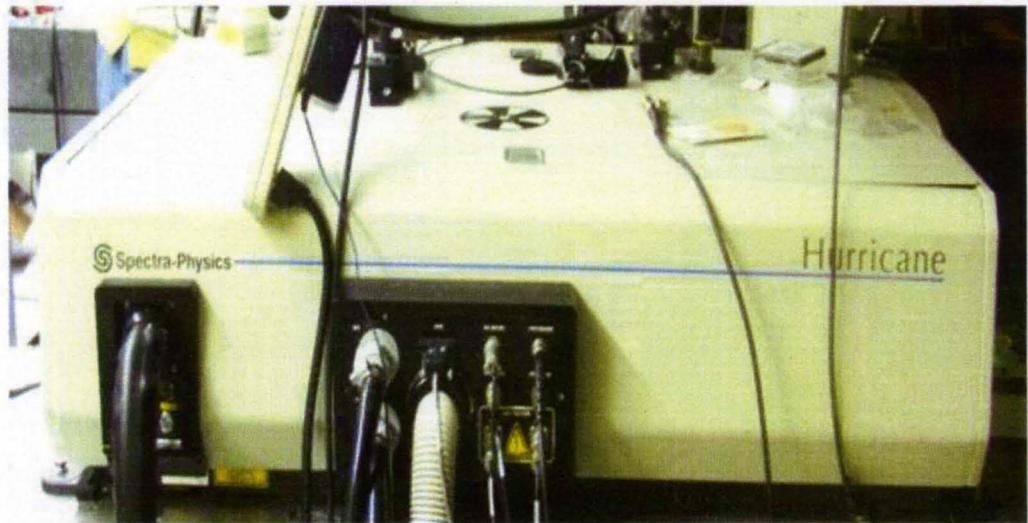


Figure 3.1: Excitation source, "Hurricane" laser system

Hurricane is comprised of three main components: Mai Tai, Evolution and Regenerative amplifier. Mai Tai generates low energy femtosecond pulses at 800 nm. Evolution is a solid-state laser used to pump Mai Tai. The low energy femtosecond pulses are amplified by Regenerative amplifier. Mai Tai, in itself, is comprised of two chambers, A continuous wave (CW) pump chamber and a pulsed output chamber containing two lasers, a CW diode-pumped laser and a mode-locked Ti: sapphire pulsed laser respectively. The CW diode pump laser is an all solid-state, high power (5W), visible CW (532 nm) single phase laser. The output of the laser diode (825nm) pumps the Nd3+ ions doped in a yttrium vanadate crystalline matrix (Nd: YV04) which start lasing at 1064 nm due to the

population inversion in the crystal matrix. The resulting 1064 nm output is converted to visible (532 nm) through a frequency doubling or second harmonic generation using a 90°, non-critically phase matched, temperature-tuned lithium triborate (LBO) nonlinear crystal as doubling medium. The pulsed chamber uses this CW laser (532 nm) output as the pump beam for the Ti: sapphire amplifier fitted with an acousto-optic modulator for mode locking purposes. In a mode locked laser the longitudinal modes are locked in phase such that they constructively interfere to create a single circulating pulse. An output pulse is generated every 12.5 ns which corresponds to the arrival of the intra-cavity pulse at the partially reflective output coupler. Collectively, Mai Tai delivers a low power (~0.75 W to .90 W) femtosecond (~120fs) mode locked continuously tunable pulsed output over a range of near infrared wavelengths from 750 nm to 850 nm at a repetition rate of 80 MHz. The rest of the three subsystems namely stretcher/compressor, evolution and regenerative amplifier collectively constitute the chirped pulse amplification system which increases the power of the pulsed laser beam keeping the width of the pulse and mode-locking intact.

Using a single grating stretcher, a low energy, very short duration pulse is stretched to as much as 10,000 times. This stretched pulse is then amplified using a Ti: Sapphire regenerative amplifier which can increase the pulse energy as much as 106 times. A single grating compressor recompresses the pulse back to its original duration. The OPA consists of a single optical head that feeds on the output of the Hurricane amplifier. The infrared wavelength extension is achieved in a two-step process with white light generation and traveling-length

optical parametric amplification. The output wavelength is tuned by changing the angle of the p-Barium Borate (BBO) crystal. Wavelength tuning in the visible and near IR regions is achieved using the integrated harmonic generation (HOI and HOII). Although the OPA was used to perform all the measurements described in this dissertation, the capacitive photocurrent technique also works with a CW (continuous wave) laser in combination with a chopper and has also shown promise with white light system being the optical source.
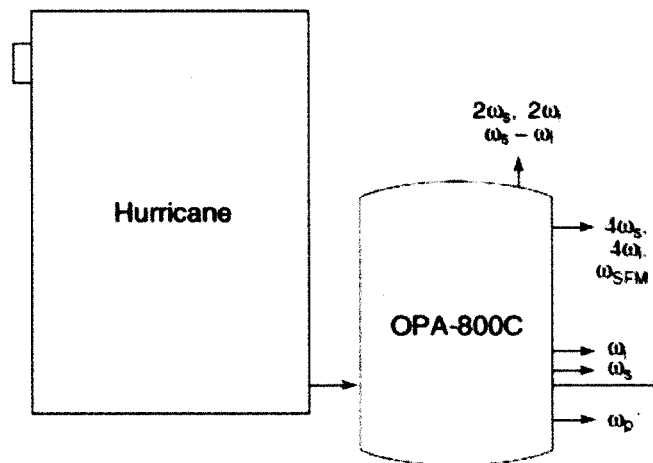


Figure 3.2: "Hurricane" laser pumping an Optical parametric amplifier (OPA-800C) schematic

## 3.2 Optical parametric amplifier (OPA):

The following section will describe the theory and working principles of Optical parametric amplifier which gives a tunable output wavelenght from 350-2400 nm.

### 3.2.1 Theory

OPAs operate on a very different principle from that of a laser. A laser derives its gain from inverted population distribution between different atomic or molecular states. These transitions have inherent line widths that govern the maximum tuning range of the laser (e.g., a dye laser tunes over a range of 30 – 40 nm per dye, while a Ti: Sapphire laser tunes over a 300 nm range). In contrast, an OPA derives gain from a nonlinear frequency conversion process. Figure 3.3 illustrates a three-wave interaction process, which could be either down conversion (a) or up conversion (b).
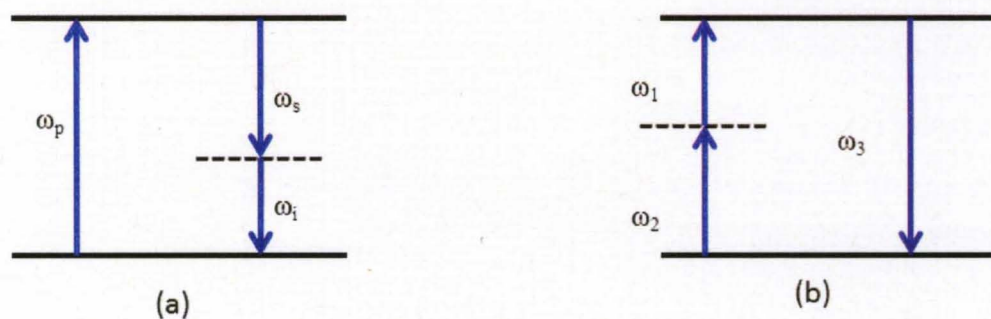


Figure 3.3 Optical frequency three-wave interaction process

This process originates from the interaction of the optical electromagnetic field with the bounded electrons in the nonlinear medium. It is governed by Maxwell's equation:

$$\nabla^2 E - \mu_0 \sigma E - \mu \varepsilon E = \mu_0 P$$

Where E is the electromagnetic field, $\mu_0$ is the vacuum magnetic permeability, $\varepsilon$ is the dielectric permeability, $\mu$ is the magnetic permeability, $\sigma$ is the ohmic conductivity, and P is the polarization. High efficient conversion from one wave to another requires: (a) high pump intensity wave or waves (b) high nonlinear polarization coefficient d and (c) a better phase match.

To have high conversion efficiency for the three wave process, a high second order nonlinear susceptibility of the nonlinear medium is desirable. In the OPA process shown in Figure 2-1, a high intensity pump is used to amplify a low energy seed beam as shown in Figure 2-2.
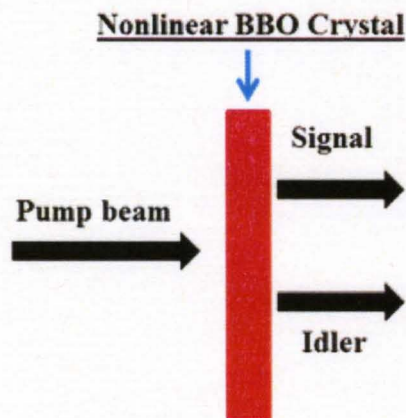


Figure 3.4 Optical Parametric Amplification in BBO crystal

## 3.3 OPA-800CF System
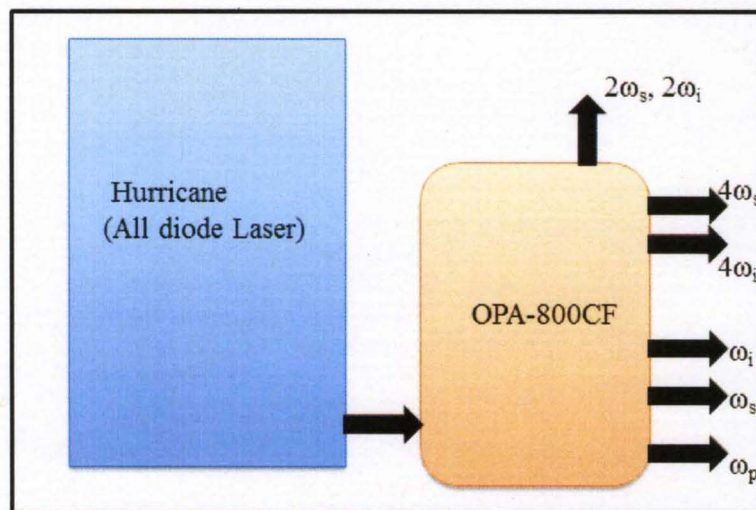


Figure 3.5 Schematic layout of a OPA-800CF pumped from the Hurricane

A type II, angle-tuned, Beta-Barium Borate (BBO) crystal is used as the nonlinear gain medium in the Spectra-Physics OPA-800CF. For the type II phase matching process, the signal beam is of opposite polarization to that of the pump and idler beams. This makes wavelength separation of the signal and idler beams straightforward using polarization-sensitive optics. Figure 2-4 shows the typical dependence of the signal and idler wavelengths upon phase matching conditions (usually the crystal angle) for a type I and a type II process. Unlike the type I phase-matching process that normally exhibits very large phase-matching bandwidths near degeneracy, the bandwidth of the signal and idler pulses are relatively independent of the phase-matching conditions. In fact, for a type II

process, it is possible to tune right through the degeneracy point without obtaining pulses with abnormally large bandwidth. The signal and idler waves actually undergo a polarization flip at the degeneracy point. (This is sometimes referred to as type IIb phase matching.)

The OPA-800CF can be pumped with any output wavelength from the Hurricane amplifier, which is tunable in the range from 750-840 nm. However the performance specifications are based upon pump energies up to 1 mJ pulse widths of <130, <80 and <50 femtoseconds at 800 nm for an OPA-800CF. Figure 2-5 shows the typical tuning curves for 1 mJ pump conditions. The signal and idler outputs provide pulses with up to 80 μJ of energy with broad wavelength coverage from 1.1 μm to 3.0 μm.



(a) Type I Phase Match

(b) Type II Phase Match
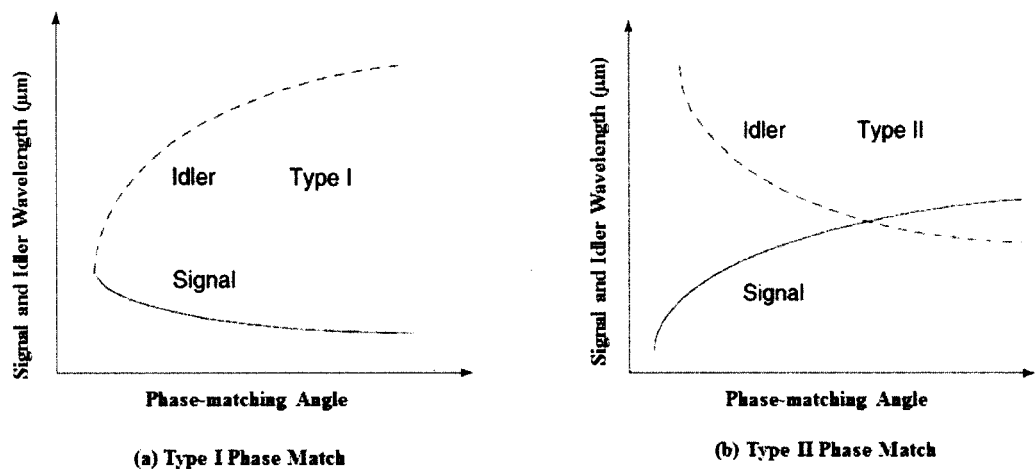
Figure 3.6: Wavelength vs. Phase-Matching Angle of Type I and Type II Crystals

### 3.3.1 Tuning Curve for OPA-800CF
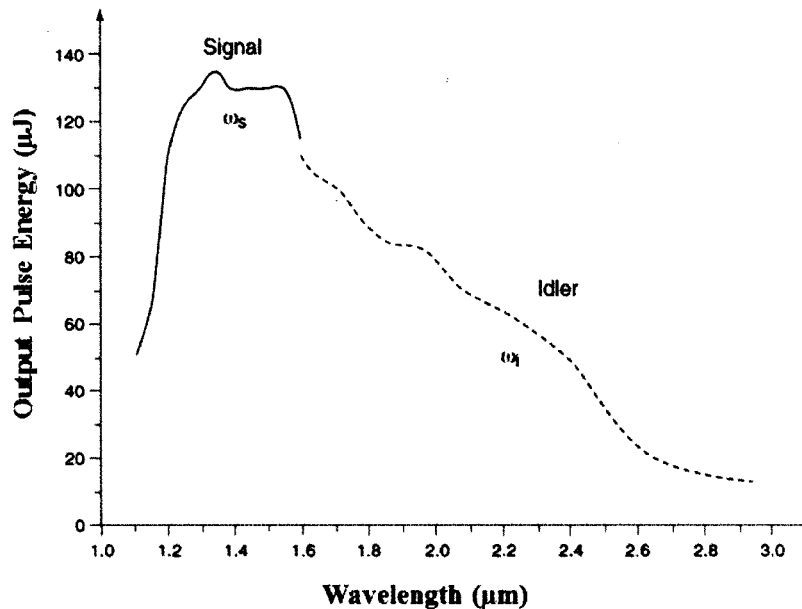


Figure 3.7 Typical output Tuning curves for an OPA-800C

The tuning range for the Type II BBO crystal from the Hurricane amplifier output is in the range of 750 nm to 840 nm. However, the due to the performance specifications which are based upon pump energies which is up to 1 mJ with a pulse width of < 130 femtoseconds are best obtained at 800 nm. The OPA-800CF can be pumped with any other wavelengths, but the pump energy required to pump an OPA (1 mJ) would be lower, thus it is advisable to pump the OPA-800CF at 800 nm.

Output energy graphs for the 2<sup>nd</sup> and 4th harmonic generation, DFM and SFM:



**Second Harmonic Option**

**Fourth Harmonic Option**
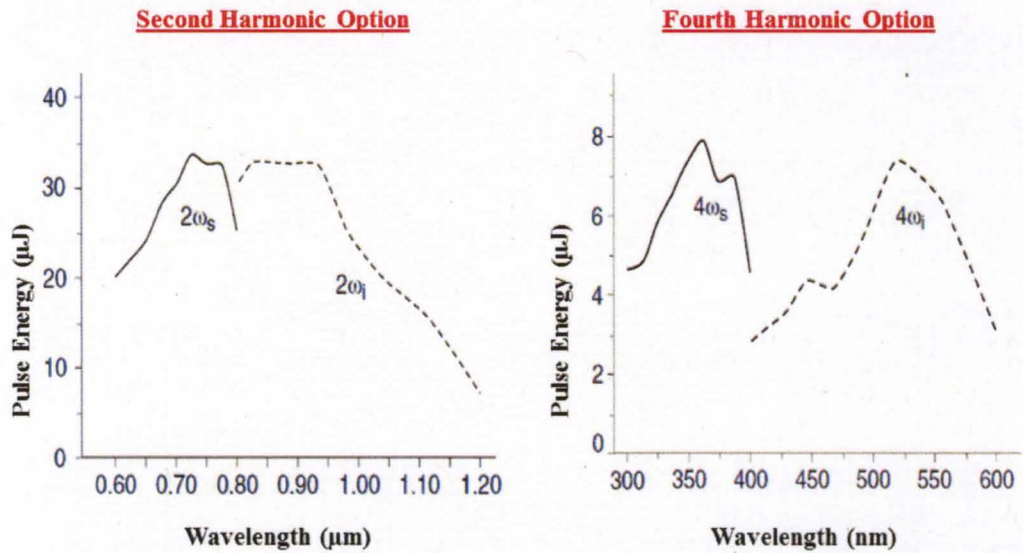
Figure 3.8 Typical output tuning curves for the 2<sup>nd</sup> and 4<sup>th</sup> Harmonic Generation



**Sum-Frequency Mixing Option**

**Difference-Frequency Mixing Option**
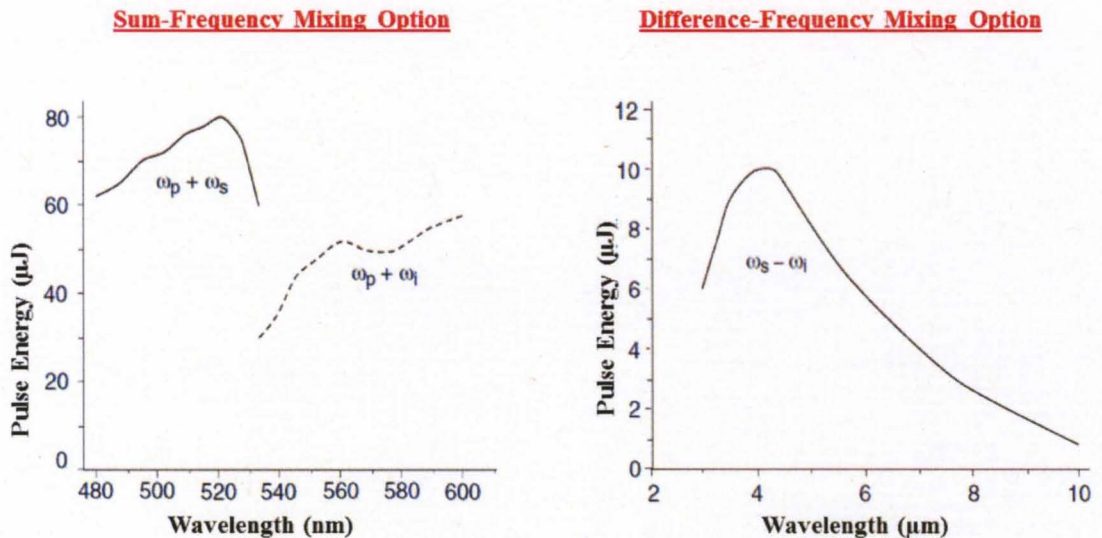
Figure 3.9 Typical output tuning curves for the Sum Frequency Mixing and Difference-Frequency Mixing

### 3.3.2 Configuration

The fs OPA-800CF layout is shown in Figure 2-8. The input amplified Ti: Sapphire beam is first reflected off two mirrors that flip the polarization from horizontal to vertical, and then is split into two legs. In the first leg, approximately 96% of the energy is transmitted and used for pumping the OPA. The remaining <4% is reflected by beam splitter BS1 to produce a white light continuum that provides the seed pulse for the OPA. A half waveplate and a thin film or cube polarizer control the beam energy, and a lens focuses the beam into a solid-state material where the continuum is generated. It is re-collimated and relayed to the OPA crystal through variable delay stage DELAY 1.

In the second leg, the major portion of the amplified beam is split into two pump beams, each of which is down-collimated to pump the OPA-800C crystal. About 15% of the beam is used to pump the first pass or pre-amplification stage, and the remainder is used to pump the second pass or power amplifier stage. In the pre-amplification stage, the pump beam is steered to the OPA- 800CF crystal using dichroic mirror D1, which is a high reflector from 750 to 840 nm and highly transparent for longer wavelengths. This dichroic mirror combines the pre-amplification pump beam with the white light that is generated in the WL arm. The white light is temporally overlapped and amplified by the pre-pump beam by optimizing DELAY 1. The signal and idler beams generated in the BBO crystal in the pre-amplification stage then pass through dichroic mirror D2. In an OPA-800CF, the amplified idler beam is reflected back through the OPA-800CF crystal by mirrors WLR3 and WLR4. This returned beam provides the seed pulse for the

power amplifier stage. The power amplifier stage pump beam is steered to the crystal by five mirrors and the 800 nm dichroic mirror, D2, where it is overlapped collinearly with the returning idler (signal) beam in the BBO crystal for final amplification. R3 and R4 are mounted on delay translation stage DELAY 2 to temporally overlap the power pump beam with the pre-amplified white light returning from WLR4. The amplified signal and idler output wavelengths are determined by the phase-matching angle of the BBO crystal. For femtosecond system, wavelength tuning is accomplished by changing the BBO phase-matching angle and adjusting each delay stage for optimum output energy. The residual 800 nm beam is separated from the amplified signal and idler beams by dichroic mirror D4, and the signal and idler are then either separated and made available through different exit ports or are sent to the harmonic generation leg for wavelength extension through second and fourth harmonic generation.

The following abbreviations will be used frequently in the OPA-800CF operation Manual:

| | | |
|---|---|---|
| **BS1, 2 Beam Splitter** | **L1–4 Lenses** | **R0–5 Reflectors for 800 nm** |
| **CL Collimating Lens** | **OR1–3 Reflectors** | **T1, 2 Telescopes** |
| **D1–4 Dichroic Mirror** | **I1–2 Irises** | **WLP White-light Plate** |
| **FL Focusing Lens** | **P Polarizer** | **WLR1–4 White-light Reflectors** |
| **PS1, 2 Periscope** | | **WP Waveplate** |
| **PS1, 2 Periscopes** | | |

The figure 2-8 shows the complete beam path for the OPA-800CF, including the white light path, pre-amp beam path and power amp beam path.

Figure 3.10: Complete beam path for OPA-800CF

42

### 3.3.3 OPA-800CF Specifications

| | Pump Pulse Requirement | Output Performance | |
|---|---|---|---|
| | | Signal | Idler |
| Pulse Energy | 1.0 mJ | 75 µJ | 35 µJ |
| | 0.5 mJ | 35 µJ | 20 µJ |
| | 0.3 mJ | 18 µJ | 10 µJ |
| | 0.7 mJ at 50 fs | 53 µJ | 25 µJ |
| Pulse Width | < 130 fs | < 130 fs | < 130 fs |
| Tuning Range | 800 nm ± 5 nm | 1.10-1.60 µm | 1.60-3.00 µm |
| Repetition Rate | 1-5 KHz | 1-5 KHz | |
| Energy Stability | < 3% | < 3% | |
| Polarization | Horizontal | Linear, Horizontal | |

Table 2-1: OPA-800CF Specifications for the Idler and Signal output, energy, pulse width and tuning range

The wavelength coverage range for the Idler is from 1.60 µm – 2.40 µm (1600 – 2400 nm) and the wavelength range for Signal is from 1.10 µm – 1.60 µm (1200 nm – 1600 nm). The second harmonic generation for the Idler has a wavelength range from 800 – 1200 nm, SHG for Signal is from 600 -800 nm, FHG for Idler has a range from 400 – 600 nm and the FHG for Signal has the wavelength range from 300-400 nm, the total wavelength coverage for the output of the OPA, including the Signal, Idler, first harmonic of the Signal and Idler and the Second harmonic generation of the Signal and Idler is 400 – 2400 nm.

### 3.3.4 Specifications of OPA-800CF Wavelength Extension Options:

| Option | Wavelength Range | Pulse Energy | Pulse Width | Energy Stability |
|---|---|---|---|---|
| $\omega_i$ | 1.6 μm - 3.0 μm | 35 μJ at 2.0 μm | < 130 fs | < 3% |
| $\omega_s$ | 1.1 μm - 1.6 μm | 75 μJ at 1.3 μm | < 130 fs | < 3% |
| HG1/HGII $2\omega_i$ | 800 - 1200 nm | 10 μJ at 900 nm | < 130 fs | < 5% |
| HG1/HGII $2\omega_s$ | 580 - 800 nm | 15 μJ at 650 nm | < 1300 fs | < 5% |
| HG1/HGII $4\omega_i$ | 400 - 600 nm | 3 μJ at 450 nm | < 130 fs | < 7.5% |
| HGII $4\omega_s$ | 300 - 400 nm | 3 μJ at 300 nm | < 200 fs | < 7.5% |
| DFM | 3.0 μm – 10 μm | 3 μJ at 4.0 μm | — | < 5% |

Table 2-2: OPA-800CF Specifications for the Idler and Signal, 2nd and 4th harmonic of signal and idler, wavelength range, pulse energy pulse width

3.3.5 The overall wavelength range for the OPA is covered from 300 nm – 2400 nm.

| Output Specification | Wavelength Range |
|---|---|
| Signal | 1200 – 1600 nm |
| Idler | 1600 – 2400 nm |
| First Harmonic: Signal (S2) | 600 – 800 nm |
| First Harmonic: Idler (I2) | 800 – 1200 nm |
| Second Harmonic: Signal (S4) | 300 – 400 nm |
| Second Harmonic: Idler (I4) | 400 – 600 nm |

Table 2.3: The configurations available in OPA-800 CF with the wavelength range

## 3.4 OPA crystal images

The following are the images of the various crystals used for wavelength selection and the optical layouts for the OPA-800CF which has the options to use the output from the Signal only, Idler only, Second Harmonic Generation of the Signal, Second harmonic Generation for the Idler, Fourth harmonic Generation of the Signal and Fourth harmonic Generation of the Idler and the extended wavelength option for the wavelength selection in the range from 3.0 µm to 10.0 µm.

### 3.4.1: Optical Images of the crystals and Periscope for wavelength tuning in the OPA-800CF:
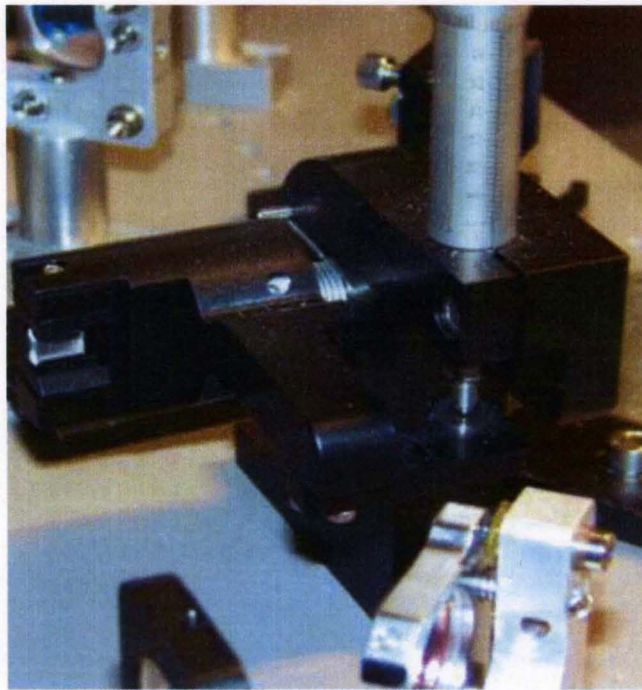


Figure 3.11 Optical Image of the Beta Barium Borate (BBO) crystal inside the OPA
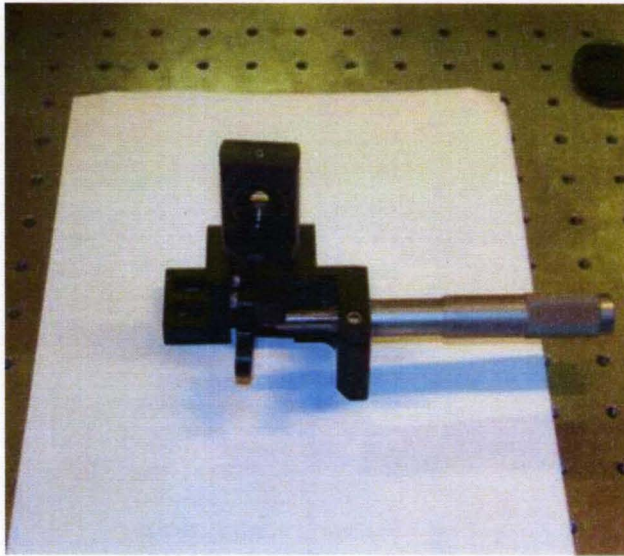
Figure 3.12 Optical image of the Horizontal Crystal used in SHG and FHG
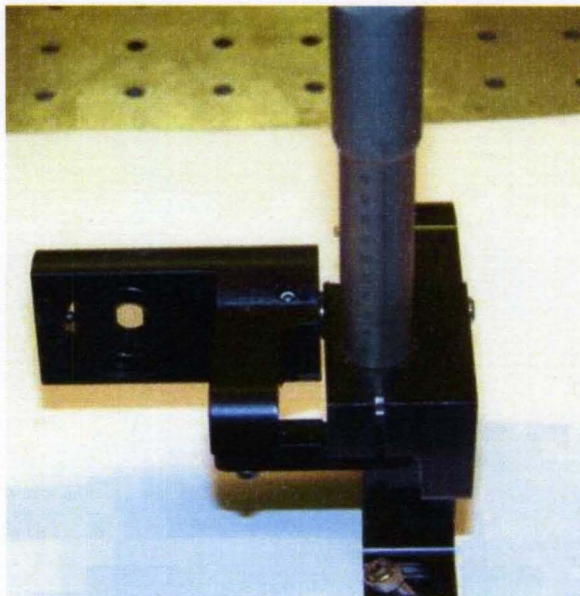


Figure 3.13 Optical image of the Vertical Crystal used in SHG and FHG
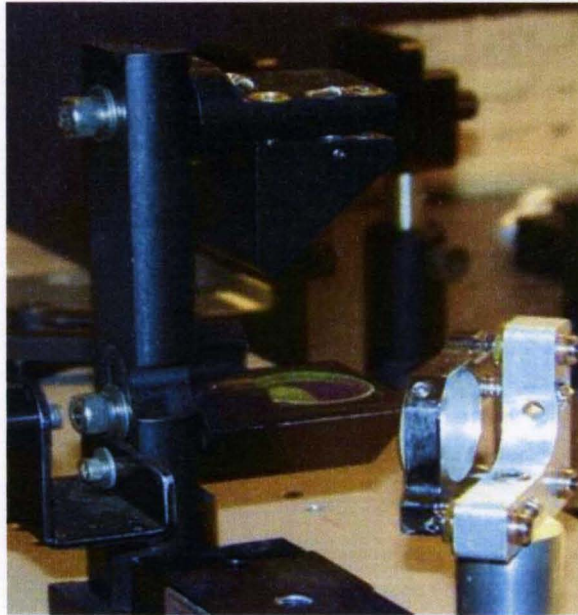
Figure 3.14 Image of Periscope for the selection of the Signal and Idler
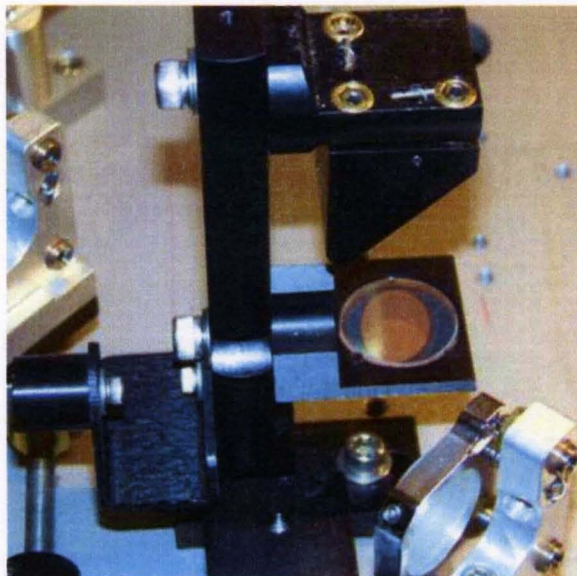


Figure 3.15 2<sup>nd</sup> view of the Periscope used for Idler or Signal selection
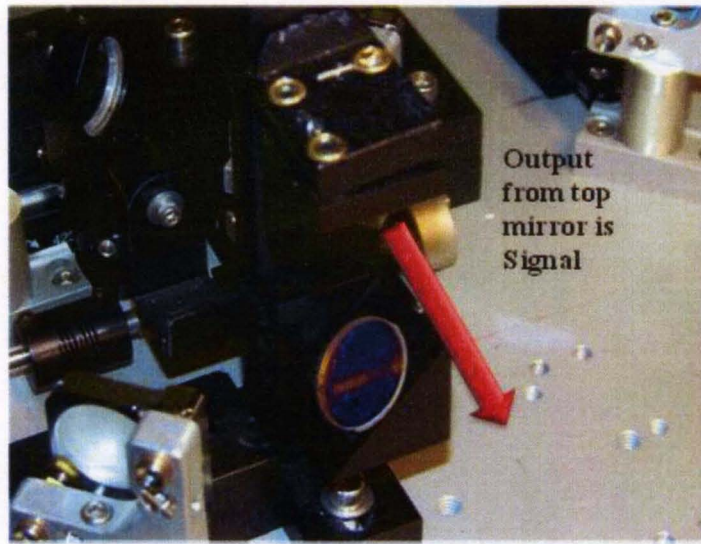
Figure 3.16 Optical view of the configuration for the Signal output beam
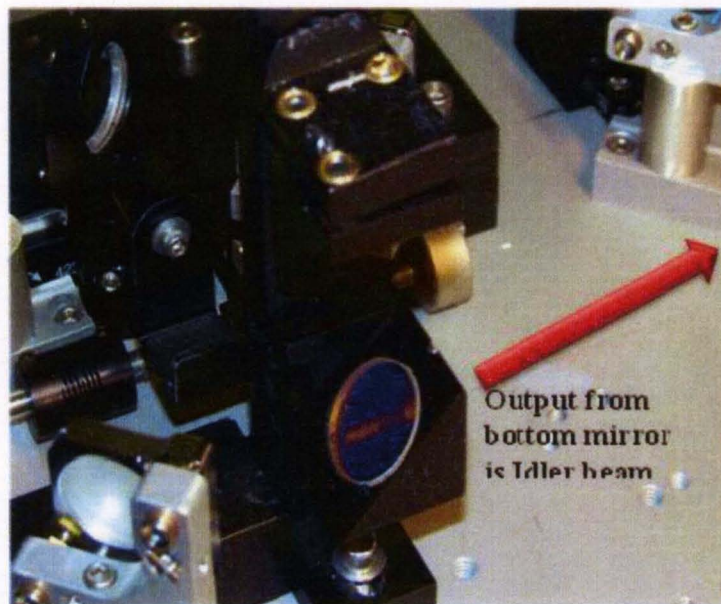


Figure 3.17 Optical image for the configuration for the Idler output beam

## 3.4.2: Images of the optical set up for various wavelength selections:



Figure 3.18 Optical alignment set up for Signal and Idler output

The output beam coming out of the vertical mirror at the bottom of the periscope is Idler and the beam bouncing out from the top mirror of the periscope is Signal. The wavelength range for the Signal is 1.1 μm to 1.6 μm. The wavelength range for the Idler is 1.6 μm to 3.0 μm. The periscope at the end of the OPA-800CF selects the polarization beam separating the Signal and the Idler beams.
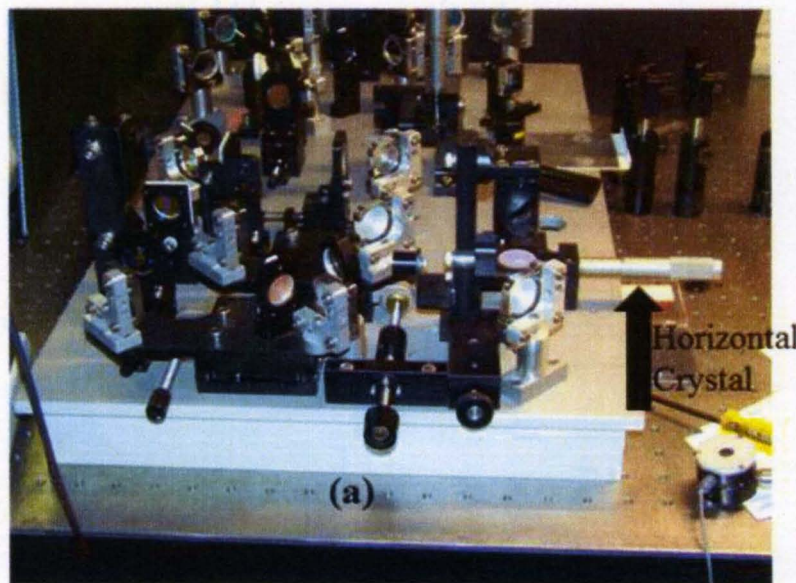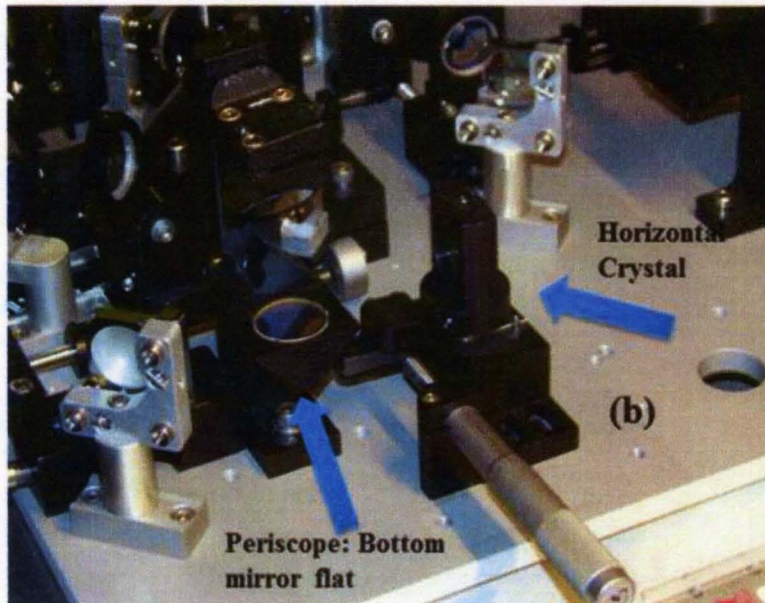
Figure 3.19 (a) and (b) Optical alignment for Second Harmonic Generation of the Idler

The SHG of Idler covers the wavelength range from 800 to 1200 nm. The

periscope is not used for the SHG of the Idler.
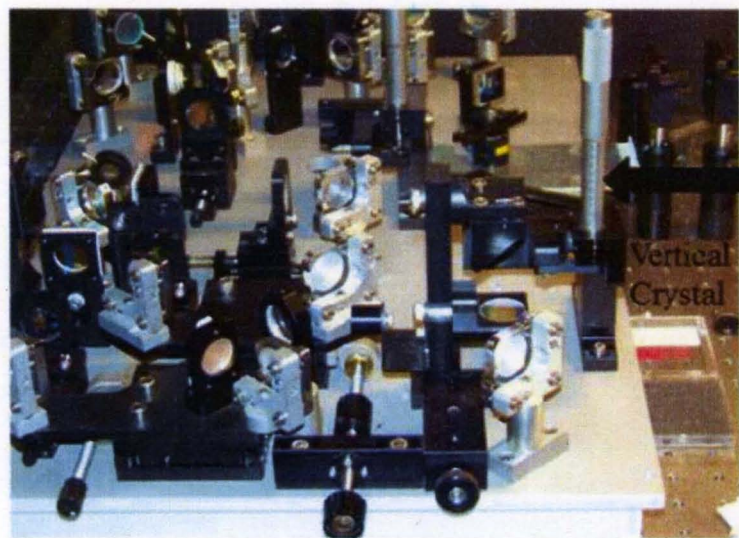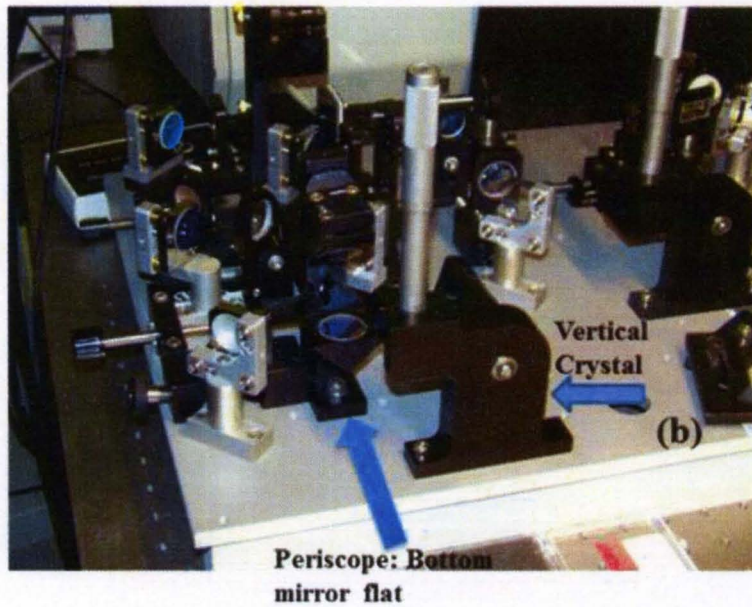
Figure 3.20 (a) and (b) Optical alignment for SHG of the Signal.

The SHG of the Signal covers the wavelength range from 600 to 800 nm. The periscope is not used for the SHG of the Signal as the crystal selects the polarization.
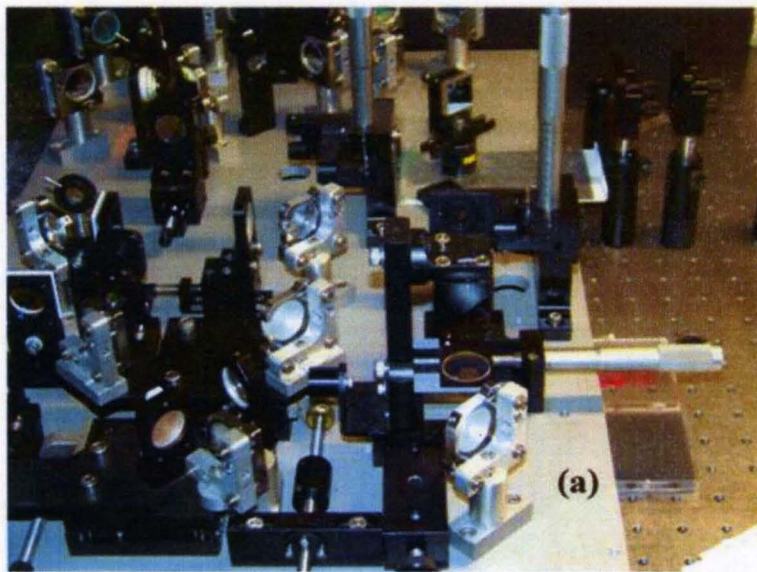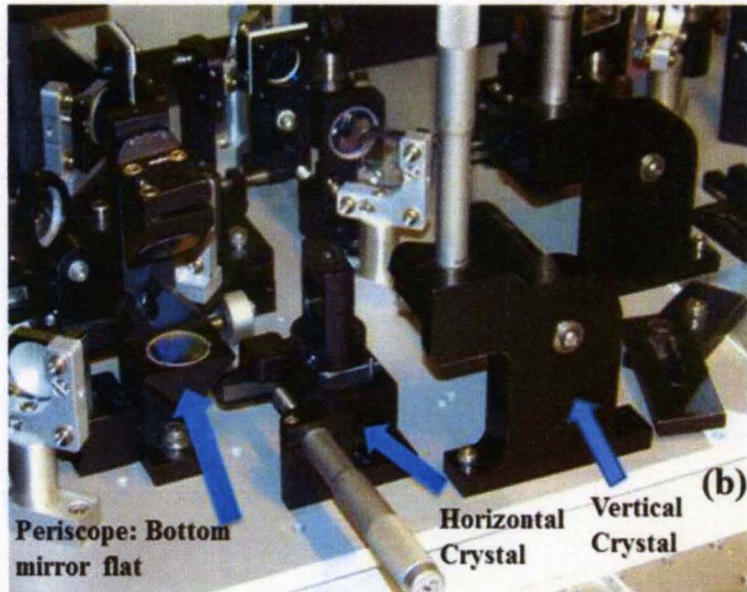
Figure 3.21 (a) and (b) Optical alignment for FHG of the Idler.

The FHG of the Idler covers the wavelength range from 400 to 600 nm. The periscope is not used for the FHG of the Idler as both the crystals select the polarization.
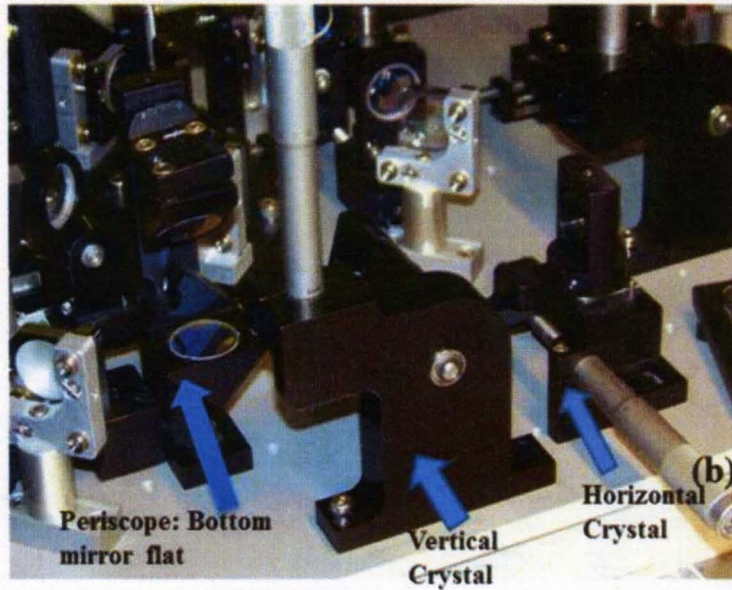
Figure 3.22 Optical alignment of FHG of Signal.

The Fourth Harmonic Generation of the Signal covers the wavelength ranges from 300 – 400 nm. The periscope is not used for the FHG of the Signal as both the crystals select the polarization.

# CHAPTER IV: CHARACTERIZATION OF MDMO-PPV: PCBM SOLAR CELLS: ABSORBANCE AND PHOTOVOLTAGE

## 4.1 Device Fabrication

In this section, fabrication procedures are described for the samples used in the preliminary characterization of the MDMO-PPV: PCBM bulk heterojunction solar cells.

### 4.1.1 Bulk Heterojunction Solar cell Fabrication

The organic solar cell starts with a transparent conducting metal oxide; Indium Tin Oxide (ITO) as the anode. Pre-deposited ITO slides were purchased from Sigma-Aldrich with sheet resistance of 20-25 $\Omega/\square$ and a thickness of 60 nm. First, a thorough cleaning of the ITO slides was done, consisting of a sonication bath in acetone, followed by a sonication bath in iso-propyl alcohol and finally a deionized water rinse. The cleaned ITO slides were then annealed at 80 $^0$C to evaporate any moisture that might have been left on the surface. Finally the slides were allowed to cool down to room temperature and transferred in to a desiccator which was held at vacuum.

The active layer mixture was prepared by mixing 1 part MDMO: PPV with 4 parts $PC_{60}BM$ in ortho-dichloro benzene. The weight ratios of the two components of the active layer were 8 mg of MDMO: PPV and 32 mg of $PC_{60}BM$.

The ratio of 1:4 parts was selected, because it is reported to give the highest power conversion efficiencies in bulk heterojunction solar cells. The mixture was subjected to magnetic stirring for 72 hours at 40 $^0$C. The magnetic stirring was performed to ensure maximum dispersion of the two materials, the elevated temperature facilitates the dispersion process. After magnetic stirring for 72 hours the hot plate temperature was turned off and the sample was allowed to cool to room temperature. The active material solution was then placed in a vacuum connected desiccator to ensure that the sample was not exposed to any moisture.
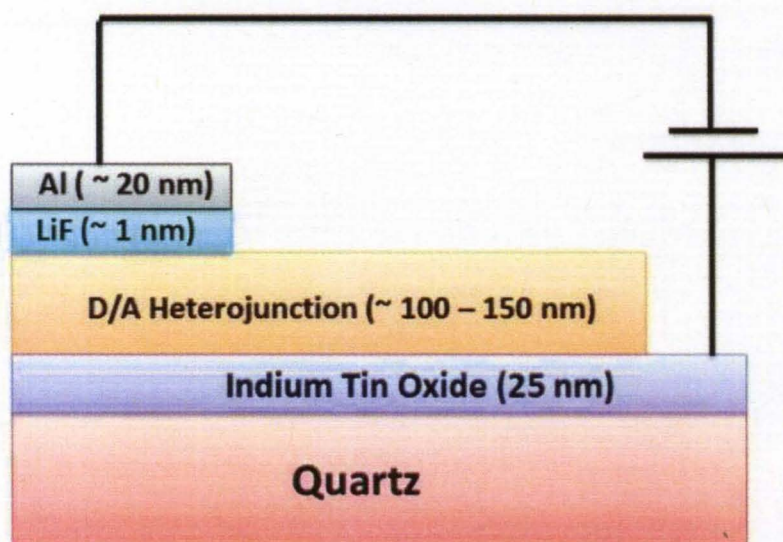


Figure 4.1: Device structure of Organic Bulk Heterojunction solar cells

The pre-cleaned ITO slides were spin coated with the mixture to form the photoactive film. After several trial and error runs, the spin speeds were chosen

to be 1000-1100 rpm to get a final film thickness of 100-150 nm. (The active material films need to be thick enough to avoid pinholes, but thin enough to allow for exciton diffusion to the contacts.) The film was then subjected to a soft bake at 80 0C for 40 minutes. The soft baking of the sample is done to promote the crystallization of the polymer chains with the PC60BM molecules. If the crystallization between polymer chains and PC60BM molecules is not optimized, the overall output power conversion efficiency is significantly reduced. After soft bake, the photoactive film was covered with an aluminum foil, and a small opening was made to create a shadow mask. A top contact consisting of 1 nm LiF and 20 nm of aluminum was then evaporated on the sample surface. LiF was deposited to ensure that aluminum metal does not penetrate through any pinholes in the film and create a leakage page between the aluminum and the ITO.

### 4.1.2 Device fabrication for UV-Vis-IR absorbance measurements

### 1. Absorbance of MDMO-PPV polymer

The quartz slide was thoroughly cleaned with acetone, iso-propyl alcohol and rinsed with DI water. 8 mg MDMO-PPV polymer was dissolved in 1 ml ortho-dichlorobenzene and a thin film was spin coated on the quartz slide at 1100 rpm resulting in ~ 100 – 150 nm thick film. The film was dried in ambient conditions

### 2. Absorbance of PCBM electron acceptor

18 mg of PCBM was dispersed in 1 ml of ortho-dichlorobenzene and the mixture was subjected to magnetic stirring for 72 hours. A film of PCBM on

quartz was made my drop casting method. The resulting film was ~ 8 – 10 microns thick.

## 3. Absorbance of MDMOMO-PPV: PCBM.

The same mixture used for fabrication of organic solar cell was used to form a thin film of the mixture of MDMO-PPV: PCBM for absorbance measurements. Film was spin coated at 1100 rpm resulting in a ~ 100 – 150 nm film. The sample was dried in ambient conditions before performing UV-Vis-IR absorbance measurements.

## 4.2: Sample Characterization Results

This section presents the results of UV-Vis-IR absorbance measurements performed on MDMO-PPV, PCBM and MDMO: PPV – PCBM mixture and open circuit photovoltage measurements of the MDMO-PPV:PCBM solar cell.

## 4.2.1 Absorbance measurement of MDMO-PPV
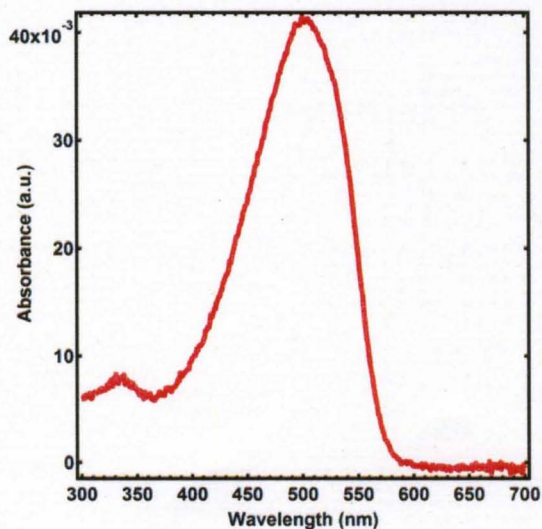


Figure 4.2: Absorbance measurements of MDMO: PPV thin film

Figure 4.2 shows the absorbance measurements of the polymer MDMO-PPV. A strong transition in the absorbance measurement was observed at ~ 500 nm. This transitions is attributed to the optical band-gap of the polymer where absorbance is maximized. A smaller transition is also observed at ~ 320 nm which is attributed to higher energy exciton transitions in the polymer.

## 4.2.2 Absorbance measurement of PCBM
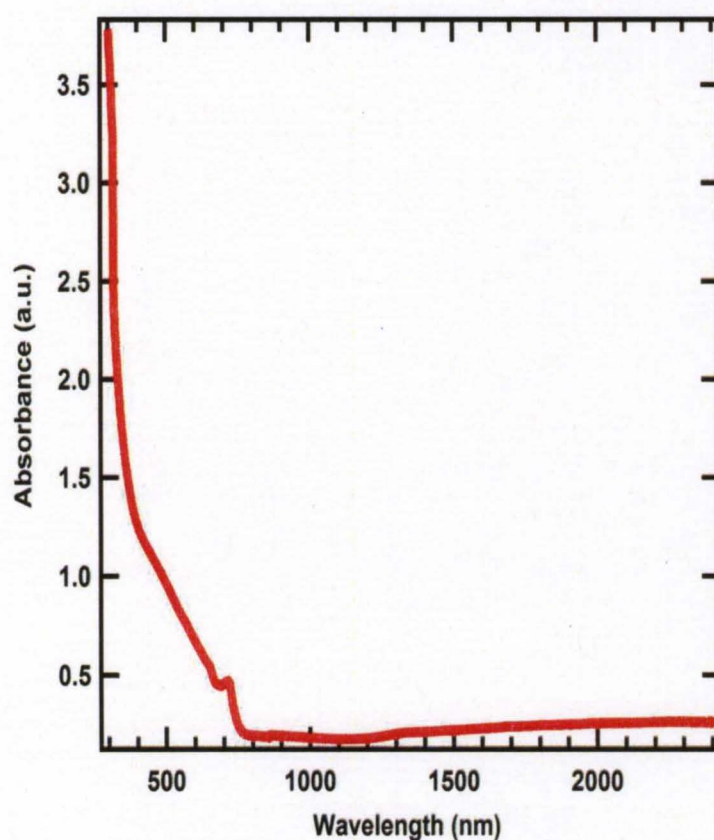


Figure 4.3: Absorbance measurements for PCBM

Figure 4.3 shows the absorbance measurements for PCBM. A small feature was observed at 720 nm which is attributed to the singlet exciton transition of PCBM. This transition is forbidden due to optical selection rules and

has a small absorbance cross-section because of the symmetry of PCBM molecules. PCBM has a large absorbance below 400 nm attributed to the optical band-gap and to the charge transfer processes between neighboring PCBM molecules.

### 4.2.3 Absorbance measurement of MDMO-PPV: PCBM mixture
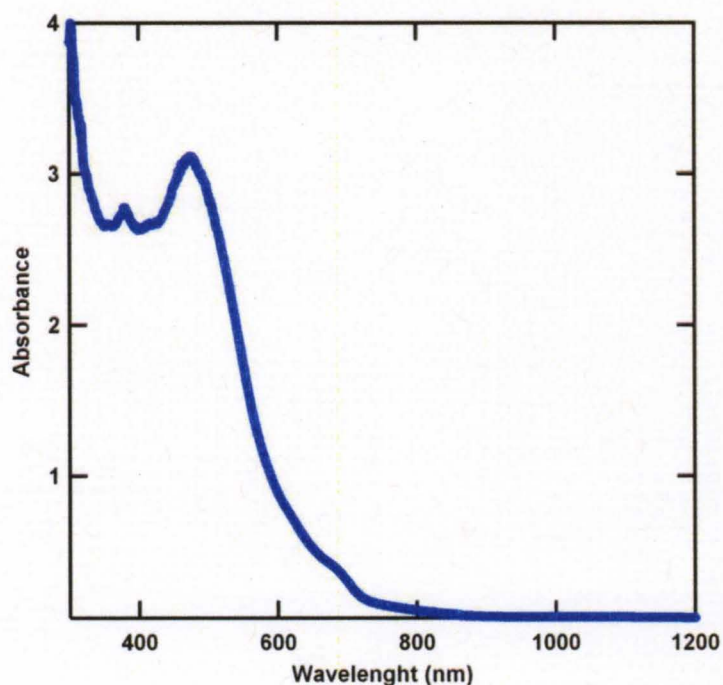


Figure 4.4: Absorbance of MDMO-PPV: PCBM thin film

Figure 4.4 shows the absorbance data for a MDMO-PPV: PCBM thin film. All the transitions attributed to the polymer and PCBM were resolved. Transitions due to the polymer at ~ 500 nm and transitions due to PCBM ~ 720 nm and below 400 nm were resolved as shown in the data.

## 4.2.4 Photovoltage measurements of MDMO-PPV: PCBM solar cell

The excitation source used for the photovoltage measurements of the bulk heterojunction solar cells was a 1 KHz Quartz Tungsten Halogen lamp source, resolved with an "Acton research" monochromator. The wavelength range of the resolved spectrum was between 380 – 800 nm. The output power of the resolved white light source in the wavelength range of 380 – 800 nm was 15 – 20 $\mu$W/cm$^2$. The monochromator resolved light was chopped using an optical chopper at a frequency of 13 Hz. The output of the device was connected to a lock-in amplifier which was synched at 13 Hz frequency from the chopper. Sample was loaded in a cryostat and was maintained in vacuum conditions better than 10$^{-6}$ Torr.

Figure 4.5 shows the open circuit photovoltage data measured for a MDMO-PPV: PCBM blend based organic solar cell device which was fabricated in the configuration shown in Fig. 4.1. The data shows a main photovoltage transition at ~ 500 nm which is attributed to the optical band-gap of the polymer and the small bump at 720 nm attributed to singlet transition in PCBM. Figure 4.6 shows data retrieved from literature for comparison. The photovoltage data matches well with the literature where similar transitions due to MDMO-PPV and PCBM were observed.
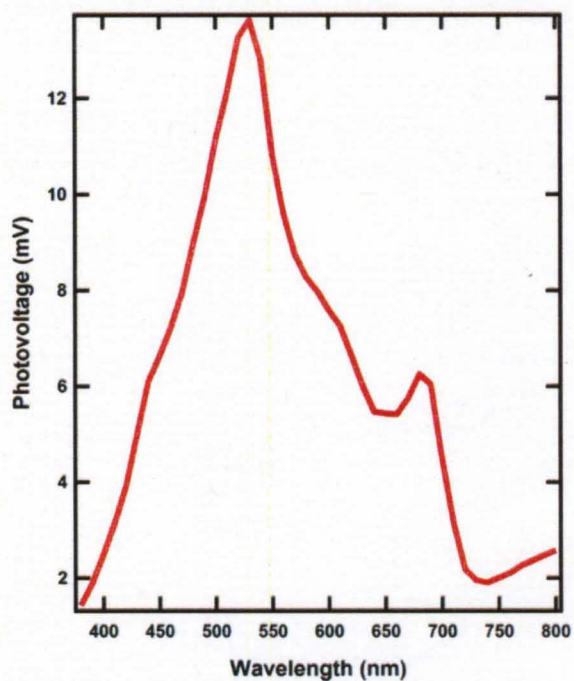
Figure 4.5: Open circuit photo-voltage measurement of MDMO-PPV: PCBM solar cell
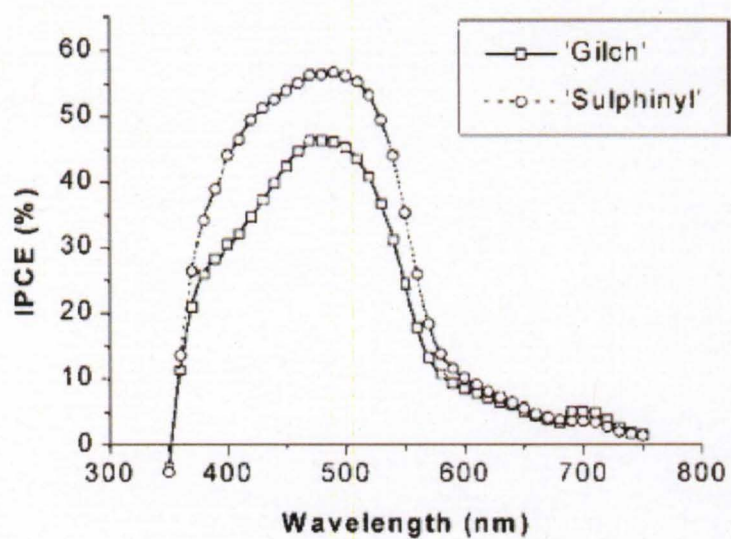


Figure 4.6: IPCE measurement of MDMO-PPV: PCBM solar cell

# CHAPTER V: CAPACITIVE PHOTOCURRENT SPECTROSCOPY

This chapter describes the capacitive photocurrent technique, together with the experimental set-up, device fabrication and optical measurements on MDMO-PPV: PCBM using capacitive photocurrent spectroscopy.

## 5.1 Experimental Setup and Device fabrication for CPS
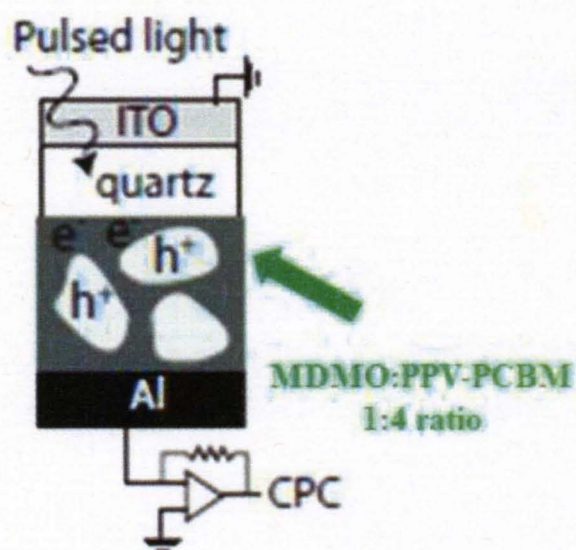


Figure 5.1: Basic device setup for capacitive photocurrent spectroscopy

The device architecture for capacitive photocurrent is shown in figure 5.1 above. A parallel plate capacitor is made by spin coating a thin film of the MDMO-PPV: PCBM mixture on a quartz slide, which acts as a transparent substrate and is used as the dielectric medium for the capacitor structure. Indium tin oxide (ITO) is coated on the other side of the quartz and forms the counter electrode for optical characterization. ITO was chosen as the transparent conducting substrate because of its high transparency and low resistivity. The capacitor structure is then anchored to a copper block in an optical access flow cryostat. An aluminum electrode is deposited on top of the active layer film, and the copper electrode is set at the ground potential to the outside of the cryostat. The output of the capacitor structure is sent through a current amplifier, and then monitored using a lock-in amplifier synched to the laser repetition rate (1 kHz). This ensures that only the photocurrent generated by the pulsed laser is measured, and improves the signal-noise ratio. The ITO electrodes provides a stable signal due to its high conductivity, reducing any fluctuations in the measurements. Absorbance of light in the active layer produces electrons and hole pairs at the D-A interface between the polymer and the PCBM. The separation of charges at this D-A interface produces an ac voltage whose magnitude is proportional to: 1. the amount of excited charge, and 2. the charge separation distance d.

## 5.2 Operational principle of capacitive photocurrent spectroscopy

The operational principle of capacitive photocurrent technique is outlined in figure 5.2. The electrode potential $V_p$ is measured relative to the donor-

acceptor active film layer which is held at ground potential. With the absence of light, $V_p$ is given by the work function difference between the donor-acceptor interface and the electrode, and any additional built-in potential which may be present due to the trapped charge within the quartz or the active film. The band diagram is similar to a MOS capacitor, with the semiconductor replaced by the active film. Light incident on the sample excites electron hole pairs. If the excited electron-hole pairs (ehps) separate, due to the internal and/or external electric field, an additional potential is created, which to first approximation is given by:

$$\Delta V p = Q d / \in$$

where Q is the total charge per area generated, and $d$ is the charge separation distance. Since the probe electrode is floating, its potential increases by an amount $\Delta V p$ to match the potential change. This measured voltage reflects the absorbance in the active region. Since ITO is used as transparent metal, its transparency with the excitation source was measured.
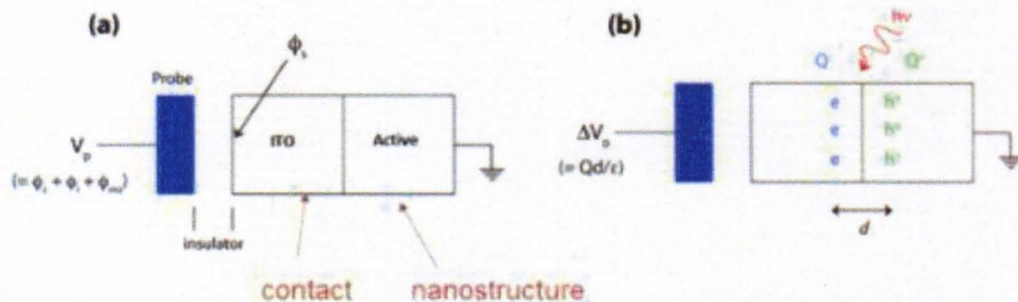


Figure 5.2: ITO/Active heterojunction measured using capacitively coupled probe electrode with (a) light and (b) without light

Preliminary measurements were performed on a p-type silicon sample to compare the CPS results with standard two terminal DC photocurrent measurements. Figure 5.3 plots the capacitive photocurrent as a function of excitation photon energy. The photocurrent is relatively low until the excitation energy is in the vicinity of the band gap of silicon (1.1 eV). When the excitation energy equals the band gap energy, the photocurrent increases and remains relatively constant. The turn on point of the photocurrent can be quite accurately matched with the absorption spectrum for p-type silicon which confirms the availability of CPS as a standard spectroscopy technique.
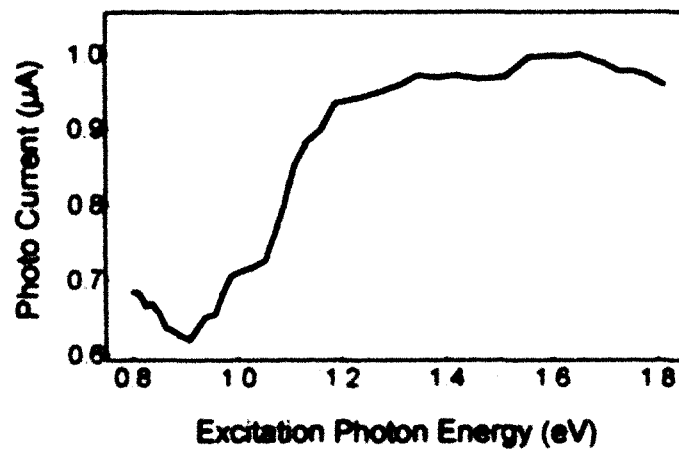


Figure 5.3: Capacitive photocurrent measurement performed on a p-Si sample [57-58]

## 5.3. Capacitive photocurrent spectroscopy of BHJ solar cell materials

Device fabrication for capacitive photocurrent measurements and preliminary results of organic bulk heterojunction solar cells materials will be discussed in the following section.

### 5.3.1 Preliminary measurements using CPS

The following section will discuss CPS measurements of BHJ solar cell materials, power dependence and comparison of CPS measurements with absorbance and photovoltage measurements.

### 5.3.1.1 CPS measurements of BHJ solar cell materials

As seen in figure 5.4, the capacitive photocurrent measurement of the bulk heterojunction active film made from MDMO-PPV:PCBM showed very interesting results. The main absorbance peak attributed to the electron donating polymer was resolved at 520 nm, but a second and even larger peak in magnitude was resolved at 720 nm. This peak is attributed to the first optically allowed transition for electron acceptor PCBM. Ideally this transition of PCBM has a low absorbance cross-section because of the symmetry selection rules for optically forbidden transitions. However, in the capacitive photocurrent measurement a large photocurrent peak was resolved. This experimental evidence demonstrates that although the absorbance cross-section of this first allowed singlet transition of PCBM is low; the photocurrent charge dissociation generated from this transition is relatively high.
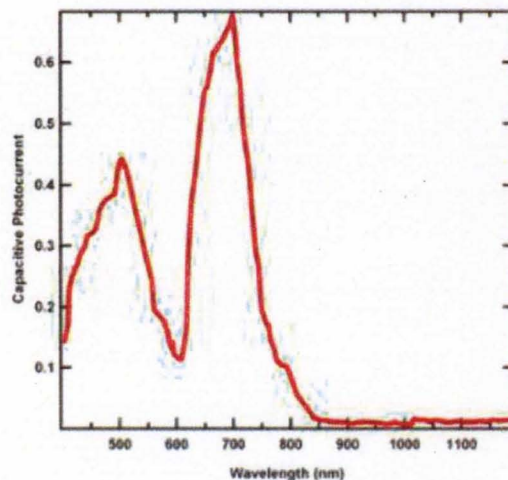
Figure 5.4: Capacitive photocurrent measurement of MDMO-PPV: PCBM active layer

## 5.3.1.2 Absorbance vs. CPS comparison of MDMO-PPV: PCBM

For direct comparison between the UV-Vis-IR absorbance and the capacitive photocurrent measurement, figure 5.5 shows the two data sets plotted together. It can be clearly seen that the main absorbance transition attributed to the optical band-gap of the polymer is resolved in both measurements at 520 nm but the second transition due to PCBM at 720 nm which appears to be a small bump in the absorbance measurements, is resolved as a very large magnitude peak in the capacitive photocurrent measurements. The main conclusion from this result was that the charge dissociation rate of PCBM is much higher even with small absorbance of light. This agrees with work reported in the literature where the charge dissociation rate of PCBM was found to occur on femtosecond time scales.
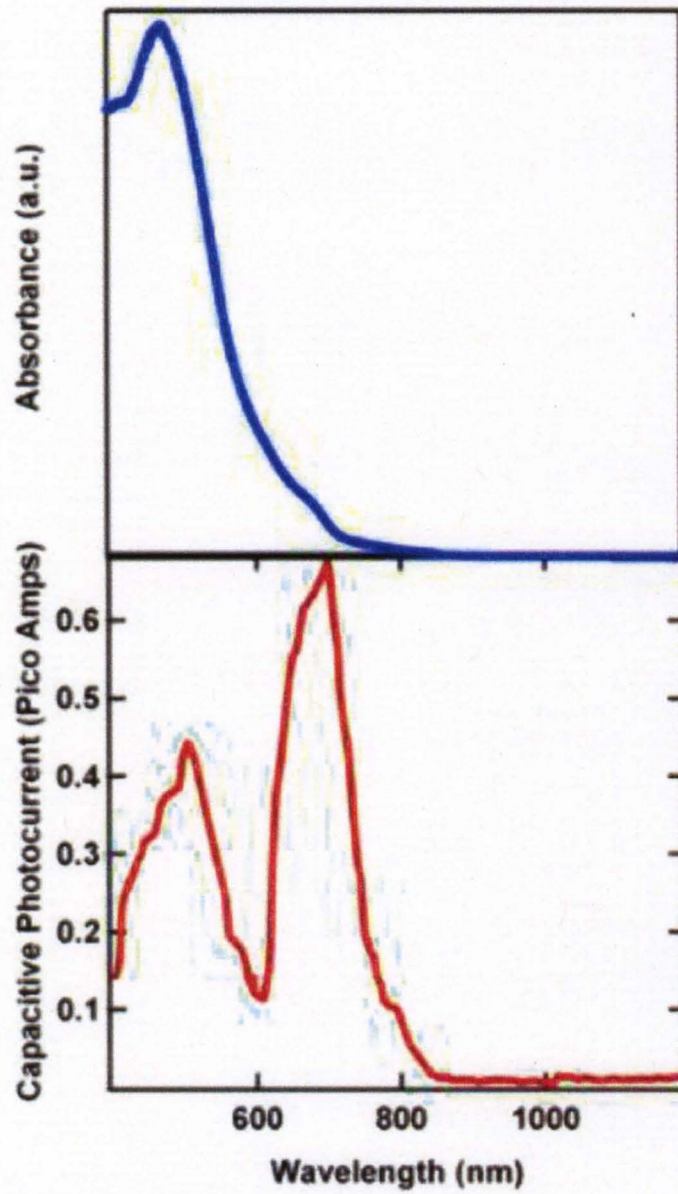
Figure 5.5: Absorbance vs. capacitive photocurrent measurement for active film

### 5.3.1.3 Power dependence of CPS measurement

The use of a femtosecond pulsed laser raises the possibility of anomalies occurring due to the high powered pulses. This could result in two photon absorbance or the breaking of symmetry rules of the materials under study. To confirm that no such anomalies existed in the capacitive photocurrent measurements, the photocurrent was measured as a function of increasing power. If two photon absorbance processes are happening, the power dependence will be quadratic, and if it was a one photon process, the power dependence will be linear.
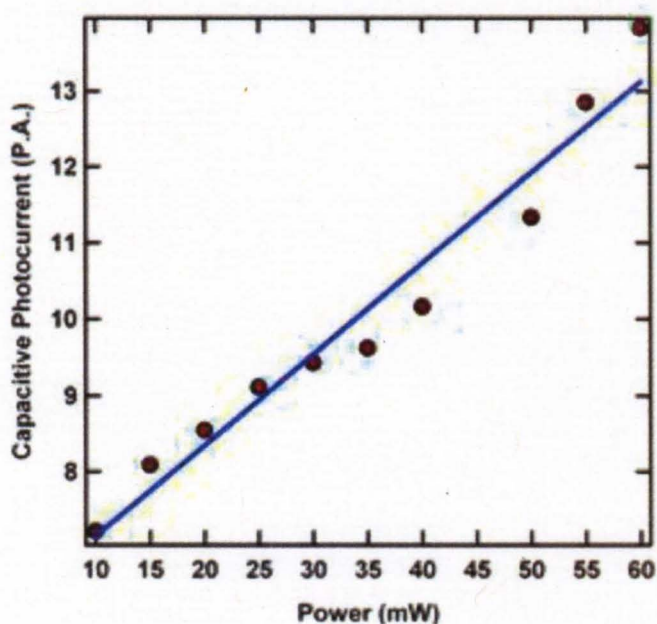


Figure 5.6: Power dependence of CPS at 720 nm laser excitation

Figure 5.6, shows the power dependence of the capacitive photocurrent measurements. Because the electron acceptor PCBM peak was so large, the power dependence was performed by exciting the laser light at the peak

wavelength of this transition (720 nm). Excitation of light from the laser was maintained at 720 nm and subsequently, the power was increased in small step sizes. As seen in figure 16, the power dependence looks almost linear in behavior at least in the lower power regime where the entire capacitive photocurrent measurements were performed. (The power used for the wavelength scan in CPS was 10 mW.) There is some deviation from linear power dependence, but only at higher powers .Thus the power dependence confirmed that the capacitive photocurrent peak was in-fact due to one photon absorbance.

### 5.3.1.4 Photovoltage vs. capacitive photocurrent measurements

Figure 5.7 shows the comparison of DC photovoltage measurement with capacitive photocurrent measurement. Just as was observed in absorbance measurements, the main absorbance peak for the polymer was resolved at 520 nm and a small bump was observed at 720 nm which was attributed to the PCBM first allowed singlet transition. The first allowed singlet transition of PCBM which is known to have low absorbance generates low photocurrent as observed in DC photovoltage measurement but the capacitive photocurrent measurements confirmed that although the absorbance is low, the photocurrent generated is relatively high.
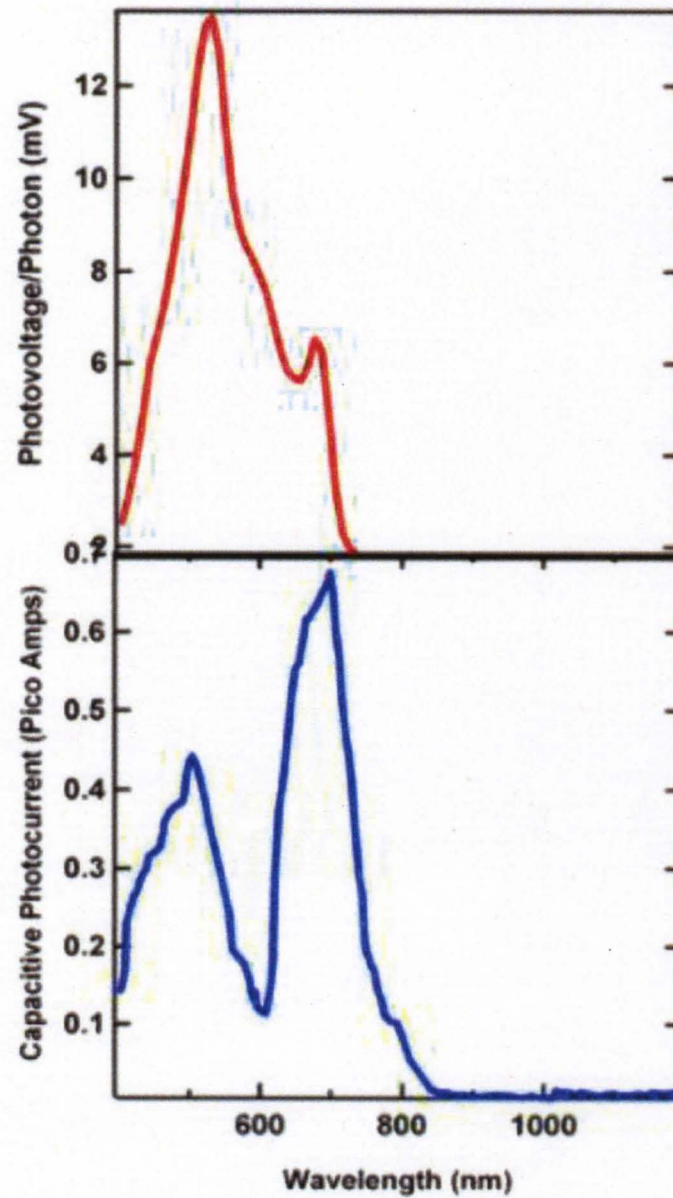
Figure 5.7: Photovoltage vs. capacitive photocurrent for MDMO-PPV: PCBM

## 5.4. Photovoltage bleaching experiments

The results of capacitive photocurrent measurements demonstrated that the electron acceptor PCBM has a high dissociation rate when compared to the absorbance. This information, led to designing new experiments to understand the role of PCBM in the charge generation, charge dissociation and charge collection at the counter electrodes in organic bulk heterojunction solar cells.
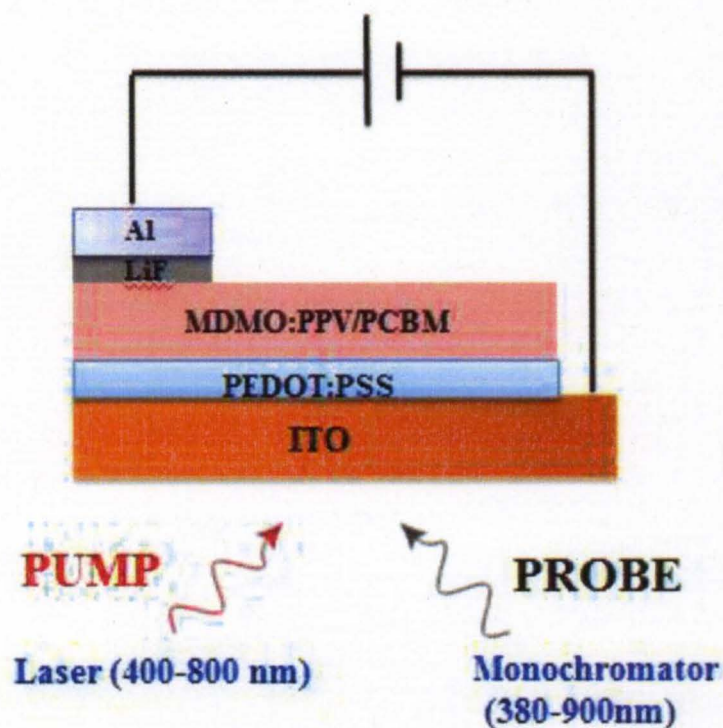


Figure 5.8: Experimental schematic for photovoltage bleaching experiments

Figure 5.8 shows the experimental schematic for photovoltage bleaching experiments. A simple experiment was designed to understand the role of PCBM photo-generated states. The idea was to make a two terminal solar cell as demonstrated in figure 19 and populate certain states at higher energies and lower energies and observe the effect of this population on the charge collection at the counter electrodes under monochromatic white light resolved wavelength scans.

The experiment was designed such that; using the laser a certain energy level would be populated where there is some absorbance both in the polymer and the electron acceptor. After the state is populated with a specific energy level, using the output beam from the monochromator the entire wavelength scan was performed to measure the photovoltage response. Initially the laser was set at a low energy wavelength and let it populate a low energy transition in the solar cell, after which the output light from the monochromator was scanned in the wavelength and response was recorded to measure the photo-voltage of the solar cell. Thus, the output of the laser was only used to populate certain energy levels but not to measure the response of the laser. The photovoltage response due to the light shining from the monochromator output light was used to record the data.

A tungsten halogen white lamp source rated at 1 KHz was resolved using a monochromator output in the wavelength range from 380 – 800 nm. The output of the wavelength (exciting only one wavelength at a time) was scanned from 400 – 800 nm. Thus the laser was used as a pump source and the

monochromator output beam was used a probe beam for measuring the photovoltage response. Figure 5.9 shows the photovoltage response of a bulk heterojunction solar cell made from MDMO-PPV: PCBM under different illumination of light from the laser to populate various energy states and the response is measured as the open circuit photovoltage generated due to the monochromator output beam. The monochromator output beam was chopped using an optical chopper at 13 Hz and kept constant at this frequency value. The lock-in amplifier was synched at 13 Hz to record the response of the solar cell only at this frequency which was used to chop the output of the monochromatic light.
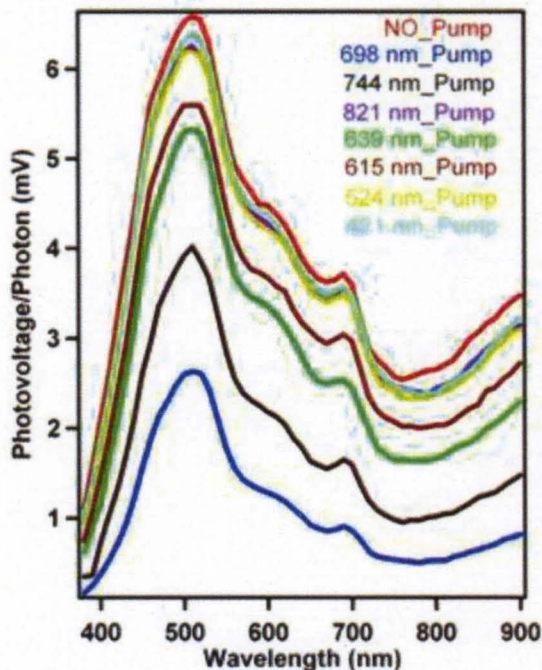


Figure 5.9: Photovoltage response of MDMO-PPV: PCBM solar cell in the photovoltage bleaching experiments

The photovoltage bleaching data was very interesting as it demonstrated some unique properties of the charge dissociation process involved in this complex bulk heterojunction system. As seen in the graph in Fig. 5.9, when high energy excitation light (wavelength = 421 nm) was illuminated on the solar cells, the photovoltage signal only dropped by a small amount. When the sample was illuminated at 524 nm, the change was a little higher and the photovoltage signal dropped a little more, similarly when the laser excitation was 615 nm the drop in the photovoltage signal was even higher than previously observed.

The most interesting aspect of this data set was the excitation of the laser light illuminating the sample at lower energies. When the excitation from the laser light was 744 nm, the photovoltage signal bleached down substantially. The highest amount of photovoltage bleaching was observed for laser excitation at 700 nm. However, if the same behavior was expected the magnitude of the photovoltage signal should have bleached higher for laser excitation at 744 nm, but that was not the case. In-fact when the output of the laser excitation was at the lowest energy; 821 nm, the photovoltage bleaching signal did not show a substantial drop in the signal. As seen from the data, some change was observed from the signal but it was almost comparable to the photovoltage bleaching signal observed for 421 nm (high energy excitation). The photovoltage bleaching experiments proved that there was a clear wavelength dependence on the photovoltage bleaching response. Figure 5.10 shows the photovoltage plotted as a function of pump beam wavelength for photovoltage bleaching, the integration of all the data sets for photovoltage bleaching and comparison with

capacitive photocurrent data. The entire experiment was performed on two similar devices. Although, there is some deviation in the data of the two devices, the main experimental observations remain the same.
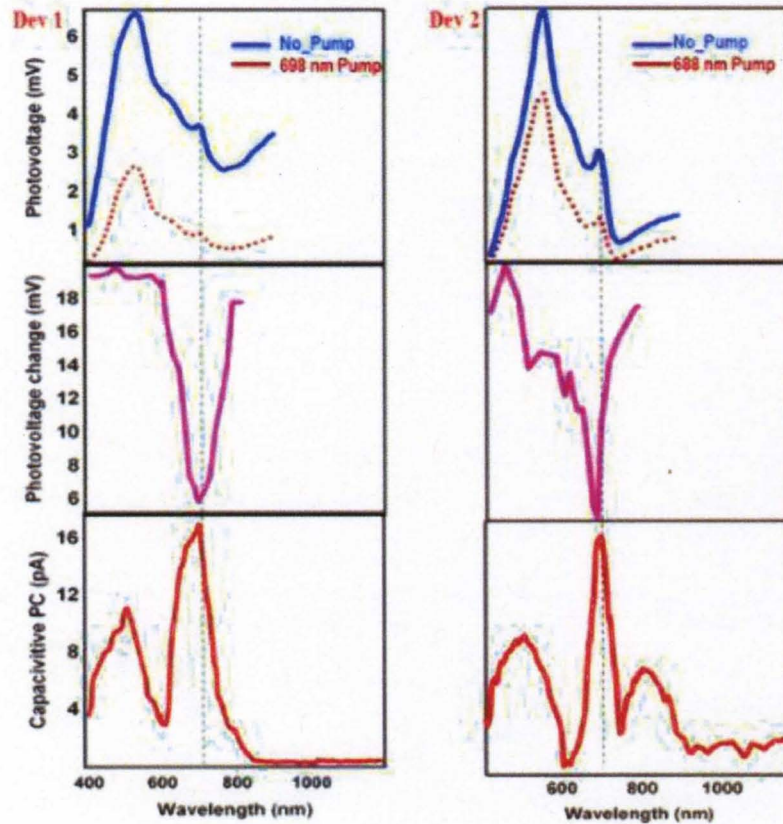


Figure 5.10: Photovoltage bleaching vs. capacitive photocurrent measurement [59]

## 5.5 Discussion

As seen from the capacitive photocurrent measurements, the peak at 700 nm (which has a larger magnitude than the main absorbance peak due to the polymer) is attributed to the first allowed optical transition for the electron acceptor PCBM. This clearly demonstrates that populating the energy states at the peak transition energy at 700 nm for the electron acceptor enhances the charge recombination process by either impeding the charge to be collected at the counter electrodes or promoting recombination of the higher energy states

It is striking that such large photovoltage bleaching occurs under exposure to low energy light even though the absorbance in this regime is relatively weak. In contrast, little or no bleaching is observed under exposure to high energy light corresponding to the main absorbance peak. This shows that the effect is not simply due to heating of the sample through absorption of the laser or through low-frequency transients of the femtosecond pulses. Instead, the bleaching must be a consequence of population of the singlet state of electron acceptor PCBM. One possibility is that population of the PCBM exciton and the subsequent charge dissociation creates an electric field which blocks the flow of additional charge to the contacts. However, direct measurement shows that the CPS peak corresponds to a voltage difference of only 30μV, which is far less than the change of 10 mV observed in the standard photovoltage. In addition, no bleaching is observed under exposure to high energy light even though a similar or a large blocking voltage is created. The bleaching results show that low energy excitation near the PCBM state impedes the charge collection process.

Both our CPS experiments and previous PIA (photo induced absorption) measurements show however, that charge dissociation from PCBM exciton is extremely efficient, and the state itself is not occupied long enough to have an influence on the charge collection. This means that some fraction of the PCBM excitons must decay into a long lived state, which itself acts to reduce charge collection efficiency. Experiments have shown that charge dissociation in BHJs results in the creation of two types of polaron states—a high energy polaron with high mobility and fast recombination time, and a low energy polaron which is localized and long lived. It has been shown recently that the localized polaron is preferentially generated by low-energy, below gap optical excitation. Despite having long recombination times, this polaron does not contribute to the photocurrent.

Our results suggest that this polaron also acts to increase the recombination rate for higher energy excitations, either by acting as a recombination centeror by forcing higher energy polarons into short lived statesthat recombine before being collected by the contacts. Thefact that the bleaching correlates with the PCBM excitonsuggests thatcharge dissociation from the PCBM preferentiallygenerates such long-lived localized polaron states. White light excitations consisting of all wavelengths generate photo-excitations both in the electron donating polymer and electron acceptor PCBM. Charge generation due to photo-excitations can create electron donor: acceptor bound pairs either by charge transfer process from the polymer or by energy transfer process from the PCBM.

Photo-excitation in the PCBM can generate bound radical pairs of PCBM anions and cations by internal charge transfer process within the neighboring PCBM molecules. The bound pair of electron donor and acceptor can be converted to mobile charges through charge transfer state energy from bound radical pairs of PCBM where if enough energy is provided to break apart the bound pairs of electrons and holes free charges could be generated or these bound pairs could end up recombining.
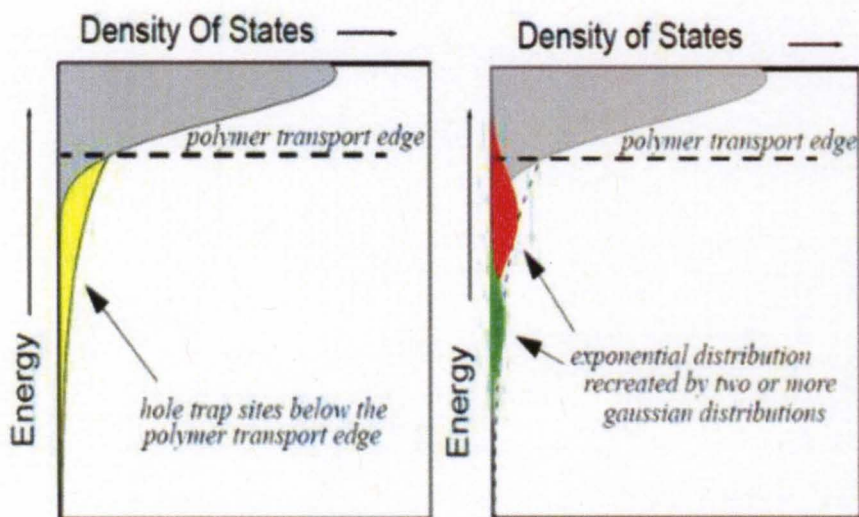


Figure 5.11: Energy vs. Density of states for photo-generated carriers in polymers

The key observation in photovoltage bleaching experiment where a sharp decrease in the photovoltage signal was observed at the singlet state energy of PCBM suggests that the mobile charges generated from gaining the energy to break apart the bound pair of electron and hole could undergo a recombination

process due to filling up of the trap states below the transport edge of the polymers. As seen in figure 5.11, the density of states for organic polymers has a long and extended tail at lower energies. Some polymers could also have an exponential distribution which could be created by two or more Gaussian distributions. Excitation of the singlet state transition of PCBM, which is at a lower energy than the optical band-gap of the polymer, seems to populate this exponential distribution of trap states with the free charge carriers generated by higher energy.

The photovoltage bleaching results counter intuitively demonstrate that increasing the amount of light on a bulk heterojunction solar cells causes the open circuit photovoltage to go down. This implies that the efficiency of these solar cells could be improved by filtering out a narrow band of light corresponding to the singlet state transition of PCBM at 1.7 eV.

## 5.6 Role of ITO plasmon states in bleaching:

At the time these results were published, the role of the ITO plasmon states was not investigated in the photovoltage bleaching mechanism. As will be seen in chapter 6, the next set of experiments on the optical properties of methanofullerene derivatives provides an alternative explanation for the photovoltage bleaching process, including the possibility that the ITO plasmon states block the charge dissociation process.

Plasmon modes in ITO thin film and nanoparticles have gained attention due to their presence in the low energy regime, where there is considerable

interest in the solar cell community. The next set of experiments were performed on methanofullerene derivatives on ITO substrate, the results of which show charge transfer happening from ITO into PCBM. This correlated with the fact that low energy excitation in PCBM fills the states and higher energy carriers do not have a pathway to make it to the contact resulting in either their recombination or creation of short lived states. The details of the experimental set-up, device architecture and results will be discussed in the next chapter.

# CHAPTER VI: SPECTROSCOPY OF METHANOFULLERENE DERIVATIVES

This chapter will introduce the theoretical properties of fullerene derivatives 1-(3-methoxycarbonyl)-propyl-1-phenyl-(6,6)C61 commonly known as PC60BM and (Phenyl-C71-Butyric-Acid-Methyl Ester) commonly known as PC70BM. Following the discussion on theory, optical and other experimental results will be discussed in detail.

## 6.1: Introduction

Since the development of organic electronics C60 (bucky balls) have been widely studied in various device architectures such as thin film transistors, electroluminescent devices and organic solar cells. Fundamental properties of C60 have been studied widely including their electrical, optical properties, magneto transport properties and superconductivity to name a few. In organic electronics the major challenge of using C60 arises from the fact that plastic solar cells are usually spin coated from solutions and the poor solubility properties of C60 raises some major challenges to form a good dispersion with various polymers. To overcome this challenge, various derivatives of C60 have been synthesized to enhance their solubility in organic solvents. The most common methanofullerene derivative of C60 is 1-(3-methoxycarbonyl)-propyl-1-phenyl-(6,6)C61 commonly known as PC60BM. PC60BM is the most commonly used

electron acceptor in organic solar cells and its use with electron donating polymers have shown the highest power conversion efficiencies.

Initial bulk heterojunction devices based on MDMO-PPV: PCBM blends demonstrated the highest power conversion efficiencies when polymer to PCBM ratio was 1:4. The concentration of PCBM was varied from 60-90% to study how the efficiency was affected. It is worth noting that PCBM was the major constituent in these solar cells however, little characterization results are reported for this fullerene derivative in its pristine form. The literature also reports different values for the HOMO and LUMO levels of the functionalized derivatives of methanofullerenes. Only recently it has been demonstrated that the dispersion relation of C60 can be perturbed when placed in close proximity with high conducting substrates. More work needs to be done, to understand the optical properties of fullerene derivatives in their pristine form and on different substrates (conducting/non-conducting substrates).

C60 in its pristine form is crystalline in nature and, similar to nanotubes; is held together by Van der Walls forces of attraction. It has been reported that the C60 molecule-molecule interactions leads to relaxation of the optical transition rules compared to individual C60 molecules leading to a reduced band gap of C60 molecules. The photoconduction band-edge of C60 is reported to be at 1.7 eV which leads to the first allowed optical transition but the symmetry of this state is not completely relaxed. Figure 6.1 shows the band diagram for PCBM molecules [54].
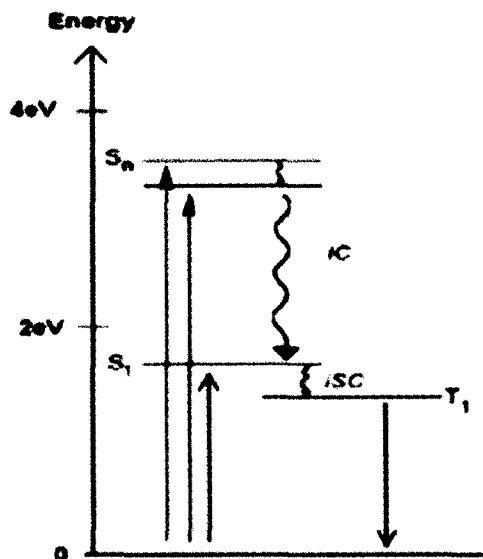
Figure 6.1: Energy band diagram for PCBM [54]

As seen in the diagram, the first allowed transition is at 1.7 eV. However, this transition is optically forbidden, and it thus has a small absorbance cross-section. The transition below this is the triplet state transition at 1.5 eV, but due to spin conservation, it is optically inactive. A higher energy singlet state transition can populate the dark states at the triplet energy levels through inter-system crossing. The thermal band-gap is reported to be 2.2 eV. The close proximity of these molecules leads to internal charge transfer process within the PCBM molecules. Two of the most dominant charge transfer states are at 2.43 eV and 3.5 eV.

As seen in figure 6.1, all the optically allowed transitions are at energies greater than 1.7 eV or higher. No optical transitions are reported below 1.7 eV. Through inter-system crossing from singlet state, triplet state transitions can exist but due to optical selection rules these transitions are completely optically

forbidden. Theoretical calculations have predicted no optically allowed transitions below 1.7 eV. However, very recent studies have reported on the relaxation of fullerene derivative PCBM perturbing their density of states. Reports have mentioned that although PCBM is transparent below 1.7 eV, under certain conditions optical transitions below the band-gap can be observed.

The existence of low energy states is important to enhance the power conversion efficiency of organic solar cells. The solar community has mostly focused on enhancing absorbance coefficients of polymers especially in the infra-red regime, since most of the polymers have absorbance in the visible spectrum. Low energy transitions in PCBM molecules could open areas for designing new architectures for enhancing power conversion with other materials which could be tailored to enhance the charge generation, charge transport and collection in bulk heterojunction or bi-layer devices.
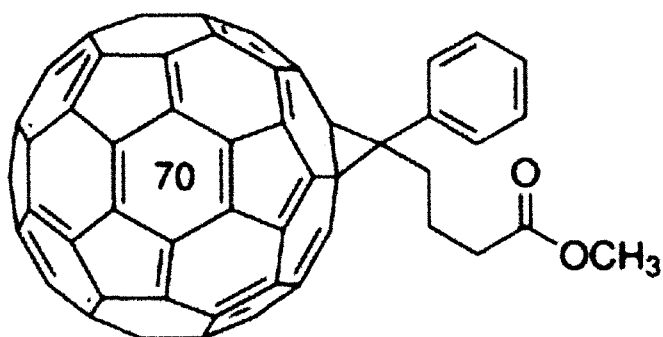


Figure 6.2: Functionalized fullerene derivative PC70BM

Figure 6.2 shows the schematic of the functionalized fullerene derivative PC70BM (Phenyl-C71-Butyric-Acid-Methyl Ester) for which the parent molecule is C70. Similar to C60, C70 has poor solubility in organic solvents and is functionalized with a butyric acid methyl ester side chain to enhance its solubility. PC70BM is also a very commonly used electron acceptor along with PC60BM. C70, the parent molecule of PC70BM is known to have higher absorbance of light. This makes it a useful electron acceptor in organic solar cells. PC70BM is reported to have a relaxed symmetry of C70 molecule compared to C60 which is attributed to be the reason for higher absorbance. The second reason is the presence of 10 extra carbon atoms present on the equator of this molecule compared to C60 which give enhanced absorbance in the visible regime of the solar spectrum.

## 6.2: Preliminary Results

This section will discuss the device fabrication for capacitive photocurrent measurements, followed by optical spectroscopy results of fullerene derivatives PC60BM. Absorbance measurements will be compared with capacitive photocurrent measurements, power dependence, and bias dependence.

## 6.2.1: Device fabrication and experimental procedure for capacitive photocurrent spectroscopy of PC60BM.

Figure 6.3 shows the device schematic of the structure made for capacitive photocurrent spectroscopy.
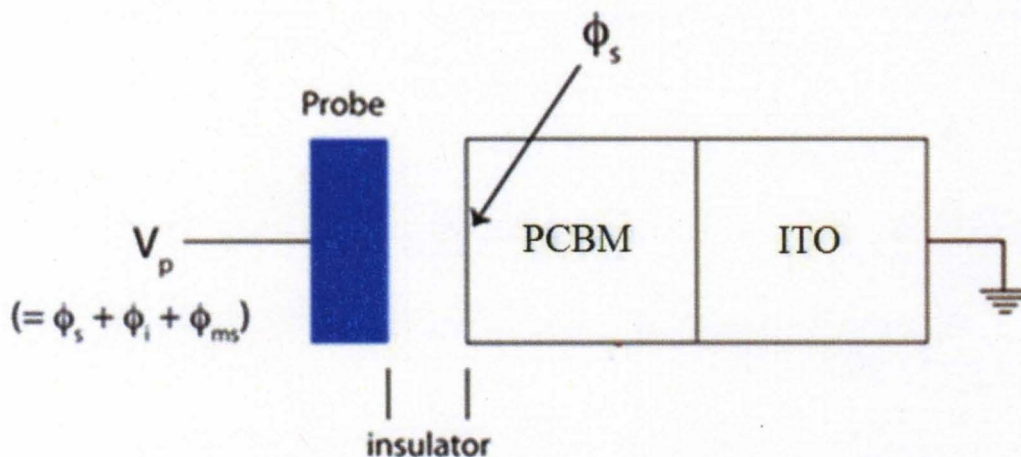


Figure 6.3: Device schematic for CPC measurement of PCBM

A thin film of PCBM was drop casted on pre-cleaned highly conducting ITO substrate (20-25 $\Omega$/square). Sputter coated ITO slides were purchased from Sigma Aldrich and used after thorough cleaning procedure was performed to ensure no organic contaminants were present on the electrode. The film was allowed to dry under ambient conditions overnight. An ITO coated slide was used because of its optical transparency to the laser light, and high conductivity which enhances charge transport. Electrical contact to the PCBM film was made by a small drop of silver paste partially connecting to PCBM and the ITO surface, and a copper wire was connected to the silver paste for charge collection from the

PCBM. The counter electrode for the capacitive measurement was the aluminum block on which the sample was placed. The dielectric for the capacitive photocurrent measurement was the quartz slide. Thus the two electrodes for the capacitor were PCBM/ITO and the opposite electrode was aluminum. The entire device was placed inside an optical access flow cryostat. The output of the device was connected to a current amplifier to measure small signals. The output of the current amplifier was connected to a lock-in amplifier on which an out of phase signal was measured. The lock-in amplifier was synched to the frequency of the laser which was 1 KHz. Only the optical signals generated at 1 KHz were measured ignoring any femtosecond pulsed laser transients. The excitation source was a femtosecond pulsed laser which had a pulse width less than 130 femtoseconds and pulse repetition rate of 1KHz. The laser was scanned in the wavelength range from 380 − 2400 nm (3.26 eV − 0.5 eV). During the entire scan the power of the laser was maintained at a constant value of 5 mW. Output of the laser power was pretty stable without fluctuations.

### 6.2.2: Optical spectroscopy results:

Optical spectroscopy results of PC60BM will be discussed in the following section.
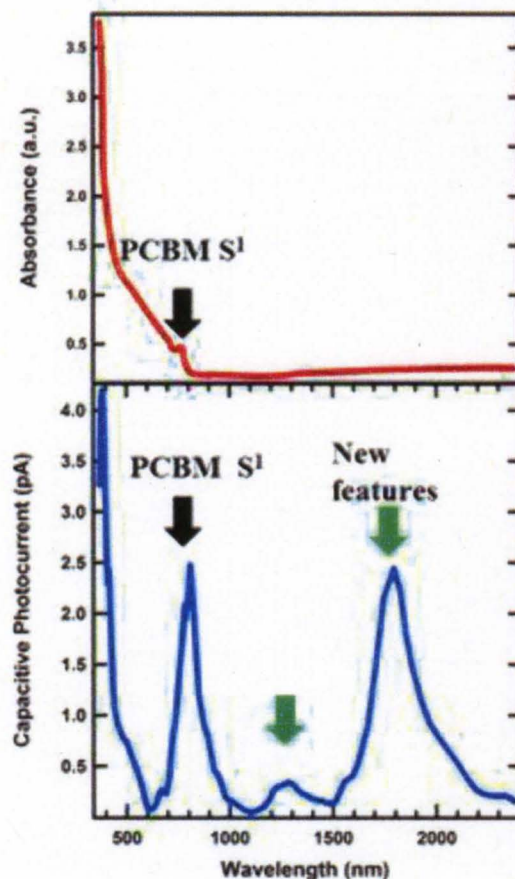
Figure 6.4: Absorbance vs. Capacitive photocurrent of PC60BM

Figure 6.4 shows a comparison of the capacitive photocurrent measurement with UV-Vis-IR absorbance. As it can be seen in the data, the capacitive photocurrent measurement shows the high energy feature below 400 nm which is attributed to the above gap transitions for PCBM. In addition, the capacitive photocurrent measurements a number of interesting below gap features in the PCBM. The first singlet transition state of PCBM (which has a small absorbance cross-section due to optical selection rules) appears as a small peak in the absorbance measurement, but appears as a much larger peak in the capacitive photocurrent measurement. This suggests that the charge dissociation

of this state is relatively high even though the absorbance cross-section for this state is small. In addition, two new features were resolved - a small feature observed at ~ 1250 nm and a big peak resolved at 1800 nm (0.7 eV). These low energy transitions have not been observed before for PCBM. The density of states calculations for PCBM do not predict any transitions in this energy range, thus it was interesting to observe some new features that have not been seen previously.

## 6.3 Optical spectroscopy of PC70BM

The following section will discuss the optical experiments performed on fullerene derivative PC70BM including absorbance capacitive photocurrent measurements.

PC70BM (Phenyl-C71-Butyric-Acid-Methyl Ester) is a functionalized derivative of C70 parent molecule. Similar to C60, C70 has poor solubility in organic solvents and is functionalized with a butyric acid methyl ester side chain to enhance its solubility. PC70BM is also a very commonly used electron acceptor along with PC60BM. C70, the parent molecule of PC70BM is known to have higher absorbance of light. This makes it a useful electron acceptor in organic solar cells because along with the light absorbance property of the electron donating polymer, if electron acceptor too absorbs light the power conversion efficiency of these solar cells would be more.

The first reason for the higher absorbance of PC70BM is the relaxed symmetry of the C70 molecule compared to C60. The second reason for higher absorbance is the presence of 10 extra carbon atoms on the equator of the molecule compared to PC60BM.
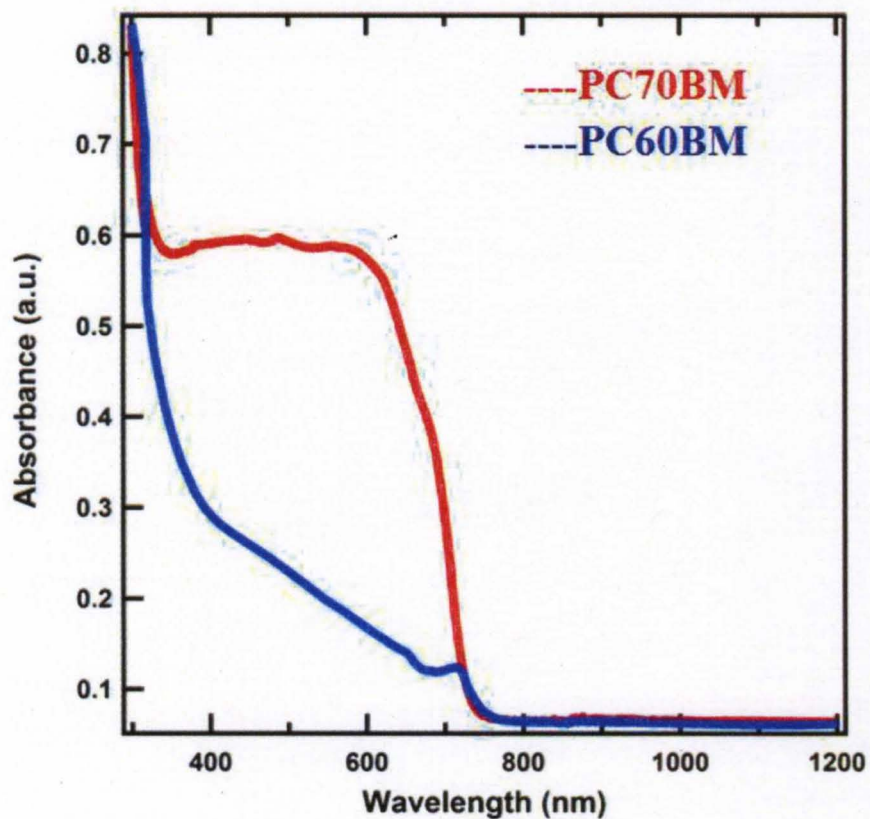


Figure 6.5: UV-Vis-IR absorbance measurement for PC70BM

Figure 6.5 shows the UV-Vis-IR absorbance measurements for PC60BM and PC70BM. The absorbance measurements were performed by dissolving 18 mg of PC70BM in 1ml of ortho-dichlorobenzene. The solution was left on a

magnetic stirrer for 72 hours to ensure PC70BM was uniformly dispersed in the organic solvent. The film for the absorbance measurements was made by drop casting the solution on a quartz slide. The film was let dry in ambient conditions overnight before the absorbance measurements were performed. The absorbance measurements were performed from 380 – 1200 nm. As seen in figure 6.16, as expected PC70BM show a higher absorbance in the visible region compared to PC60BM.

The relaxed symmetry for PC70BM makes it a useful candidate for electron acceptor in organic bulk heterojunction devices as higher power conversion efficiencies are achieved due to the higher absorbance coefficient of PC70BM compared to PC60BM. Using capacitive photocurrent measurement technique, new features were observed in PC60BM which previously had not been seen before. Thus, it was important to investigate if the same low energy transitions observed in PC60BM could be observed in PC70BM.

### 6.3.1 Capacitive photocurrent spectroscopy of PC70BM

The following section will discuss the device fabrication and capacitive photocurrent measurements of PC70BM.

Figure 6.6 shows the capacitive photocurrent measurement for PC70BM on a highly conducting ITO substrate. The sample used for the capacitive photocurrent spectroscopy of PC70BM was made in a similar way as PC60BM. 99.9 % pure PC70BM was purchased from Sigma Aldrich and used as received without further purification. 18 mg of PC70BM was dispersed in ortho-

dichlorobenzene and left on a magnetic stirrer for 72 hours. As purchased highly conducting ITO slides were used as a transparent electrode for efficient charge transport. The electrical connection to PC70BM/ITO was made by a small silver paste contact to which a copper wire was connected for external connection to
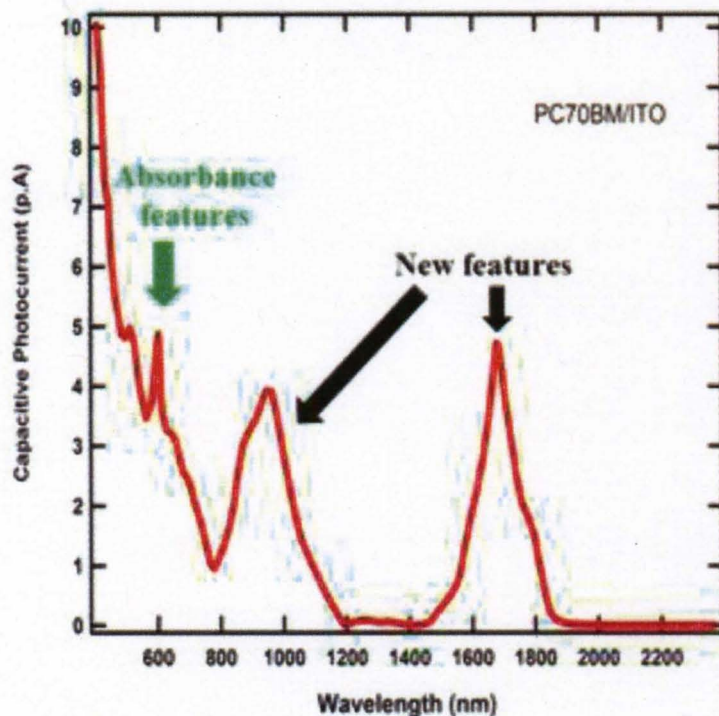


Figure 6.6: Capacitive photocurrent spectroscopy of PC70BM on ITO surface

the electronic equipment. The sample was placed in an optical access flow cryostat where the counter electrode of the capacitor strucutre was a copper electrode. Thus the two plates of the capacitor structure were PC70BM/ITO and the counter electrode was copper in the optical cryostat. The dielectric sepeating the two electrodes was quartz on which the ITO was sputtered.

The capacitive photocurrent spectrum of PC70BM/ITO shows the same absorbance features below 700 nm as seen in the UV-Vis-IR absorbance measurements. However, two new features in PC70BM were observed at lower energies. A new transition was resolved at 947 nm (1.31 eV) and a second transition was observed at even lower energy; 1667 nm (0.74 eV). These transitions in PC70BM on ITO substrate have not been previously reported. Even though the capacitive photocurrent measurement was performed at 0 V bias a high photocurrent signal was still observed which shows that just as was the case for PC60BM, the charge dissociation rate of PC70BM is pretty high as well, even though the absorbance of PC70BM at low energy light is relatively low. The lowest energy transition in PC70BM at 1667nm is believed to be due to the ITO plasmon state donating charge to PC70BM as was observed in PC60BM. The observation of new features resolved in PC70BM could used to develop new device architectures for higher power conversion efficiencies to take advantage of the newly observed transitions, partciularly at lower energy.
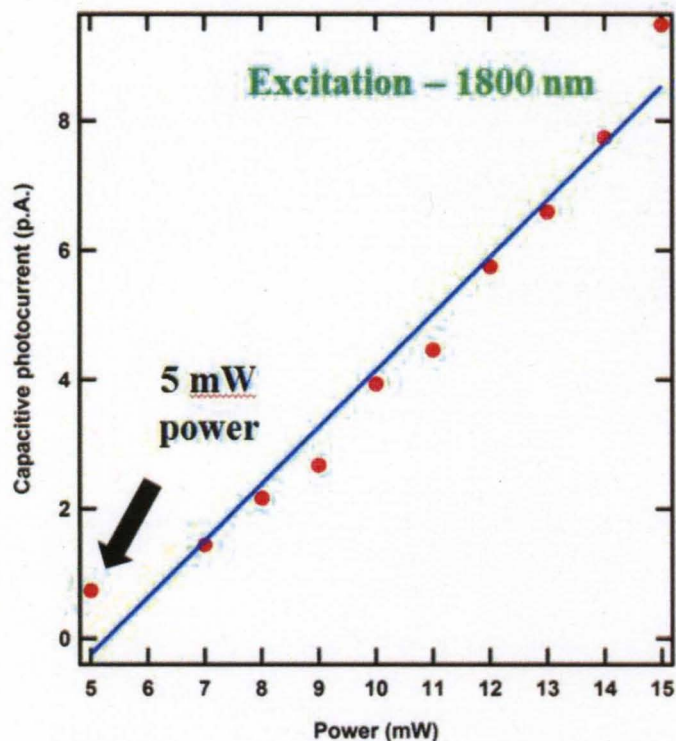
Figure 6.7: Power dependence for 1800 nm transition

## 6.3.2 Power dependence for capacitive photocurrent measurement

Power dependence of low energy transitions was performed to confirm the observed low energy peaks were not due to two photon absorbance. Figure 6.7 shows the power dependence of the low energy transition at 1800 nm observed in PC60BM. The laser was set at 1800 nm and a constant signal was obtained after which the laser power was successively increased in small steps. As seen in the data, the power dependence shows almost a linear dependence. For the entire capacitive photocurrent measurement a fixed power of 5 mW was used. Especially in the low power regime the data looks quite linear suggesting that the capacitive photocurrent measurement was due to a single photon effect and that there were no laser transient effects that could have affected the measurement.

## 6.4 CPC measurements of PCBM on conducting and non-conducting substrates

The following section will discuss the experimental results of PCBM on various substrates.

Following the review of theoretical/experimental studies of C60 molecules on different substrates, capacitive photocurrent measurements of PC60BM were performed on different substrates. The capacitive photocurrent data for PC60BM on different substrates will be presented in the following section.Figure 6.8 shows the comparison of the capacitive photocurrent data performed for PCBM on two different substrates.

Figure 6.8 shows the CPC data for PCBM on an ITO substrate where low energy transitions were observed, as described above. After a literature review, it was thought that the low energy transitions in PCBM might be due to the presence of highly conducting substrate ITO. It was important to confirm this hypothesis. Thus, PCBM was deposited on a transparent non-conducting substrate quartz to see if the low energy transitions still existed.

As seen in figure 6.9, the above gap transitions in PCBM below 400 nm were resolved. The first allowed singlet state transition for PCBM was also resolved. The singlet state transition on quartz substrate also showed a high dissociation rate as was observed in CPC measurements of PCBM on ITO. However, the most interesting fact of this data set was the absence of the low

energy transition at 1800 nm. As seen in figure 8, the signal was almost zero for the entire low energy scan from 1400 – 2400 nm.

This experiment confirmed that for the existence of the low energy transitions in PCBM it is important to have a high conducting substrate in close proximity with PCBM. The interface between ITO and PCBM is essential for the low energy transitions to be made accessible. The experimental evidence obtained in this data set was really important for the organic solar cell community as all the materials used for the fabrication of the device are the most common materials in the study of organic solar cells and at the same time the show some new experimental evidence for the existence of low energy transitions that previously have not been demonstrated using these materials.
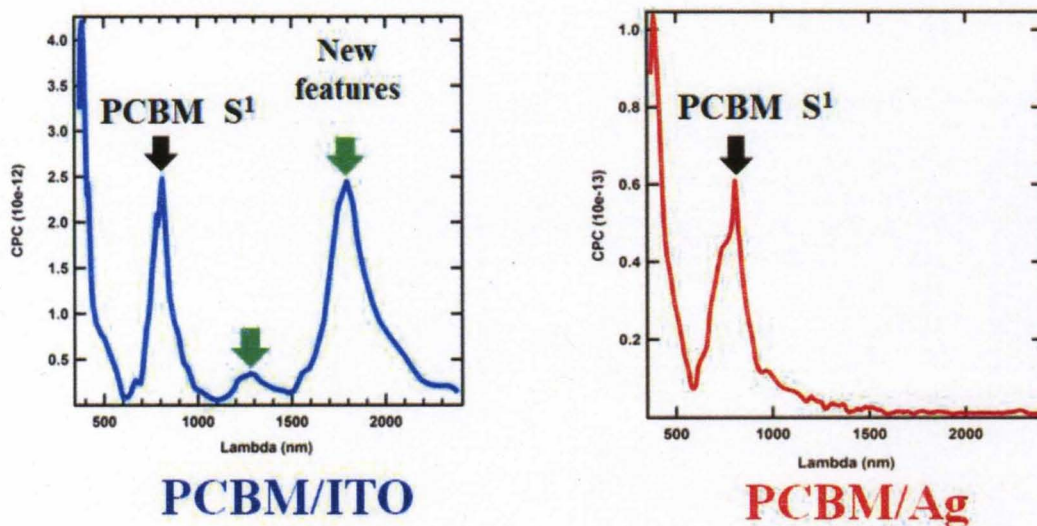


Figure 6.8: CPC device architecture and data for PCBM/ITO and PCBM/Quartz

97

## 6.4.1 Bias dependence of low energy transitions
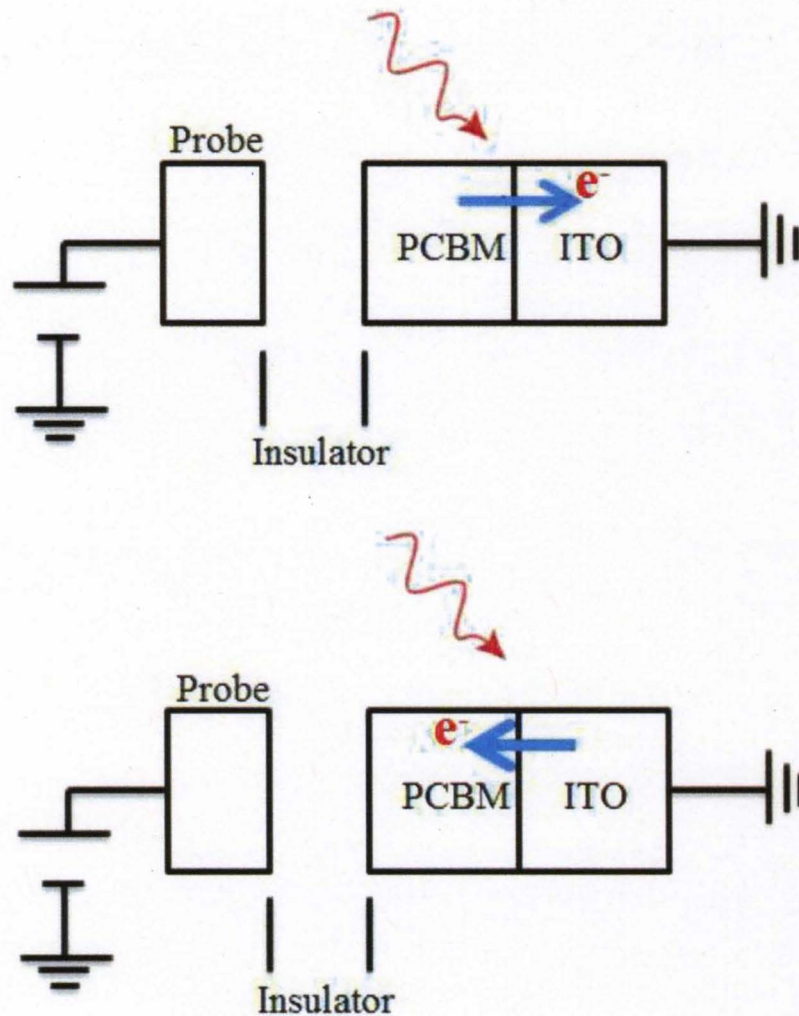


Figure 6.9 Electron transfer from PCBM to ITO and ITO to PCBM

As the low energy feature was resolved for the first time and was not observed before, bias dependence was performed for this transition to observe which direction the charge was moving. The bias was applied between ITO electrode and ground. The bias dependence was performed by setting the laser wavelength to 1800 nm and obtaining a stable signal. Using a DC source meter,

a dc bias was applied to the device from − 32 volts + 32 volts. As seen in figure 6.6 the bias dependence showed some interesting features about this transition. It was observed that the signal was increased by a large magnitude when applying a positive bias and was reduced when applying a negative bias. Even when a negative voltage was applied to device, the signal did not reduce completely to zero until negative 10 volts was applied to the device. This confirmed that the charge dissociation rate for the low energy transition was relatively high as the entire capacitive photocurrent measurement for the wavelength range of 380 − 2400 nm was performed at zero bias and no voltage had to be applied as the dissociation rate was high enough to detect a stable signal.
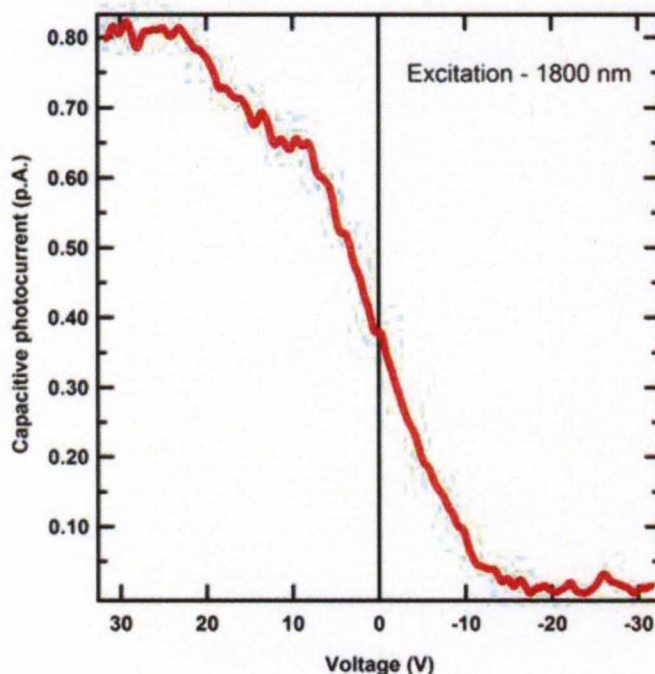


Figure 6.10: Bias dependence for 1800 nm transition

## 6.4.2 Low energy transition wavelength scan under applied potential

The bias dependence for the low energy transition shown above was only performed at the wavelength of the peak position of 1800 nm. It is thus essential to see how the wavelength scan varies under applied bias conditions. Since the signal decreases when a negative voltage is applied to the device; it was decided to apply negative voltage to the device for these measurements. The wavelength was scanned between 1600 – 2400 nm to resolve the low energy transition. Figure 6.11 shows four wavelength scans for the device under different bias conditions. As can be seen from figure 6.7, when zero bias was applied to the device the signal was the highest but when negative voltage was applied the signal started going down. At negative 10 volts, the signal was substantially smaller. This data set confirms the results of the bias dependence for the 1800 nm feature for the entire range in which the low energy transition was resolved. At negative bias, the signal is reduced.
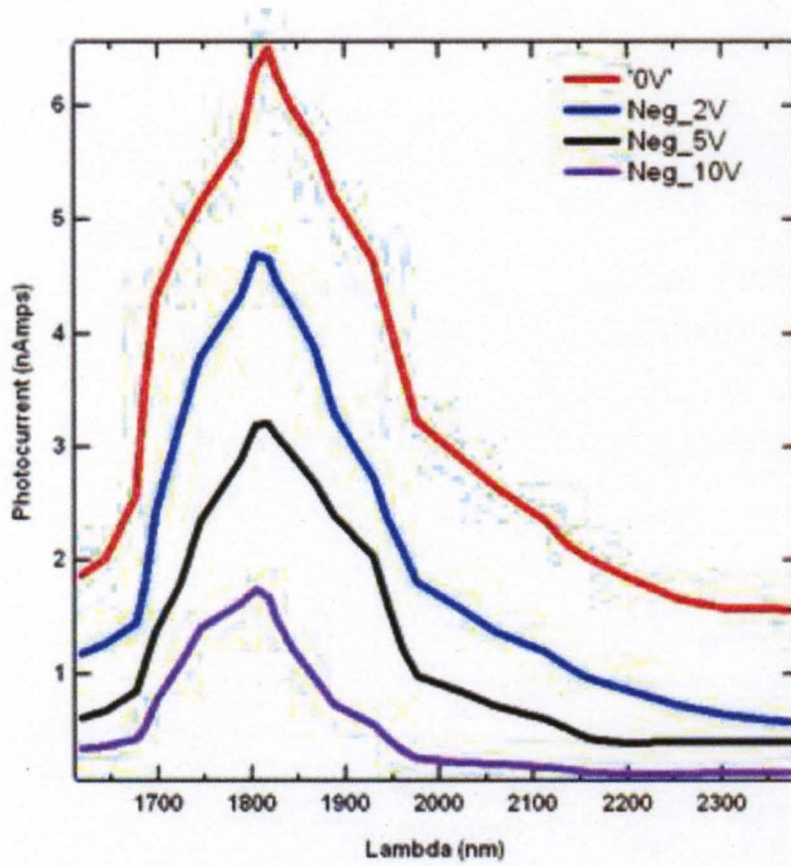
Figure 6.11: Low energy wavelength scans under different bias conditions

## 6.5 Plasmon resonance in Indium Tin Oxide

The following section will discuss the existence of plasmon states in ITO films at low energies.

As seen in the absorbance data for PCBM and ITO nanoparticles in figure 6.12, the low energy peaks which are observed at wavelengths greater than 1600 nm were initially assigned to an interfacial state between ITO nanoparticles and PCBM. An extensive literature review was performed to understand the absorbance properties of ITO nanoparticles of different dimensions and electron concentrations.

It was found that ITO nanoparticles fall in the category of conducting metal oxide nanoparticles in which there is a great deal of interest for enhancing the optical absorbance in the infra-red range.[60] Very recent reports have been published on synthesis and characterization of ITO nanoparticles with varying Indium/Tin molar ratios. Depending on the concentration of Tin in these conducting metal oxides, the surface plasmon state of ITO nanoparticles can be excited from 1618 nm up to > 2200 nm. The surface plasmon states have been studied widely in Ag and Au nanoparticles and have been used widely in the fabrication of organic bulk heterojunction solar cells. Surface plasmon states couple with the incident light in a plane and help enhance the light absorbance properties of materials. Plasmon states in solar cells are used primarily for enhancing the absorbance coefficient of various materials leading to higher power conversion efficiencies. However, there are various shortcomings of using

Au and Ag nanoparticles because they oxide easily and the peak plasmon resonance states of these materials is observed at 700 – 800 nm. No plasmon states for these materials exist in the infra-red or near infra-red region of the solar spectrum.
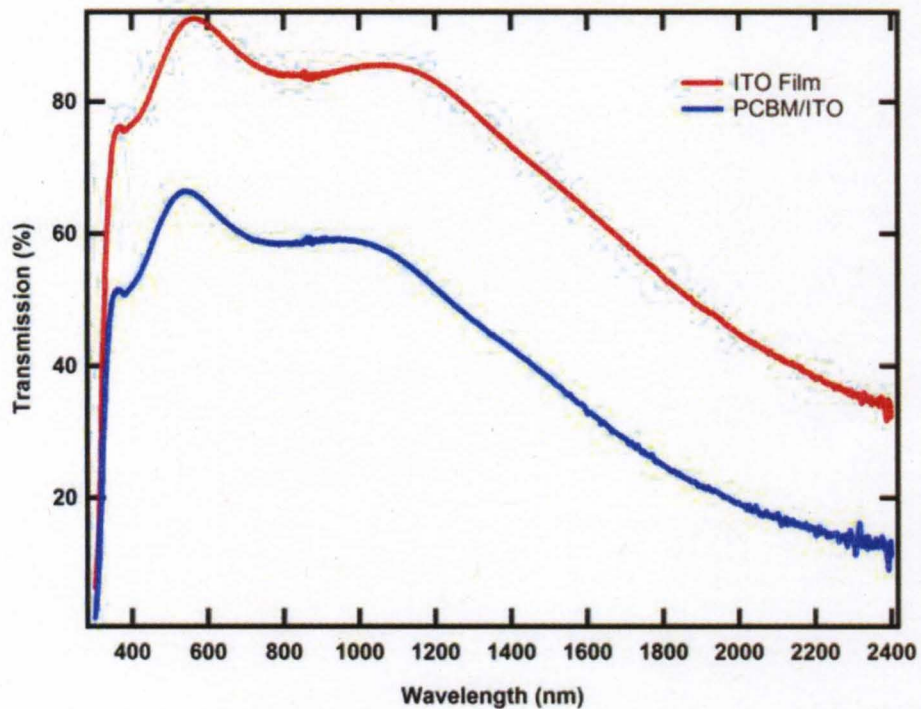


Figure 6.12 ITO transmission data with and without PCBM

For the purpose of enhancing the plasmon states in the infra-red region, various groups have worked on the controlled synthesis of highly conducting metal oxide nanoparticles including antimony doped tin oxide nanoparticles and indium doped tin oxide nanoparticles. Recent reports have demonstrated that plasmon states can be excited over a wide range in infra-red to mid infra-red spectrum. For ITO nanoparticles the plasmon states have only been reported to be excited in the infra-red and mid infra-red range. No plasmon states have been observed for either ITO nanoparticles or ITO nanocrystals in the visible or higher

energy regime. Thus, ITO nanoparticles are transparent in the visible regime for plasmon excitation.

Fig 6.12 shows absorbance measurements performed on a thin film of ITO. It can be seen that ITO is transparent in the visible range but shows some absorbance in the low energy regime. Absorbance below 350 nm is attributed to the optical band-gap of ITO. It has been reported in the literature that depending on the thickness of ITO films plasmon states at low energies can be excited.

Higher absorbance in the infra-red range due to the plasmon state could lead to higher absorbance coefficient leading to higher power conversion efficiencies. The key challenge after excitation of the plasmon state however remains the conversion of the excited plasmon to free charge that can be used for higher light to current conversion in an actual solar cell. Unless the excited plasmon leading to higher absorbance can be converted to free charge no photocurrent can be obtained.
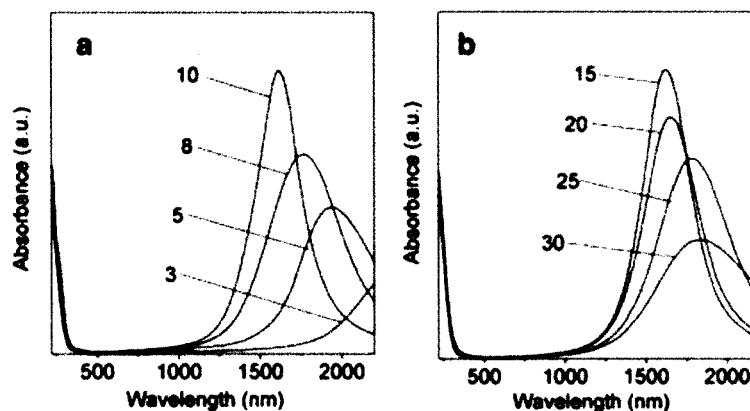


Figure 6.13: Absorbance of ITO nanoparticles due to plasmon mode [60]

## 6.6 Experimental and theoretical studies of below gap transitions in C60

Following section will review recent theoretical and experimental studies of C60 on different substrates showing evidence of low energy transitions. The existence of low energy transitions in PCBM raises questions for the reason of its existence as it is not predicted in any density of states theoretically for this material. Initially after the capacitive photocurrent experiment for PCBM was performed, it was hard to conclude the reason for the existence of the low energy transitions. A thorough literature review was performed to examine if any experimental or theoretical evidence existed to explain these transitions. It was found during the course of this extensive literature review that certain groups did predict the existence of below band-gap features for PCBM under certain conditions. For example, Tamai et al had demonstrated both experimentally and theoretically that if the parent molecule of PCBM, i.e. C60 were placed in close proximity of a highly conducting substrate, its dispersion relation could be perturbed. [55] This perturbation of the dispersion relation of C60 could give rise to new features that otherwise could not have been predicted in any theoretical calculations. The author performed theoretical calculations on density of states calculations for the lower most six carbon atoms of C60 molecules projected on top of the first three layers of copper metal. The calculations predicated the existence of a low energy transition way below the band-gap of C60. The energy at which this transition was predicted to exist was 0.7 eV (1800 nm). The author also performed photo electron emission spectroscopy of C60 deposited on top of

a copper metal and demonstrated experimentally that a low energy transition existed at 0.7 eV.
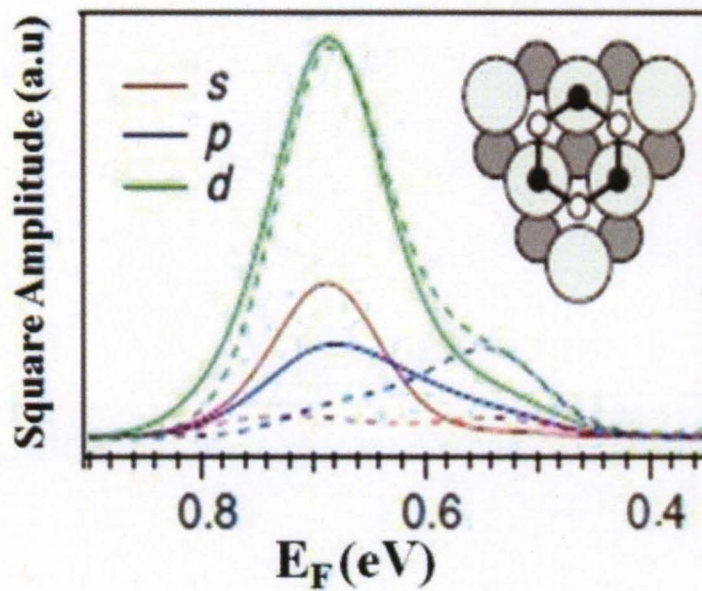


Figure 6.14: Density of states of C60 on Copper metal

## 6.7 Implications

Detailed study on the optical characterization of methanofullerene derivatives PC60BM and PC70BM reavled some interesting results. More work was needed to understand the charge generation mechansims in these fullerene derivatives as they are primarily used as the most efficient electron acceptors in organic bulk heterojunction devices.

Capacitive photocurrenet measurement of PC60BM/ITO devices showed optical transitions in wide range of wavelenghts (400 – 2400 nm). The most interesting of these transitions were those resolved in the low energy regime. Till date very materials used in different device architectures have optical transitions in such a wide range of wavelengths. The low energy transitions ( > 1600 nm) are primarily attributed to the excitation of the surface plasmon resonance state of high conducting Indium Tin Oxide. Recent reports confirmed the existence of surface plasmon mode in these conducting metal oxides. However, the interesting aspect of the work presented here is the evidence of charge transfer after the plasmon excitation. Charge transfer is the crucial process for high power conversion efficincies and the configuration of PC60BM/ITO using capacitive photocurrent technique offered two interesting aspects for this. First, plasmon mode exciation is very difficult when excitation of light is perpendicular to the surface. Using capacitive photocurrent technique, where the exciation of light was perpendicular to the surface, the plasmon mode was excited and resolved. Second, following the exciation of the plasmon mode using PC60BM in close

proximity with ITO direct charge transfer was demonstrated from the excited plasmon state of ITO to neighboring PC60BM.

Such evidence of low energy transitions in PC60BM/ITO surfaces opens a new area for study where different device architectures can be developed for harvesting light in a wide range of solar spectrum.

PC70BM is known to have higher absorbance compared to PC60BM. Using capacitive photocurrent measurements of PC70BM/ITO it was demonstrated that low energy transitions in PC70BM can also be resolved. Provided the right device configurations are developed to extract the photoexcited charges, these results are very promising for higher power conversion efficincies.

## 6.8 PCBM ITO nanoparticles spectroscopy

The following section will discuss the experiments performed on PC60BM and ITO nanoparticles bulk heterojunction films including absorbance measurements and capacitive photocurrent measurements.

Following the capacitive photocurrent measurements of PC60BM on quartz it was evident that existence of ITO layer is necessary for low energy transitions. Next experiment was designed to study if these low energy transitions can be resolved in bulk heterojunction mixture of PC60BM and ITO nanoparticles.

Figure 6.15 shows the UV-Vis-IR absorbance measurements of PCBM/ITO nanoparticles. As purchased ITO nanoparticles were used for this experiment without further purification. The size of the ITO nanoparticles ranged between 20-30 nm in diameter. PCBM and ITO nanoparticles were mixed in different ratios in ortho-dichlorobenzene and magnetically stirred for 72 hours to ensure a uniform mixture was made between the two materials. The films were made by drop casting method directly from the solvent and the film was allowed to dry under ambient conditions.

Figure 6.15 shows the absorbance data for two different ratios used for making PCBM and ITO nanoparticles bulk heterojunction mixture. As seen from the data, the 1:10 mixture where PCBM was one part and ITO nanoparticles were 10 parts showed the features of PCBM including the first singlet state transition and the high energy features but not many features were resolved in the infra-red

wavelength range. However in the absorbance measurements for 1:5 mixtures (one part PCBM, five parts ITO nanoparticles) the singlet state transitions of PCBM were resolved along with the high energy transitions but features in the infra-red range attributed to the interfacial effect between PCBM and ITO nanoparticles were also resolved.
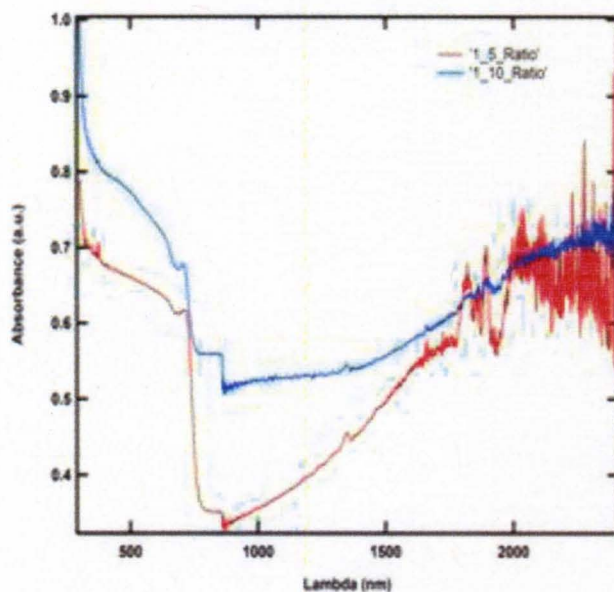


Figure 6.15: UV-Vis-IR absorbance measurement of PCBM/ITO nanoparticles

Thus for the 1:5 mixture of PCBM and ITO nanoparticles showed the absorbance features covering a wide range of the solar spectrum, starting from visible region and extending in the mid infra-red. This data can be very essential in increasing the absorbance of various bulk heterojunction materials provided the right materials and metal electrodes of varying work functions are used which could help facilitate enhanced charge generation/separation and charge collection in an actual solar cell.

110

## 6.8.1 Capacitive photocurrent spectroscopy of PC60BM/ITO nanoparticles

After the observation of sub band-gap states in PC60BM/ITO both in the capacitive photocurrent spectrosocpy and UV-Vis-IR absorbance measurements, it was important to study the optical properties of PC60BM/ITO nanoparticles. As seen in the UV-Vis-IR absorbance measurements of PC60BM/ITO nanoparticles (1:5 ratio sample), low energy transistions primarily attributed to the plasmon states of ITO nanoparticles were resolved. Capacitive photocurrent measurement of the sample ratio was performed to observe if charge separation can be observed between these two materials. Figure 6.16 shows the capacitive photocurrent device architecture for PC60BM/ITO nanoparticles. 1:5 ratios of PC60BM/ITO nanoparticles were dispersed in ortho-dichlorobenzene. Thin film of this mixture was made on a pre-cleaned ITO substrate by drop casting method. The film was allowed to dry under ambient conditions. Electrical connections were made as described in previous measurements for capacitive photocurrent spectroscopy. The dielectric separating the two electrodes was quartz.

As seen in the figure 6.17 several features were resolved for this measurement. The high energy transitions below 400 nm are primarily due to the thermal band-gap of PC60BM. The singlet state transition S1 of PC60BM was also resolved but along with this transition there were several other transitions at energies close to the singlet state transition of PC60BM which were also resolved.
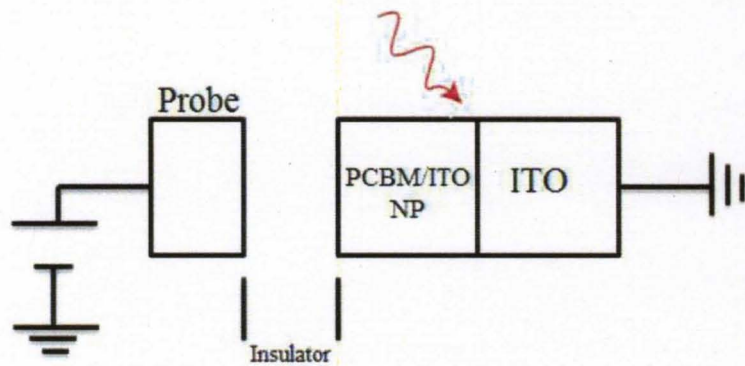
Figure 6.16: Device architecture for CPS of PCBM/ITO NP
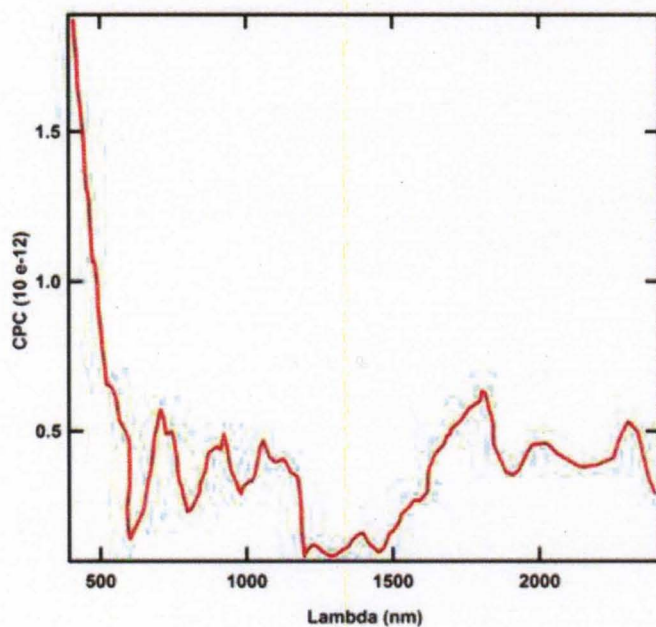


Figure 6.17 Capacitive photocurrent spectroscopy of PC60BM/ITO nanoparticles.

The interesting fact of this data set was the photocurrent measured at lower energies. As seen in PC60BM/ITO film measurement, the 1800 nm low energy transition was resolved but along with that several other transitions were also seen, at energies up to 2400 nm (0.5 eV). As can be seen from the UV-Vis-IR data of PC60BM/ITO nanoparticles (1:5 ratios) in figure 9, there are several features in the low energy range due to the plasmon state of ITO. Similar to those transitions, photocurrent transitions were resolved in the same low energy regime. This measurement is a direct evidence of charge generation and charge transfer between PC60BM and ITO nanoparticles and PC60BM and ITO film (as previously seen). This measurement demonstrates that for bulk heterojunction devices made out of PC60BM and ITO nanoparticles light absorbance creates charge and this charge can be separated and extracted for a wide range of wavelength range from 400 nm – 2400 nm (3 eV – 0.5 eV).

Using the right combination of counter electrodes with separate work functions and charge acceptance favorability; a two terminal bulk heterojunction solar cell can be made using PC60BM/ITO nanoparticles which would have light absorbance and charge generation on wavelength scales that previously have not been seen or reported before.

# CHAPTER VII: CONCLUSIONS AND FUTURE WORK

## CONCLUSIONS:

Capacitive photocurrent measurements of bulk heterojunction solar cell materials revealed interesting information about the charge dissociation rate of the commonly used electron acceptor; PCBM. PCBM is known to have a small absorbance cross-section but its charge dissociation rate was measured to be relatively high. This experimental evidence led to design of a new experiment; photovoltage bleaching.

Photovoltage bleaching experiments clearly helped identify a direct channel promoting recombination in an organic bulk heterojunction device. It was demonstrated counter-intuitively that shining more light on an organic solar cell the photovoltage output goes down. In fact for a narrow band of light it was shown that the photovoltage signal reduces by ~ 71 %. This narrow band of light coincided with the singlet state S1 transition of PCBM which is known to have a small absorbance cross-section. It was concluded that the excitation of light for the energy transition of singlet state of PCBM impedes the charge dissociation either by enhancing the recombination rate of higher energy generated charge or by blocking the free charge carriers from making to the contacts.

114

It was thus concluded that filtering out a narrow band of light at the excitation energy S1 transition of PCBM the overall output of organic solar cells can be enhanced. Most commonly used electron acceptors such as PCBM have received little attention compared to the polymers although they constitute a major portion of the bulk heterojunction solar cell active material. Capacitive photocurrent spectrum revealed several low energy transitions which are believed to be below the optical band-gap of PCBM. It was found that these low energy transitions were due to plasmon mode excitation of a high conducting substrate ITO which was in close proximity of PCBM to facilitate charge transfer. Although plasmon modes in ITO have been reported in the past, for the first time clear evidence of enhanced charge transfer by the plasmon mode of ITO to PCBM was shown using capacitive photocurrent spectroscopy. These plasmon modes were excited at energies as low as 0.7 eV and charge transfer due to these excitation was also shown at such low energies. The same measurements were also shown for a second methanofullerene derivative; PC70BM which is also a very commonly used electron acceptor in organic bulk heterojunction solar cells.

Combining methanofullerene derivatives with high conducting ITO substrate/nanoparticles, light absorbance and charge transfer was demonstrated for broad range of wavelengths (400 – 2400 nm). Till date very few materials have been reported to have absorbance accompanied with charge dissociation for such a large range of energies.

Most commonly used electron acceptors such as PCBM have received little attention compared to the polymers although they constitute a major portion of the bulk heterojunction solar cell active material. Capacitive photocurrent spectrum revealed several low energy transitions which are believed to be below the optical band-gap of PCBM. It was found that these low energy transitions were due to plasmon mode excitation of a high conducting substrate ITO which was in close proximity of PCBM to facilitate charge transfer. Although plasmon modes in ITO have been reported in the past, for the first time clear evidence of enhanced charge transfer by the plasmon mode of ITO to PCBM was shown using capacitive photocurrent spectroscopy. These plasmon modes were excited at energies as low as 0.7 eV and charge transfer due to these excitation was also shown at such low energies. The same measurements were also shown for a second methanofullerene derivative; PC70BM which is also a very commonly used electron acceptor in organic bulk heterojunction solar cells.

Combining methanofullerene derivatives with high conducting ITO substrate/nanoparticles, light absorbance and charge transfer was demonstrated for broad range of wavelengths (400 – 2400 nm). Till date very few materials have been reported to have absorbance accompanied with charge dissociation for such a large range of energies.

**FUTURE WORK:**

As demonstrated with the photovoltage bleaching experiments future experiments could be conducted using narrow band filters to cut out those energy levels which promote recombination process and study its effect on the power conversion efficiencies of organic solar cells. There is a great potential to enhance the power conversion efficiencies of these solar cells narrowing certain optical energy transitions.

Capacitive photocurrent measurements demonstrated plasmon excitation modes of ITO resulting in charge transfer to PCBM over a wide range of wavelengths (400 – 2400 nm). Future experiments could be conducted on real solar cells with the right configuration of working electrodes to enhance charge collection over this large energy range. There is huge potential of high power conversion efficiencies in solar cells using bulk heterojunction configurations of PCBM and ITO nanoparticles as few materials till date have demonstrated absorbance or charge separation over such large energy range.

# REFERENCES

[1]http://energy.senate.gov/public/index.cfm?FuseAction=Hearings.Testimony&Hearing_ID=6b73efcf-3b49-4211-bdec-88f4cc257831&Witness_ID=d8642eec-126d-4c6d-bebc-f1c1505d658e

[2] http://gcep.stanford.edu/pdfs/DyUMPHW1jsSmjoZfm2XEqg/1.4-Ziagos.pdf

[3] Service, R. F. (2005). "Solar energy - Is it time to shoot for the Sun?" Science 309(5734): 548-551.

[4] http://www.econbrowser.com/archives/2011/08/economic_conseq_2.html

[5] http://energy.gov/science-innovation/energy-sources

[6] http://www.nrel.gov/solar/

[7] M. Tao, The Electrochemical Society Interface, 2008, 17, 30

[8] R. Hezel, Progress in Manufacturable High-Efficiency Silicon Solar Cells, Advances in Solid State Physics Series, Vol. 44 (Springer, Berlin / Heidelberg, 2004).

[9] Gregg, B. A. (2003Journal of Physical Chemistry B 107(20): 4688-4698.

[10] Ghosh, A. K. and T. Feng (1978). Journal of Applied Physics 49(12): 5982-598[11] Tang, C. W. (1986) Applied Physics Letters 48(2): 183-185.

[12] Reyes-Reyes, M., K. Kim and D. L. Carroll (2005). Applied Physics Letters 87(8): 083506.

[13] Koide N, Yamanaka R, Katayama H. Recent advancesof dye-sensitized solar cells and integrated modules at SHARP. MRS Proceedings 2009; 1211: 1211-R12-02.

[14] Morooka M, Ogura R, Orihashi M, Takenaka M. Development of dye-sensitized solar cells for practical applications. Electrochemistry 2009; 77: 960–965.

[15] http://www.konarka.com.

[16] http://www.solarmer.com.

[17] Ni Zhao, Tim P. Osedach, Liang-Yi Chang, Scott M. Geyer, Darcy Wanger, Maddalena T. Binda,Alexi C. Arango, Moungi G. Bawendi, and Vladimir Bulovic. AVS Nano 4, 3743, 2010

[18] Shenqiang Ren, Liang-Yi Chang, Sung-Keun Lim, Jing Zhao, Matthew Smith, Ni Zhao§Vladimir Bulovi Moungi Bawendi, and Silvija Gradecak Nano Lett. 2011, 11, 3998–4002

[19] Jiang Tang, KyleW. Kem, Sjoerd Hoogland, Kwang S. Jeong, Huan Liu Larissa Levina,Melissa Furukawa, XihuaWang, Ratan Debnath, Dongkyu Cha, KangWei Chou, Armin Fischer,Aram Amassian, John B. Asbury and Edward H. Sargent Nature Materials 10, 765, 2011

[20] Daisuke Mori, Hiroaki Benten, Junya Kosaka, Hideo Ohkita, Shinzaburo Ito, and Kunihito Miyake ACS Appl. Mater. Interfaces 2011, 3, 2924–2927

[21] Martin A. Green, K. E., David L. King, Yoshihiro Hisikawa, Wilhelm Warta, (2006). "SHORT COMMUNICATION Solar cell efficiency tables (version 27)." Progress in Photovoltaics: Research and Applications 14(1): 45-51.

[22] Schmidt-Mende, L., U. Bach, R. Humphry-Baker, T. Horiuchi, H. Miura, S. Ito, S. Uchida and M. Gratzel (2005). Advanced Materials 17(7): 813

[23] Komiya, R., L. Y. Han, R. Yamanaka, A. Islam and T. Mitate (2004 Journal of Photochemistry and Photobiology a-Chemistry 164(1-3): 123-127.

[24] van Hal, P. A., M. M. Wienk, J. M. Kroon, W. J. H. Verhees, L. H. Slooff, W. J. H. van Gennip, P. Jonkheijm and R. A. J. Janssen (2003). Advanced Materials15(2): 118-121.

[25] Liu, J. S., E. N. Kadnikova, Y. X. Liu, M. D. McGehee and J. M. J. Frechet (2004). Journal of the American Chemical Society 126(31): 9486-9487.

[26] Beek, W. J. E., L. H. Slooff, M. M. Wienk, J. M. Kroon and R. A. J. Janssen (2005). Advanced Functional Materials 15(10): 1703-1707.

[27] Huynh, W. U., J. J. Dittmer, W. C. Libby, G. L. Whiting and A. P. Alivisatos (2003). Advanced Functional Materials 13(1): 73-79.

[28] Gur, I., N. A. Fromer, M. L. Geier and A. P. Alivisatos (2005Science 310(5747): 462-465.

[29] Shockley, W. and H. J. Queisser (1961). 32: 510.32. Ellingson, R.

[30] Kim, Y., S. Cook, S. A. Choulis, J. Nelson, J. R. Durrant and D. D. C. Bradley (2004). Chemistry of Materials 16(23): 4812-4818.

[31] Granstrom, M., K. Petritsch, A. C. Arias, A. Lux, M. R. Andersson and R. H. Friend (1998). Nature 395(6699): 257-260.

[32] Shaheen, S. E., C. J. Brabec, N. S. Sariciftci, F. Padinger, T. Fromherz and J. C. Hummelen (2001). Applied Physics Letters 78(6): 841-843

[33] J. J. M. Halls, C. A. Walsh, N. C. Greenham, E. A. Marseglia,R. H. Friend, S. C. Moratti, A. B. Holmes, Nature 1995, 376, 498 – 500.

[34] G. Yu, A. J. Heeger, J. Appl. Phys. 1995, 78, 4510 – 4515.

[35] J. Xue, S. Uchida, B. P. Rand, S. R. Forrest, Appl. Phys. Lett.2004, 84, 3013 – 3015.

[36] N. S. Sariciftci, D. Braun, C. Zhang, V. I. Srdanov, A. J. Heeger, G. Stucky, F. Wudl, Appl. Phys. Lett. 1993, 62, 585 – 587.

[37] M. Granstrom, K. Petritsch, A. C. Arias, A. Lux, M. R. Andersson, R. H. Friend, Nature 1998, 395, 257 – 260.

[38] Physics of Organic Semiconductors Wiley-VCH  Edited by W.Brutting 2005

[39] C. J. Brabec, N. S. Sariciftci, J. C. Hummelen, Adv. Funct.

Mater. 2001, 11, 15 – 26.

[40]R. Koeppe, N. S. Sariciftci, Photochem. Photobiol. Sci. 2006, 5,1122 – 1131.

[41] Photoinduced Electron Transfer (Eds.: M. A. Fox, M. Chanon), Elsevier, Amsterdam, 1988.

[42] Polymer–fullerene bulk heterojunction solar cells Carsten Deibel and Vladimir Dyakono Rep. Prog. Lhys. 73, 096401, 2010

[43] P. A. van Hal, S. C. J. Meskers, R. A. J. Janssen, Appl. Phys. A 2004, 79, 41– 46.

[44] Y.-X. Liu, M. A. Summers, S. R. Scully, M. D. McGehee, J. Appl. Phys. 2006, 99, 093521

[45] J. J. Benson-Smith, L. Goris, K. Vandewal, K. Haenen, J. V. Manca, D. Vanderzande, D. D. C. Bradley, J. Nelson, Adv. Funct. Mater. 2007, 17, 451– 457.

[46] V. Chukharev, N. V. Tkachenko, A. Efimov, D. M. Guldi, A. Hirsch, M. Scheloske, H. Lemmetyinen, J. Phys. Chem. B 2004, 108, 16377 – 16385.

[47] H. Bässler, Physica Status Solidi B: Basic Research 175, 15-56 (1993).

[48] I. Montanari, A. F. Nogueira, J. Nelson, J. R. Durrant, C. Winder, M. A. Loi, N. S. Sariciftci, and C. Brabec, Applied Physics Letters 81, 3001-3003 (2002).

[49] S. C. J. Meskers, P. A. van Hal, A. J. H. Spiering, J. C. Hummelen, A. F. G. van der Meer, and R. A. J. Janssen, Physical Review B: Condensed Matter and Materials Physics 61, 9917-9920 (2000).

[50] T. Offermans, S. C. J. Meskers, and R. A. J. Janssen, Journal of Chemical Physics 119, 10924-10929 (2003).

[51] Brabec, C. J., A. Cravino, D. Meissner, N. S. Sariciftci, T. Fromherz, M. T. Rispens, L. Sanchez and J. C. Hummelen (2001Advanced Functional Materials 11(5): 374-380.

[52] Wang, X., E. Perzon, J. L. Delgado, P. De la Cruz, F. Zhang, F. Langa, M. Andersson and O. Inganas (2004). Applied Physics Letters 85(21): 5081-5083.

[53]12M. Hallermann, I. Kriegel, E. Da Como, J. M. Berger, E. Von Hauff, and J. Feldmann, Adv. Funct. Mater. 19, 3662 2009.

[54] Steffan Cook  Hideo Ohkita, Youngkyoo Kim Jessica J. Benson-Smith Donal D.C. Bradley   James R. Durrant  Chemical Physics Letters 445 (2007) 276–280

[55] A. Tamai, A. P. Seitsonen, F. Baumberger, M. Hengsberger, Z.-X. Shen, T. Greber, and J. Osterwalder  Physical Review B 77, 075134 2008

[56] Spectra-Physics, "Hurricane" Diode pumped Kilohertz Ti: Sapphire Regenerative Amplifier System, User's Manual 2001

[57] A. Mohite PhD Thesis University of Louisville 2007

[58] T. Bansal PhD Thesis University of Louisville 2010

[59] H. M. Shah, Applied Physics Letters, 97, 263301, 2010

[60]Masayuki Kanehara, Hayato Koike, Taizo Yoshinaga, and Toshiharu Teranish J. AM. CHEM. SOC. 2009, 131, 17736–1773

# CURRICULAM VITAE

## HEMANT M. SHAH

1516 S.2<sup>nd</sup> st, Apt # 2A,                 hemant.m.shah@gmail.com

Louisville, KY                                             502-593-7290

## RESEARCH INTERESTS

- Optical & electrical characterization of Semiconductors &Nanostructures

- Charge dissociation processes in photovoltaics & 1D systems

- Band- gap tuning & magnetism in graphene

- Nano-scale device design, fabrication & analysis

## EDUCATION

| | | |
|---|---|---|
| **PhD** | **Electrical Engineering** | **May 2012** |
| | University of Louisville, Louisville, KY | |
| **M.S** | **Electrical Engineering** | **2008** |
| | University of Louisville, Louisville, KY s | |
| **P. G. Diploma** | **Solid State Electronics** | **2004** |
| | M. S. University, Baroda, India | |
| **B.S** | **Instrumentation & Control Engineering** | **2003** |
| | M.S.University, Baroda, India | |

## RESEARCH ACCOMPLISHMENTS (In chronological order)

- Proposed strategy for improving quantum efficiency of organic and dye sensitized solar cells by harvesting the spin-triplet exciton states.

- Developed capacitive method to directly probe the exciton dissociation in organic photo-voltaics.

- Used capacitive photocurrent technique for measuring properties of a variety of individual nanostructures without complex lithography – technique can provide direct measure of photo-voltage generated by charge separation in two or more interface systems.

- Fabricated a nanotube based strain sensor with gauge factor of over 1000 and tunable over a large wavelength regime.

- Developed techniques to deposit and pattern Graphene Nano Ribbons for fabrication of Graphene transistors.

- Among the first few groups to demonstrate a nanotube SPIN-FET (field effect transistors) using a short channel (< 20 nm) fabrication technique.

- Contributed to several proposals based on development of Graphene interconnects, THz sources, Carbon nanotube Strain sensors, and Organic photovoltaics to name a few.

## PEER REVIEWED PUBLICATIONS

- **H. M. Shah,** A. D. Mohite, T. Bansal & B. W. Alphenaar "Photovoltage Bleaching in Bulk Heterojunction Solar Cells through Occupation of the Charge Transfer State" **Submitted to Physical Review Letters, April 2010**

- **H. M. Shah,** B. W. Alphenaar & M. Sunkara "Solid state Dye sensitized solar cells based on Tin Oxide Nanowires" **manuscript in preparation, 2010**

- T. Bansal, A. D. Mohite, **H. M. Shah** & B.W.Alphenaar "Measurement of the electronic density of states versus oxygen coverage in oxidized graphene" **manuscript in preparation for Nano Letters, May 2010**


## ORAL TALKS AT CONFERENCES

- **H. M. Shah,** A. D. Mohite, T. Bansal & B. W. Alphenaar "Resolving the charge transfer state in bulk heterojunction solar cells by occupation of the charge transfer state" presented at the American Physical Society March meeting, Portland, OR 2010.

- T. Bansal, A. D. Mohite, **H. M. Shah** C. Galande, P. Ajayan & B. W. Alphenaar "Measurement of the electronic density of states versusoxygen coverage in oxidized grapheme" presented at the American Physical society, March meeting, Portland, OR 2010.

- **H. M. Shah**, T. Bansal, A. D. Mohite, P. Ajayan & B. W. Alphenaar "Photoexcitation and dissociation of charge in organic nanostructures

and photovoltaic devices" presented at University of Lexington, KY,

Lexington, KY, 2009

**TECHNICAL SKILLS**

- Expertise in multidisciplinary research in areas of Opto-electronics, Micro/Nanofabrication, Semiconductor Device Physics and Material Science.

- Organic Solar Cell fabrication and electrical/optical characterization techniques.

- clean room (Micro/Nanofabrication) semiconductor processing techniques – optical /e-beam lithography (sub 10 nm gaps), wet/dry etching, diffusion, lapping and polishing (CMP).

- thin film deposition techniques like CVD, PECVD, ALD, Oxidation, e-beam/thermal evaporation, sputtering and spin coating polymers, films of nanomaterials.

- Expertise with state of art lasers and optical systems like Spectra-Physics femtosecond pulsed Laser; Hurricane (Mai- Tai, Evolution, Regenerative Amplifier) pumped OPA-800 CF, Argon-Ion, Ti-Sapphire, dye, diode lasers and optical components.

- microscopy and surface characterization techniques like AFM/MFM,SEM, EDAX,WYKO,DEKTAK, NSOM,InGaAs detectors, single molecule fluorescence microscopy.

- spectroscopy techniques like Raman, Fluorescence, UV-Vis-IR absorbance, Photoconductivity, Transient absorbance,Pump-probe, Capacitive photo-voltage and FTIR.
- cryogenic measurement techniques like dilution refrigerators, optical flow cryostats.

### OPTO-ELECTRONICS & SPECTROSCOPY

- Developed an innovative spectroscopy technique, ("Capacitive Photocurrent Spectroscopy") for optical characterization of carbon nanotubes and nanowires.
- Performed extensive experiments on photoconductivity and luminescence of nanowires and carbon nanotubes for the development of photodetectors and photovoltaic applications.
- Designed experiments on electroluminescence from CNT devices.
- Studied the vibrational energy spectrum of Single Wall and Double Wall nanotubes using micro Raman Spectroscopy.

### SPIN TRANSPORT & MAGNETO-OPTICS

- Photocurrent measurements on Europium Chalcogenites (EuX) compounds as spin filtering tunnel barrier.
- Magnetic switching in Single-wall carbon nantoubes with ferromagnetic contacts.
- Conducted experiments on Magnetic switching in Nickel contacted Nano junctions.

- Performed Experiments on Optical Spin Injection from ferromagnetic contact into Quantum Heterostructures (GaAs/AlGaAs/InGaAs/GaAs).

## MICROFABRICATION & SEMICONDUCTOR DEVICE PHYSICS

- Fabrication and testing of Carbon Nanotube & Nanowire MOSFETs.

- Design and fabrication of break junctions using electromigration technique for development of single-molecular transistors.

- Detailed experiments on achieving low resistance contacts to nanostructures.

- Understanding the role of Schottky barrier contacts to carbon nanotubes for opto-electronic transport.